Title
EFFECTS OF ANGULAR MOMENTUM ON GAMMA-MY PRODUCTION IN COMPOUND NUCLEUS REACTIONS

Author
Mollenauer, James Frederick.

Publication Date
1961-06-01

UCRL 9724

UNIVERSITY OF CALIFORNIA

Ernest O. Lawrence

Radiation Laboratory

EFFECTS OF ANGULAR MOMENTUM ON GAMMA-RAY PRODUCTION IN COMPOUND NUCLEUS REACTIONS

DISCLAIMER

UCRL-9724
UC-34 Physics
TID-4500 (16th Ed.)

UNIVERSITY OF CALIFORNIA

Lawrence Radiation Laboratory

Berkeley, California

Contract No. W-7405-eng-48

EFFECTS OF ANGULAR MOMENTUM ON GAMMA-RAY PRODUCTION IN COMPOUND NUCLEUS REACTIONS

James Frederick Mollenauer

(Thesis)

June 1960

Printed in USA. Price $2.25. Available from the
Office of Technical Services
U. S. Department of Commerce
Washington 25, D.C.

EFFECT OF ANGULAR MOMENTUM ON GAMMA-RAY PRODUCTION IN COMPOUND-NUCLEUS REACTIONS

Contents

EFFECTS OF ANGULAR MOMENTUM ON GAMMA-RAY PRODUCTION IN COMPOUND-NUCLEUS REACTIONS

James F. Mollenauer
(Thesis)

Lawrence Radiation Laboratory and Department of Chemistry
University of California, Berkeley, California

June 1961

ABSTRACT

The yields and spectra of gamma rays produced in compound nucleus reaction were measured by a coincidence technique. Pulses from the gamma detector were required to be in coincidence with pulses indicating the removal of a charged particle from the beam. The effect of the angular momentum of the compound system was studied by using pairs of targets producing the same compound nucleus when bombarded with helium and with carbon ions.

For the carbon-ion reactions studied, the total energy appearing in gamma rays was greater than the neutron binding energy. This result disagrees with the assumption of evaporation theory that nucleon emission is preferred when possible. The increased gamma yield was shown to depend on angular momentum at constant excitation energy.

The anisotropy of the gamma radiation indicated that the transitions involved in the de-excitation were primarily quadrupole when the angular momentum brought in was approximately 10 to 15 units. A greater fraction of dipole transitions was apparent for larger angular momenta. Both the anisotropy and the average photon energy were inconsistent with predictions based on single-proton transitions. Collective modes are probably involved in the radiative processes; the average and total gamma energies are more consistent with vibrational than with rotational transitions.

I. INTRODUCTION

In the study of compound-nucleus reactions, it is generally assumed that if an excited nucleus can emit a nucleon, it will. Above the neutron emission threshold, the probability of de-excitation by emission of gamma rays is considered negligible. In most cases, this assumption is good, but the presence of large amounts of orbital angular momentum adds a complicating factor. The peaks of the excitation functions for evaporation reactions are consistent with reasonable values of the nuclear temperature when little angular momentum is brought in by the bombarding particle. When heavy ions are used as the projectile and orbital angular momenta averaging 40 $\hbar$ or more are brought in, the peaks of the excitation functions are shifted upward in energy.

Such effects have been seen by Choppin with 60 to 120-Mev carbon ions on isotopes of tellurium,[1] and by Karamyan and associates with carbon and nitrogen ions on vanadium at lower energies.[2] The magnitude of the energy shift is about 3x Mev, where x is the number of neutrons evaporated. However, the shift has not been seen[3] in the reaction $Pr^{141}(C^{12}, 4n)Tb^{149}$. Morton has measured the angular distribution of the recoil nuclei for carbon ions on tellurium and praseodymium.[4] He found that by proper choice of temperature he could fit a calculation based on the Jackson model to the distribution of Tb^{149} recoils in the praseodymium bombardments, but not the Ce^{137m} recoils in the tellurium case. In the latter, it was necessary to assume that extra energy was carried off by gamma rays (about 10 Mev at an excitation energy of 80 Mev) in order to get a fit.

Effects of high angular momentum have also been seen in the case of fission. Gilmore bombarded several rare earths with oxygen and neon ions and found that fission yields increased with average angular momentum (that is, using a heavier projectile) at the same excitation energy.[5] The angular distribution of fission fragments from carbon-ion bombardments of gold was examined by Gordon,[6] who found it consistent with a nucleus rotating as a liquid drop with high angular momentum at the moment of fission.

We may expect high angular momentum to cause an increase in gamma emission on the following qualitative grounds: because the binding energy of the emitted neutrons is considerably greater than their

kinetic energy, they carry off most of the excitation but relatively little of the original angular momentum. As the excitation energy decreases, the number of final states available with sufficiently high spin should become quite small. Consequently, neutron emission should be slowed considerably while the energy is still above the threshold. If it is slowed enough, photon emission will begin to compete favorably. The gamma rays are not required to carry a large binding energy and, compared with neutron emission, may go to final states of higher energy where the density of states is higher.

From the classical point of view, the whole nucleus may be considered as set into rotation by the impact of the projectile. Its energy will then consist of thermal energy and rotational energy. The thermal energy may contribute to the evaporation of neutrons, while the rotational motion may not. The equivalence of these two points of view, and their application to particle emission, is discussed by Ericson and Strutinsky.[7]

The gamma-ray yields were observed in reactions showing a shift of the excitation functions, to determine whether there is a correlation between the yields and the increase in the energy appearing as gamma rays. In addition, it was hoped that the energy spectra and angular distribution of the gamma rays might furnish clues to the mechanism of gamma de-excitation.

Tellurium and barium targets were bombarded with carbon and helium nuclei respectively to form cerium compound nuclei. This pair of targets was chosen because of the excitation shifts observed by Choppin and the recoil angular distribution work then in progress by Morton on tellurium. Because of the relatively thick targets required by the experiment, natural materials were used.

The Coulomb barrier for carbon on tellurium prevented bombardments leading to the same excitation energy in both targets. This end was achieved by using vanadium and cobalt for a second pair. The excitation shift for vanadium was known from Karamyan's work;[2] in addition, both elements are monoisotopic.

Since the copper and cerium nuclei are spherical, several other nuclei were bombarded in order to observe the effects of nuclear deformation. Holmium and tantalum were bombarded with alpha particles; holmium was also bombarded with carbon ions.

II. REACTION THEORY FOR HIGH ANGULAR MOMENTUM

A. Formation of High Angular Momentum States

For high angular momentum quantum numbers, a classical approximation may be used in calculating the distribution in angular momentum of the compound states formed in bombardment. The assumption may also be made that direct reactions corresponding to the absorption of only a part of the projectile are negligible (experimental evidence to the contrary will be discussed in Sec. IV). The sum of the Coulomb and centrifugal barriers for the projectile is:

$$E_{c.m.} = \frac{Z_T Z_P e^2}{R_T + R_P} + \frac{\ell(\ell+1)}{2\mu(R_T+R_P)^2} \quad \ell(\ell+1) \sim \ell^2 . \tag{1}$$

From which we obtain

$$\ell_{max} = \left[2\mu(R_T+R_P)^2 \, (E_{c.m.} - B)/\hbar^2\right]^{1/2}, \tag{2}$$

where R_T and R_P are the radii of the target and projectile, B is the Coulomb barrier, and μ is the reduced mass of the system. In this approximation, we have $\bar{\ell} = \ell_{max}/\sqrt{2}$, where $\bar{\ell}$ is the average and ℓ_{max} is the maximum angular momentum.

In a better approximation, Thomas[8] used Blatt and Weisskopf's square-well model[9] with $R = 1.5\ A^{1/3}$, and found very good agreement with the classical model at energies above the Coulomb barrier. He also did a calculation on the basis of a diffuse-well model, assuming a parabolic well top and calculating the transmission coefficients after Hill and Wheeler.[10] The transmission for the ℓth partial wave is

$$T_\ell = 1/\left[1 + \exp \frac{2\pi\,(B - E_{c.m.})}{\hbar\omega}\right]^{-1}$$

where ω is the vibrational frequency of the harmonic oscillator having a potential-energy function given by the negative of the function describing the barrier. The partial-wave cross section is

$$\sigma_\ell = \pi \lambda^2 (2\ell+1) T_\ell , \tag{3}$$

and the average value of ℓ is

$$\frac{\Sigma_\ell \ell \sigma_\ell}{\Sigma_\ell \sigma_\ell} .$$

The formation of higher and higher angular-momentum states cannot go on indefinitely. At a sufficiently high bombarding energy, a projectile of any given mass will not be bound when its rotational kinetic energy exceeds its binding energy. This case is discussed by Knox, Quinton, and Anderson.[11] At energies attainable by present heavy-ion accelerators, such effects are confined to the light elements.

Since the classical approximation was found by Thomas, one is presented with a choice in describing the compound state formed; it may be regarded as a rotating drop with energy separated into thermal and rotational parts, or one may use the statistical model in its spin-dependent formulations. These models are discussed below. The collective model, with its features determined by pairing energies and residual interactions, may not be so valid. At spin values over a critical J_c, the energy gap is washed out and rotational bands in the usual sense vanish.

Pik-Pichak evaluated J_c, by comparing the energy of rotation with the change of energy connected with the formation of nucleon pairs.[12] If Δ is the magnitude of the gap, G the level density at the Fermi surface, and $\Im$ the moment of inertia, we have

$$\frac{\hbar^2 J_c^2}{2\Im} \simeq \frac{\Delta^2 G}{4} . \qquad (4)$$

Then J_c is approximately 7 for A ~50, and 15 for A ~250. These results apply independently of thermal excitation which also tends to wash out the gap.

A more sophisticated approach by Mottelson and Valatin introduced a Coriolis term to the nuclear wave functions.[13] Their results are comparable, giving $J_c \sim 12$ for A ~ 180, and $J_c \sim 18$ for A ~ 238. Above these values of the spin, the density of states should be given by the statistics of a Fermi Gas. The momentum of inertia should be that of a rigid body, representing a sharing of the rotational energy by all the particles rather than by a surface wave.

B. The Statistical Model For High Angular Momentum

In the statistical model for nuclear reactions, it is assumed that the compound nucleus has had time to reach a thermodynamic equilibrium before it decays by emission of particles or photons. The available excitation energy is then distributed over all degrees of freedom of the system, according to Fermi statistics. In considering states of high angular momentum, one must use care in applying commonly used approximations valid for low angular momentum.

By analogy with statistical mechanics, Weisskopf defined the entropy of the nucleus:[14]

$$S(U) = \log \omega(U), \tag{5}$$

where U is the energy above the ground state, and ω the density of levels at energy U. The temperature T is then

$$T(U) = dU/dS. \tag{6}$$

Assuming the entropy to be the same before and after particle emission, he derived the well-known equation for the spectrum of evaporated particles:

$$W(\epsilon) = \text{constant} \cdot \epsilon\, \sigma(U,\epsilon) \exp\,[-\epsilon/T(U)], \tag{7}$$

where ϵ is the energy of the emitted particle, and σ is a barrier penetrability approximately equal to unity for neutrons above the threshold.

A more rigorous treatment was carried out by Bethe involving the free energy of the nucleus.[15] His equation for the level density provided an exact thermodynamic definition of the temperature t, and his method is summarized by Le Couteur[16] as follows. The free energy F at a temperature given by $1/\beta$ appears in the Laplace transform of the level density

$$\exp(-\beta F) = \int_0^\infty \omega(A,U') \exp(-\beta U')\, dU' . \tag{8}$$

The integration is over all states; summation is used where the states are discrete. Inversion of the transform gives

$$\omega(A,U)= \frac{1}{2\pi} \int_{\gamma-i\infty}^{\gamma+i\infty} d\beta \exp \beta(U-F) . \tag{9}$$

Integration is carried out by the method of steepest descents from the saddle point, at the value of $\beta(U)$ defined by

$$U = d(\beta F)/d\beta, \tag{10}$$

and gives Bethe's equation for the level density

$$\omega(A,U) = e^{S}/(2\pi dU/d\beta)^{1/2} \tag{11}$$

The relation between the experimental temperature T and the statistical temperature t is found by taking the logarithmic derivative:

$$\frac{1}{T} = \frac{d}{dU} \log \omega = \frac{1}{t} - \frac{1}{2} \frac{d}{dU} \left(\log t^2 \frac{dU}{dt}\right) . \tag{12}$$

Le Couteur points out that there is no restriction implied on the functional form of ω or T, save that ω be positive. The relation must come from a specific model; for example, the Fermi gas model gives $U \propto t^2$, while a continuous fluid leads to $U \propto t^4$.

An equation of state was derived by Lang and Le Couteur[17] as

$$U = \frac{1}{6} \pi^2 g t^2 - t, \tag{13}$$

where g is the density of states at the Fermi level. This is valid so long as we have $t \geq g^{-1}$. The level density for all spin values combined is then

$$P(U,A)= \left(\frac{8}{3} \pi^5 g_1 g_2 g t^5\right)^{-1/2} \exp 2\left(\frac{1}{6} \pi^2 gU + 1/4\right)^{1/2}, \tag{14}$$

where g_1 and g_2 are the density of neutron and proton states at the Fermi level and $g = g_1 + g_2$. Lang and Le Couteur also derive a term in the equation of state to account for surface effects, giving

$$U = \frac{At^2}{f'} - t + \frac{1}{8} A^{2/3} t^{7/3}. \tag{15}$$

The authors have fit f' = 11 Mev to experimental data, while others have used 10 or 10.5 Mev. Using t calculated from Eq. (14), a simpler expression for the level density is

$$P(U,A) = \frac{1}{12}\left(\frac{6}{g}\right)^{1/4} (U+t)^{-5/4} \exp 2\left(\frac{\pi^2}{6} gU\right)^{1/2}. \tag{16}$$

The spin dependence of the level density is derived in terms of the magnetic quantum number M. Bethe gives the probability of n nucleons of spin j adding to give M as

$$p(M) = \left[2\pi nj(j+1)\right]^{-1/2} \exp\left[-3M^2/2nj(j+1)\right] \tag{17}$$

The density of levels of spin J is the difference between the density of states having M equal to its maximum value for J (i.e., M= J) and its maximum for the next higher J value (M= J+1). This may be approximated in terms of a Taylor series:

$$\omega(U,J) = P(U,A) \left.\frac{dp}{dM}\right|_{M= J+ 1/2}. \tag{18}$$

If the exponential in $\frac{dp}{dM}$ is approximated as unity after differentiating, the level density goes as (2J+1). This approximation is not good where J is more than a few units in magnitude, but has been found to give satisfactory agreement for slow-neutron resonances.[18]

Newton has derived a more exact expression for the level density P of the Fermi gas in terms of the magnetic quantum number:[19]

$$P(U,A,M) = \frac{1}{4\pi^2}\left[g_1 g_2 g^3 A^2 \left(\frac{\pi^2}{3} gt - 3/2\right) t^7\right]^{-1/2} \exp\left[\frac{\pi^2}{3} gt - 3/2 - \frac{M^2}{m^2 gt}\right]. \tag{19}$$

Here $\overline{m^2}$ is the mean-square value of the magnetic quantum number for individual nucleons. Newton shows that

$$\overline{m^2} g \approx c, \tag{20}$$

where $c\hbar^2$ is equivalent to the moment of inertia.

Lang and Le Couteur arrive at the J dependence in a slightly different way. If we assume that all the levels result from thermal excitation, the angular momentum reduces the level density by tying up some of the excitation in rotational energy. The thermal energy is $(U - M^2/2c)$, where $c\hbar^2$ is the moment of inertia. When we have $P(U,A) \propto \exp(2U/T)$ and $U \propto T^2$, the density of states with z-component of angular momentum M is

$$P(U,A,M) = P(U,A,0) \exp(-M^2/2cT) . \tag{21}$$

The binomial theorem is used in evaluating $T(U-M^2/2c)$. We take

$$\begin{aligned} \omega(U,A,J) &= P(U,A,M= J) - P(U,A,M = J+1) \\ &= D_0^{-1}(U,A)\ (2J+1)\ \exp[-\ (J+\ 1/2)^2\ /2cT] \end{aligned} \tag{22}$$

where

$$D_0^{-1} = \pi^{-1/2}(2cT)^{-3/2}P(U,A),$$

assuming $2cT \geq 1$. (23)

Here the difference has likewise been evaluated by use of the Taylor series, but the exponential has not been taken as unity. The average value of J is about $(2cT)^{1/2}$. If $c\hbar^2$ is taken as the rigid-body moment of inertia, this expression reduces to that derived for a Fermi gas.

While the nucleus may behave like a Fermi gas at a sufficiently high excitation, the effects of nuclear shells and the energy gap are quite strong at lower energies. A number of treatments have incorporated these features into the statistics. Bloch included exchange effects and took a summation over states rather than an integration.[20] The exchange

forces reduce the density of states from the Fermi gas values, while the summation procedures act in the opposite direction. Rosenzweig[21] and Ross[22] have used shell-model energies in calculations of the level densities.

Cameron adapted Newton's work by using second differences of atomic masses to derive the density of states at the Fermi energy, and compensated for odd-even effects by varying the ground-state energy.[18] Ericson points out, however, that this procedure is not accurate.[23] Cameron must use a moment of inertia two orders of magnitude above the rigid-body value in order to fit neutron resonance data. It may also be added that his use of the $\omega(J) \propto 2J+1$ approximation is not valid for J values above the very lowest.

The level densities in the presence of the energy gap were evaluated by Ericson.[24] He found the gap sufficient to account for observed odd-even differences in the level densities. A similar calculation has been made by Le Couteur and Lang.[25] Both calculations indicate that the effect of the gap is important for low excitations, but that the level density approaches the Fermi gas value at sufficiently high excitation.

Although the exponential dependence of the level density on $J(J+1)$ or $(J+1/2)^2$ is accurate over a wide range, it breaks down where the statistical assumptions are not fulfilled. Specifically, there must be a maximum spin corresponding to complete alignment of the single-particle j values, while the exponential law gives finite level densities for all spin values. Ericson points out that up to values of $J \sim cT = \mathcal{I}T/\hbar^2$ the exponential law should be good;[26] at higher J values the level density should fall below the exponential and go to zero.

A calculation of level densities in the very high spin region was attempted by the author and J. O. Rasmussen. The independent-particle model was assumed, and nucleons were assigned to spherical shell-model orbitals[27] by a Monte Carlo procedure on an IBM 704 computer. Each time the nucleons were assigned to levels, the possible combinations of individual vectors were added in all allowed ways and totaled for each value of the resulting J. This calculation was carried out for Ne^{20} and found to be in agreement with the direct counting procedure of Critchfield and Oleksa.[28] The features expected above were displayed in the J distribution, For heavier nuclei, the larger number of single-particle states

resulted in prohibitive running times on the computer. It is expected that additional calculations will be made in the future if the program can be made to run faster.

C. Energies of a Rotating Charged Drop

Since it is feasible to separate the nuclear excitation into rotational and thermal energies,[17,12] it may be valuable to inquire into the amount of energy that may be held in rotation. The rotational energy of a rigid sphere is $(\hbar^2/2\Im)J(J+1)$, where the moment of inertia $\Im$ is given by $(2/5)AmR^2$, with M the nucleon mass and R the nuclear radius. Rotation of the nucleus, however, causes it to deform, a process which is aided by the Coulomb repulsion and opposed by the surface tension of the drop.

The equilibrium configuration of the rotating drop does not have cylindrical symmetry except below a critical value of the rotational energy. Although the end result of adding more and more rotational energy to the drop is fission along an approximately prolate shape, small rotations cause an oblate deformation. Therefore intermediate rotations do not have axial symmetry.

The nonsymmetric liquid-drop energies have been calculated analytically by Pik-Pichak,[29] using the condition that the derivatives of the total energy with respect to the deformation parameters be zero. His parameters permitted the consideration of shapes different from spheroids such as dumbbells. He carried his calculation to second order in the rotational energy and estimated its accuracy to be within 15% for $x = E_{coul}/2E_{surf} > 0.7$, where $x \cong Z^2/51A$.

For the nuclei of interest in this experiment, $x < 0.7$ and a more accurate calculation is necessary. Hiskes has calculated the energies of a cylindrically symmetric drop at large deformations.[30] For ellipsoids (the loci of whose intersections with all planes are ellipses) it is possible to calculate the energies in closed form. This has been done quite recently for figures with cylindrical symmetry by Beringer and Knox.[31]

It was proposed by J. A. Wheeler to calculate the energies for the nonsymmetric case by the addition of rotational energies and consideration of nonsymmetric shapes to the equations of Swiatecki.[32] If a, b, and c are the three semi-axes of the ellipsoid and R is the radius of a sphere of the same volume, we may describe the deformations in terms of parameters β and γ:

$$a = R \exp[\beta \cos(\gamma - 2\pi/3)],$$
$$b = R \exp[\beta \cos(\gamma + 2\pi/3)],$$
$$c = R \exp[\beta \cos\gamma].$$

Rotation of the ellipsoid is taken to be about the C axis. The type of deformation and its direction are given by γ, while the extent of the deformation is measured by β. For $\gamma=0$ and π, the shapes are prolate and oblate, respectively, with symmetry about the A axis. Similarly for $\gamma = \frac{2\pi}{3}$ and $\frac{5\pi}{3}$ we have prolate and oblate spheroids symmetric about the C axis. Because of such symmetries, we need consider only values of γ between $2\pi/3$ (prolate) and π (oblate).

The Coulomb energy of an ellipsoid is given by

$$E_c = \frac{8}{15}\pi^2 \rho_e^2 a^2 b^2 c^2 \int_0^\infty \frac{d\lambda}{[(a^2+\lambda)(b^2+\lambda)(c^2+\lambda)]^{1/2}}, \qquad (24)$$

where ρ_e is the electric charge density. This reduces to

$$E_c = \frac{3}{5} Q^2 \frac{1}{(a^2+c^2)} 1/2 \int_0^\phi \frac{dz}{(1-k^2\cos^2 z)^{1/2}} \qquad (25)$$

where $k = \left(\frac{a^2-b^2}{a^2-c^2}\right)^{1/2}$ and $\phi = \arcsin\left(\frac{a^2-c^2}{a^2}\right)^{1/2}$.

Here Q is the total charge, written as

$$Q = \frac{4\pi}{3}\rho_e abc$$
$$E_c = \frac{3}{5} Q^2 \frac{1}{(a^2-c^2)} 1/2 \; F(k,\phi), \qquad (26)$$

where $F(k,\phi)$ is the elliptic integral of the first kind.

The surface energy of a sphere may be given by

$$E_s^{\circ} = 4\pi R^2 \sigma, \tag{27}$$

where σ is the surface tension. For the ellipsoid we have[33]

$$E_s/E_s^{\circ} = \frac{ab}{2R^2} \left\{ (1-\kappa^2\alpha^2)^{1/2} (1-\alpha^2)^{1/2} + (1/\alpha - \alpha)F(\kappa, \arcsin \alpha) + \alpha E(\kappa, \arcsin \alpha) \right\}, \tag{28}$$

where $\alpha^2 = \frac{a^2-c^2}{a^2}$, and $\kappa^2 = \frac{a^2(b^2-c^2)}{b^2(a^2-c^2)}$.

Again, F is the elliptic integral of the first kind, and E is the elliptic integral of the second kind, defined by

$$E(k,\phi) = \int_0^{\phi} \sqrt{1-k^2\sin^2 z}\, dz.$$

The moment of inertia of an ellipsoid about the C axis is given in terms of its semi-axes perpendicular to C as

$$\Im = (1/5) M R^2 (a^2 + b^2). \tag{29}$$

Then the rotational energy is

$$E_{rot} = \frac{5\hbar^2 I (I+1)}{2R^2(a^2+b^2)}, \tag{30}$$

where I is the rotational quantum number. This may be separated into factors dependent and independent of the deformation:

$$E_{rot} = (E_s^{\circ} \lambda^2) \frac{1}{R^2(a^2+b^2)} = (E_s^{\circ} \lambda^2) B_{rot}. \tag{31}$$

The total change in the energy due to the deformation and the rotation is

$$\frac{\Delta E}{E_s^{\circ}} = \left(\frac{E_s}{E_s^{\circ}} - 1\right) + \frac{E_c - E_c^{\circ}}{E_s^{\circ}} + \frac{E_{rot}}{E_s^{\circ}} , \tag{32}$$

where E_c° is the Coulomb energy of the sphere. If we define $x = E_c^{\circ}/2E_s^{\circ}$, this reduces in terms of parameters B_s, B_c, and B_{rot} to

$$\frac{\Delta E}{E_s^{\circ}} = B_s - 1 + 2x \frac{E_c}{E_c^{\circ}} - 2x + \frac{E_{rot}}{E_s^{\circ}} , \tag{33}$$

$$= B_s - 1 + 2x(B_c - 1) + \lambda^2 B_{rot} . \tag{34}$$

Since the elliptic integrals are functions of two variables, published tabulations use far too coarse intervals of the arguments for the purposes of this calculation. Therefore, the calculations were programmed and run on an IBM 704. This program appears in Appendix A.

Use of the computer provides a fine enough mesh of β and γ values for any x and λ^2 (i.e., for a given nucleus and rotational quantum number) to enable the figure of equilibrium to be determined by inspection of a table. Such applications to this experiment will be discussed in Sec. IV. For the prolate and oblate limits, the results agree with those of Beringer and Knox.[31]

This simple and straightforward approach provides a description of the fission process, illustrated in Fig. 1, for a hypothetical nucleus with x = 0.9. The restriction to ellipsoids ignores the tendency of the nucleus to go to a dumbbell shape at high deformations. If the fission saddle point is reached before the deformation becomes too large ($\beta \sim 0.8$), the approximation should be good. For this reason, a high value of x is used in the illustration.

Figure 1(a) shows the nucleus with little rotation. Its equilibrium shape is very close to a sphere, but the most gradual ascent (dotted line) to the approximately prolate saddle shape starts in the oblate direction. In Fig. 1(b) the rotational energy is increased to about 3.5 Mev. The equilibrium shape is oblate, and the fission saddle point

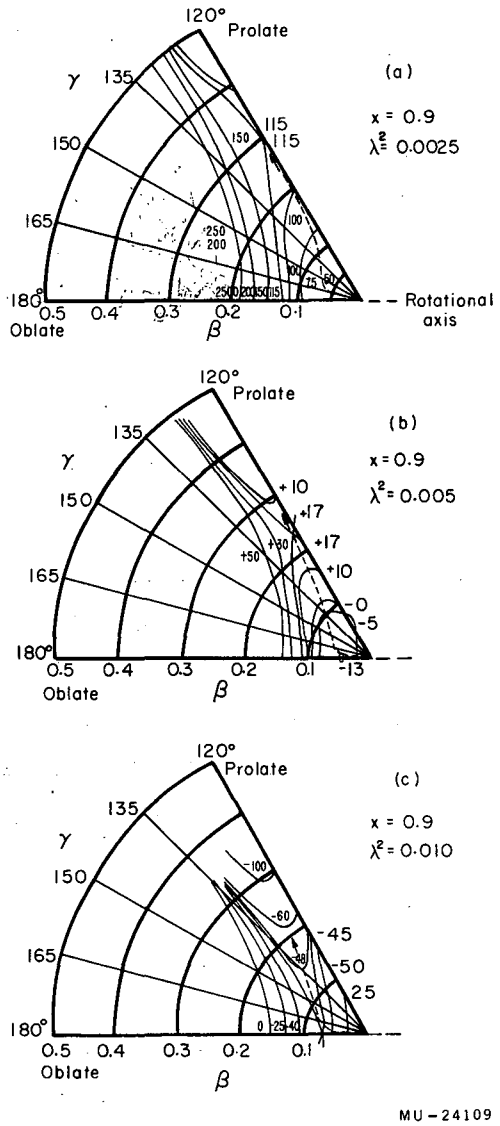

Fig. 1. Contour maps of the energy surface for a rotating nucleus. Energy contours are in units of $10^{-5}E_s^{\,o}$, where $E_s^{\,o}$ is the surface energy for the spherical shape, and $x = 0.9$. Values of $\lambda^2 \propto I^2$ are given on each map.

has moved lower, in terms of internal energy, and farther from the prolate axis. Because of the equivalence of the A and B axes, there is symmetry about $\gamma=\pi$, and the saddle point has a mirror image below the axis. With sufficient rotation, the two saddle points coalesce along the oblate axis and there is no stable shape. In Fig. 1(c) this has occurred. The steepest descent from the spherical shape, indicated by the dotted line, leads first in the oblate direction and then moves toward the prolate axis as the two parts of the nucleus start to separate. Such a path is not invariant under transformation of the coordinates; its significance is merely qualitative.

The effect of rotation on the fission barrier has been described in two ways. Halpern indicates that it should raise the barrier because of the energy that must go into rotating the nucleus.[34] Nonetheless, Pik-Pichak[29] and others[5,6] see the barrier lowered by the centrifugal force. Both may be correct. For extremely high values of x, the present calculation indicates that the energy of rotation more than compensates for the lowering of the barrier with respect to internal excitation. But for lower values of x, where the saddle-point shape is pinched in, this calculation cannot be used. The experimental results of Gilmore[5] at $x \sim 0.55$ indicate that the overall barrier is reduced by the rotation, despite the energy necessary to rotate the nucleus.

D. Particle Emission From High Angular-Momentum States

We may consider particle emission in terms of its angular distribution and the energy spectrum. One may derive expressions either on the assumption that well-defined levels of definite spin and parity are excited, or on the statistical assumption of random phases and cancellation of interference terms on the average.

The angular distribution of products from reactions passing through definite levels is treated quantum mechanically in the review of

Biedenharn and Rose.[35] A simpler treatment in the classical approximation has been made by Ericson.[36] Ericson considers transitions to individual states from an intermediate compound state where the statistical assumption is valid. This condition should be fulfilled when $I \ll 5A^{4/3}$, where I is the angular momentum brought in by the projectile. In the limit of zero spin for the final state, the emitted particle emerges perpendicular to the angular-momentum vector of the compound state in this classical approximation. If we average over all azimuthal directions we get

$$W(\theta) = \text{constant} \cdot 1/\sin\theta . \tag{35}$$

If the spin of the final state is $J_f \neq 0$, there is a decoupling of the compound-state angular momentum from that of the emitted particle. The distribution is approximately isotropic for $\theta < \theta_o = \sin^{-1} \frac{J_f}{I}$ and $\theta > \pi - \theta_o$. For $\theta_o < \theta < \pi - \theta_o$, the $1/\sin\theta$ distribution still holds.

Ericson and Strutinsky derive a similar result for the case in which the reaction goes to a statistical distribution of final states.[7] If we have $\hbar^2 I/2\Im T \leq 1$, the angular distribution is

$$W(\theta) \propto 1 + \frac{\alpha^2 \overline{I^2}\ \overline{\ell^2}}{2} \cos^2\theta ,$$

where $\overline{I^2}$ and $\overline{\ell^2}$ are averages of I^2 and ℓ^2 weighted by appropriate transmission factors and $\alpha = \hbar^2/2\Im T$. Combined with the average energy of the emitted particle 2T, this reduces to

$$W(\theta) \propto 1 + \frac{\hbar^2 R^2 I^2}{4\Im^2 T} \cos^2\theta , \tag{36}$$

where R is the interaction radius for the emitted particle.

Broeck has adapted Ericson's classical approach to the particle spectrum for the case of high angular momentum.[37] If $P(U,U_f,J)$ is the probability that an excited nucleus with energy U will make a transition from a state of spin J to a state of spin J_f and energy U_f,

and J is larger than any outgoing angular momentum that contributes appreciably to the transition, we have

$$\frac{dP}{dU_f} = \frac{8\pi^2 g}{h} \quad \frac{J}{\omega(J,U)} \int_0^{\infty} T_\ell(U_f) \left[\int_{J-\ell}^{J+\ell} \omega_f(J_f,U_f)\, d\, J_f \right] d\, \ell \,. \quad (37)$$

Here g is the statistical weight of the emitted particle, T is the barrier transmission coefficient for emission with orbital angular momentum ℓ, and ω_f is the density of final states. When ω_f is expanded in a Taylor series in terms of U_{fmax}, the maximum energy, and J, the average spin of the final nucleus, and if ϵ is the kinetic energy of the emitted particle ($\epsilon = U_{fmax} - U_f$), we have

$$\frac{dP}{dU_f} = \frac{16\pi^2 g}{h\, J} \quad \frac{\omega_f(J,U_{fmax})}{\omega(J,U)} \left(\exp \frac{-\epsilon}{T_f(J,U_{fmax})} \right)$$

$$x \quad \frac{1}{S_f(J,U_{fmax})} \quad x \int_0^{\infty} T_\ell(\epsilon) \sinh \left[\ell S_f(J,U_{fmax}) \right] d\ell \,. \quad (38)$$

where $\frac{1}{T_f} = \frac{\partial \log \omega_f}{\partial U_f}$, and $S_f \quad \frac{\partial \log \omega_f}{\partial J_f}$.

If we let $U = at^2$, we obtain from Eq. (22)

$$S_f = \frac{2}{2J+1} - \left(\frac{a}{U_{fmax}} \right)^{1/2} \quad \frac{\hbar^2}{2\Im} \quad (2J+1); \quad (39)$$

and

$$\frac{1}{T_f} = - \frac{3}{4U^{1/2}} + \left(\frac{a}{U_{fmax}} \right)^{1/2} \left[1 + \frac{\hbar^2}{4\Im} (2J+1) \right]. \quad (40)$$

The effect of high J is to increase the absolute value of S_f and therefore the contribution of particles emitted with high ℓ values. For a given total energy, the value of the temperature decreases as J increases and more energy is tied up in the rotation.

The effect of high angular momentum on nucleon emission has been studied semiclassically by Pik-Pichak,[12] who points out that at a sufficiently high rotational velocity, neutrons on the periphery may become unbound even in the absence of thermal excitation. At lower rotational velocities the neutron widths are increased for any given temperature over the nonrotating value. The average projection of the angular momentum carried by emitted neutrons increases with increasing angular momentum. The net result of the neutron cascade should be to leave the nucleus with insufficient internal excitation to evaporate another neutron, but with some energy still tied up in rotation. Hence there is a displacement upward of the excitation function. For a nucleus with $Z \sim 50$, bombarded with heavy ions to give 80-Mev excitation, this shift amounts to about 8 Mev.

E. Gamma Emission From High-Angular-Momentum States

The angular distribution of gamma rays emitted from high-angular-momentum states has been derived by Strutinsky.[38] If we assume a level density such as that given in Eq. (22), the probability of a nucleus emitting a quantum of angular momentum L is

$$\exp\left[-\hbar^2(\vec{J}-\vec{L})^2/2\mathcal{I}T\right] \sim \exp\left(-\hbar^2 JM/\mathcal{I}T\right), \tag{41}$$

where M is the projection of L on the axis of J, the spin vector of the nucleus. The probability of this photon making an angle θ with J is

$$W_J^L(\theta) = \sum_{M=-L}^{L} \left\{ \exp\left(-\hbar^2 JM/\mathcal{I}T\right) \left| Y_{LM}^{(\lambda)}(\theta) \right|^2 \right\}, \tag{42}$$

where $Y_{LM}^{(\lambda)}$ is a vector spherical harmonic. This distribution must be averaged over the azimuthal angles of J. If ϕ is the angle the photon makes with the direction of the beam, we have

$$\overline{\cos^2\theta} = (1/2)\overline{\sin^2\phi}.$$

After evaluation of the Y's and summing over M, we obtain

$$W_L(\phi) = 1 + k_L\left(\frac{\hbar^2 J}{\mathcal{I}T}\right)^2 \sin^2\phi, \tag{43}$$

where the coefficients for the different multipole orders are $k_1 = +1/8$, $k_2 = -3/8$, $k_3 = -81/64$. Dipole radiation is peaked at 90 deg to the beam, while quadrupole and octupole radiations have minima at 90 deg.

The energy spectrum of gamma rays from the capture of thermal neutrons has been calculated numerically by Strutinsky, Groshev, and Akimova.[39] A similar calculation has been published recently by Troubetzkoy.[40] Both calculations are good where the number of gamma rays is small, but Strutinsky and his associates also quote a simpler calculation by Nosov and Strutinsky (unpublished) that is valid where the fraction of excitation carried off by each photon is small. Such an approximation should apply to this experiment. The probability of emission of a gamma ray of energy E by a nucleus at an excitation U is given by

$$\omega_L(U,E)\, dE = E^K \rho\,(U-E)dE/N_L(U), \tag{44}$$

where $N_L(U)$ is a normalizing factor, $\rho(U-E)$ is the density of final states, and $K = 2L+1$. The normalizing factor is proportional to the probability of emission from excitation U over all allowed energies:

$$N_L(U) = \int_0^U E^K \rho\,(U-E)dE. \tag{45}$$

The average energy of the radiation emitted by the nucleus at excitation U is

$$\bar{E}_L\,(U) = \int_0^U E\,\omega_L\,(U,E)dE, \tag{46}$$

and the spectrum is given by

$$\nu(E)dE = dE \int_E^{U_0} \omega_L\,(U,E)\,\frac{dU}{\bar{E}_L(U)}\ , \tag{47}$$

where U_0 is the initial excitation energy of the nucleus. If we take $\rho(U) \propto \exp[2\sqrt{aU}]$ and $U = aT^2$, use of the binomial theorem for $T(U-E)$ leads to $\rho(U-E) \propto \exp\,[2\sqrt{aU}]\exp[-E/T(U)]$. The integral simplifies to yield

$$\bar{E}_L\,(U) \sim (K+1)\,T(U) = (2L+2)\,T(U). \tag{48}$$

The average number of gamma rays emitted is

$$\bar{\nu} = \int_0^{U_o} \frac{du}{\bar{E}_L(U)} , \tag{49}$$

which leads to

$$\bar{\nu} = \frac{1}{L+1} \; a^{1/2} \; U_o^{1/2} .$$

This has been derived, however, assuming that the transition probabilities are independent of J. We may add a J dependence as follows (let U'=U-E):

$$\rho(U,J) \propto (2J+1) \exp[2\sqrt{aU}] \exp\left[-\frac{J(J+1)}{2cT(U)}\right];$$

$$\rho(U',J-L) \propto [2(J-L)+1] \exp(2\sqrt{aU'}) \exp\left[\frac{(J-L)(J-L+1)}{2cT(U')}\right], \tag{52}$$

if we assume that the transition goes to J-L, which will hold for large J. Let $\hat{J} = (J-L)(J-L+1)$. Then we have

$$\bar{E}_L(U,J) = \frac{\int_0^U E^{2L+2}[2(J-L)+1] \exp[2(aU')^{1/2} - \hat{J}/2cT(U')]dE}{\int_0^U E^{2L+1}[2(J-L)+1] \exp[2(aU')^{1/2} - \hat{J}/2cT(U')]dE} . \tag{53}$$

Applying the binomial theorem for T(U-E) and cancelling factors not depending on E, we find

$$\bar{E}_L(U,J) = \frac{\int_0^U E^{2L+2} \exp[-E/T(U) - a^{1/2}\hat{J}/4cU^{3/2}]dE}{\int_0^U E^{2L+1} \exp[-E/T(U) - a^{1/2}\hat{J}/4cU^{3/2}]dE} ; \tag{54}$$

and

$$\bar{E}_L(U,J) \approx \frac{2L+2}{\frac{1}{T}\left(1+\frac{\hat{J}}{4cU}\right)} . \tag{55}$$

The value of J will decrease with the cascade; if all the gammas are of the same multipolarity,

$$J = \frac{J_o}{U_o} U. \tag{56}$$

Substituting in Eq. (55) and integrating over U, we obtain

$$\bar{\nu} \approx \frac{a^{1/2} U_o^{1/2}}{L+1} \left[1 + \frac{J_o^2}{12 c U_o} \right]. \tag{57}$$

Agreement of this prediction with the gamma yield found in the experiment should provide a measure of the role independent-particle effects play in the gamma emission. Deviations should be the result of collective effects in rotational or vibrational transitions.

III. EXPERIMENTAL PROCEDURES

A. The Counter Assembly

The first attempt to observe the direct production of gamma rays was carried out in the external beam of the Crocker Laboratory 60-inch cyclotron. The original plan was to place a 3-in. NaI (Tl) crystal near the target and ascertain the difference between the gamma spectra obtained with the target in and target out. A few trials made it evident that the background was much too high for so simple an arrangement. Any attempts to bring enough beam through the target to compete with the background resulted in piling up counts within the resolving time of the system and consequent distortion of the spectrum.

A fast-slow coincidence system was then assembled to reduce the background counts. In order to eliminate gamma rays produced when the beam was stopped, a system was needed that would provide a trigger only when a particle was removed from the beam by a reaction. Such a system had been used by Gooding at Minnesota,[41] consisting of several coincidence counters ahead of the target and an anticoincidence counter following it. An additional requirement was that the system should have a resolving and recovery time less than the RF cycle of the accelerators (14 nsec at the Heavy Ion Linear Accelerator (Hilac) and 83 nsec at the cyclotron), because whether an accelerator is pulsed or not, the particles emerge at a definite phase with respect to the RF and appear very sharply bunched at intervals equal to the RF cycle. In this experiment, it was necessary to run at beam rates low enough to minimize the chance of two particles appearing in the same RF cycle, because then there was no possibility of resolving them.

The system employed consisted of two thin fast counters and the target, through which the beam passed, and a thick plastic stopping scintillator, as shown in Figs. 2 and 3. These parts were assembled in a rigid aluminum chamber 1/2-in. thick with an inside passage 2-in. square in cross section. The third (stopping) scintillator was arranged on a sliding plate so that its position relative to the target could be varied over a 6-in. distance. The NaI (Tl) crystal was placed outside a 1/8-in. Bakelite window in this chamber and was positioned at a reproducible distance by a 2-in.-thick lead collimator. A conical hole tapering from 2-in. diameter

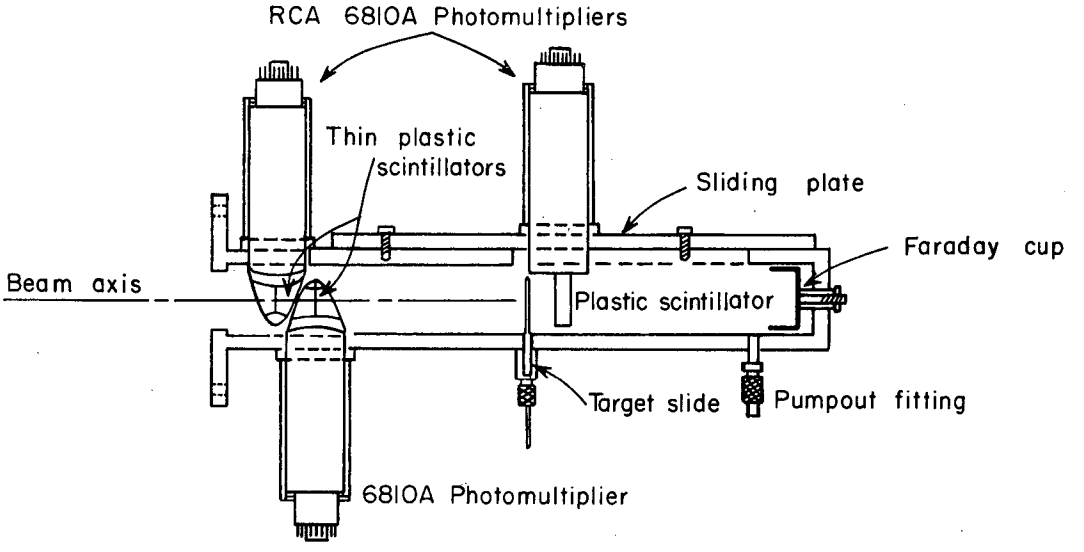

Fig. 2. Target and scintillator assembly. The stopping plastic scintillator may be moved relative to the target by means of the sliding plate.

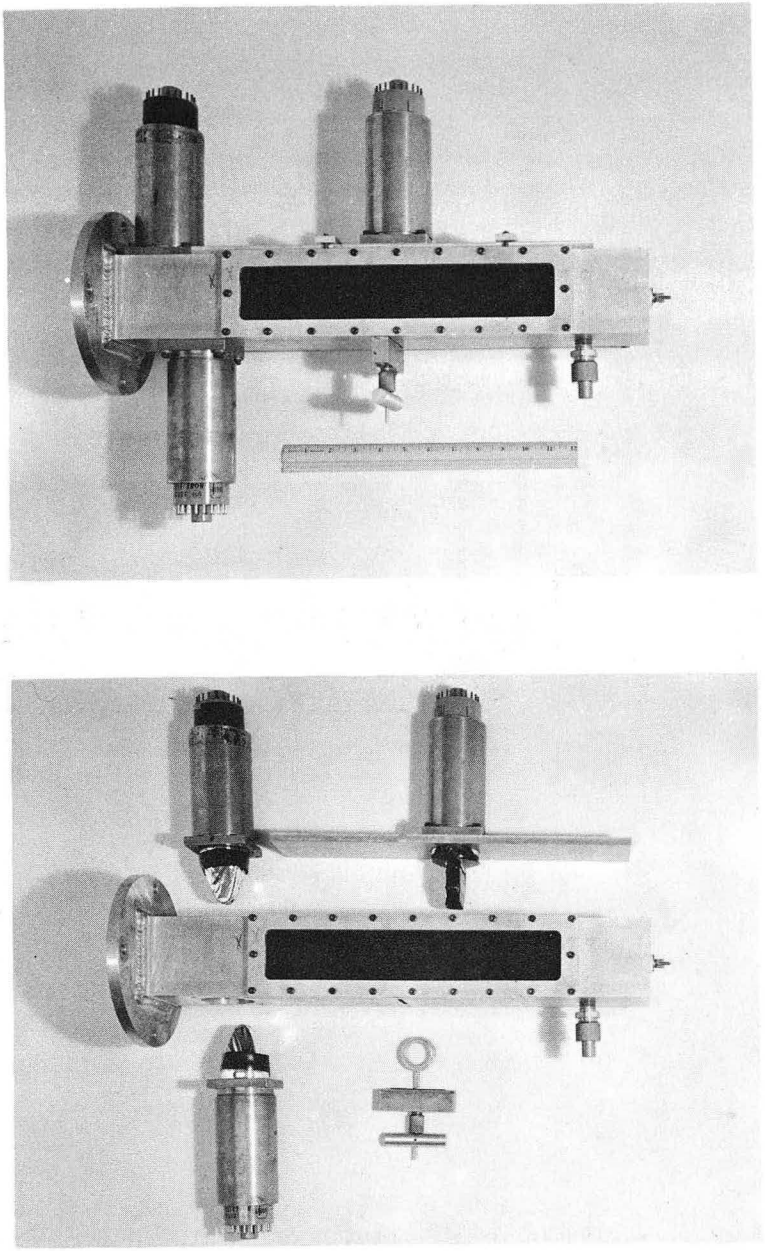

ZN-2806

Fig. 3. Target and scintillator assembly: assembled (top) and disassembled (bottom) views, showing attachment of reflector frames to the photomultipliers.

at the face of the crystal to 1 1/4-in. at the side near the target minimized scattering by the collimator. This collimator was necessary to reduce the large peak caused by photons scattered in the shield.

B. Electronic Circuits

The electronic circuit is shown in Fig. 4. Pulses from photomultipliers passed through continuously variable delay lines into two fast-coincidence circuits in parallel. One circuit served as a beam monitor; its output traveled through amplifiers, a discriminator, a Hewlett-Packard 10-Mc scaler and into standard 50-kc scalers. In the other fast-coincidence circuit, the fast pulse from the NaI detector was also required to be in coincidence. Its output, at a rate of a few pulses per second, was fed to a similar but transistorized unit where the pulse from the stopping counter was placed in anticoincidence. This procedure eliminated pulses coincident with a beam particle arriving in that counter. After passing through a transistorized discriminator and being suitably amplified, the output of this circuit served as a gate for the Penco 100-channel analyzer.

Meanwhile the slow signal from the NaI crystal (stretched to several microseconds) was amplified in a DD2 amplifier and sent on to the analyzer. This pulse was admitted by the analyzer gate only if a trigger signal was present, owing to the coincidence of a gamma pulse with pulses denoting the removal of a charged particle from the beam. If any gain shifts were noted, they were later compensated for in the computer analysis of the spectra.

Since the pulses from individual beam particles had to pass through the coincidence circuit, a high average repetition rate was needed to obtain a reasonable gamma counting rate. This last requirement posed problems with the photomultipliers. When an average rate of 10^5 8-volt pulses per sec at the cyclotron was attempted, the type 6810A phototubes became saturated, because the internal current was draining current from the divider string that supplied the dynode voltages. A power supply was obtained to provide voltages for the last five dynodes and the anode directly through cathode followers, and the saturation problem was overcome. Since the Hilac had only a 3% duty cycle, it was possible to run

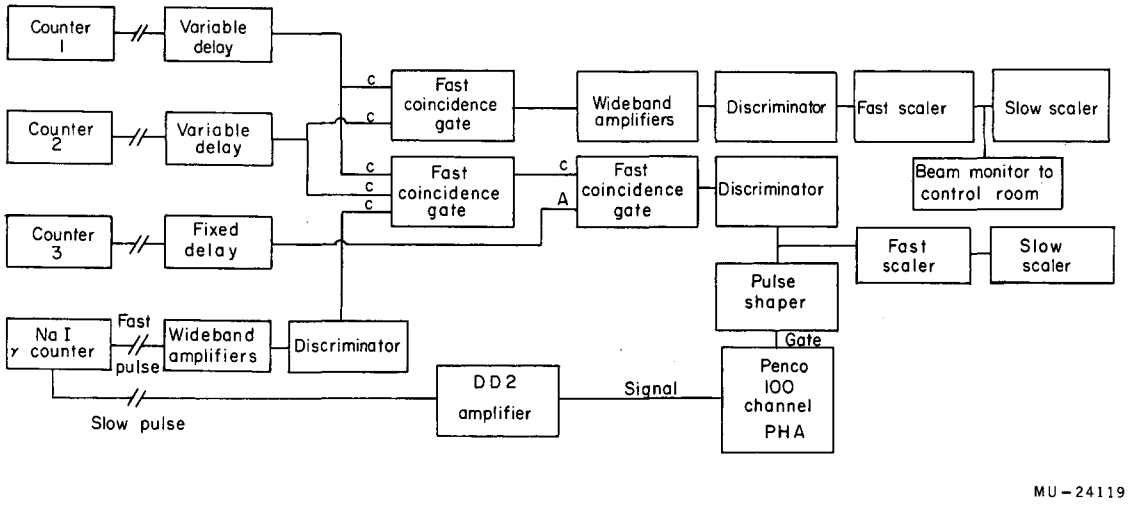

Fig. 4. Block diagram of the electronic circuit. The plastic scintillators are numbered in the order in which the beam passes through them.

at a peak rate of 5×10^5 per second with this arrangement. Apparently the capacitors in the divider string were able to keep the dynode voltages up during the 2-msec beam pulse.

The resolving time of the fast-coincidence gate was variable by means of clipping lines on the input pulses. Usually the best results were found with a resolving time of 8 nsec for the particle channels and 35 nsec for the gamma-ray channel.

Variation of the delays in the system was accomplished by means of two continuously adjustable LC-type delays with constant 125-ohm impedance and by fixed delays of various lengths of cable. In setting up the delays, a rather simple procedure was used. The fixed delay was set at a given value in the line from Counter 3. (The signal lines from Counters 1, 2, and 3, and the fast NaI signal will be denoted by Channels 1, 2, 3, and 4, respectively.) Then the output from the transistor coincidence gate was displayed on an oscilloscope with only Channel 1 in the tube unit turned on. The variable delay in Channel 1 was adjusted until the center of the anticoincidence interval was found. Then the anticoincidence signal was removed, Channels 1 and 2 both turned on, and the position of best coincidence found by adjusting the variable delay in Channel 2. This procedure was repeated for different values of the fixed delay, and the number of coincident gamma rays noted each time. The delays were considered optimized at the maximum number of gamma rays. A typical delay curve may be seen in Fig. 5.

Most of the electronic equipment used had been designed at this laboratory mainly for use at the Bevatron. It was readily adapted, with occasional modification, to this experiment. Duplicate equipment was provided at the two accelerators. The transistorized coincidence circuit and discriminator proved more reliable and stable than their tube counterparts. However, they were not able to accommodate quite as fast repetition rates and were used where speed was not so critical.

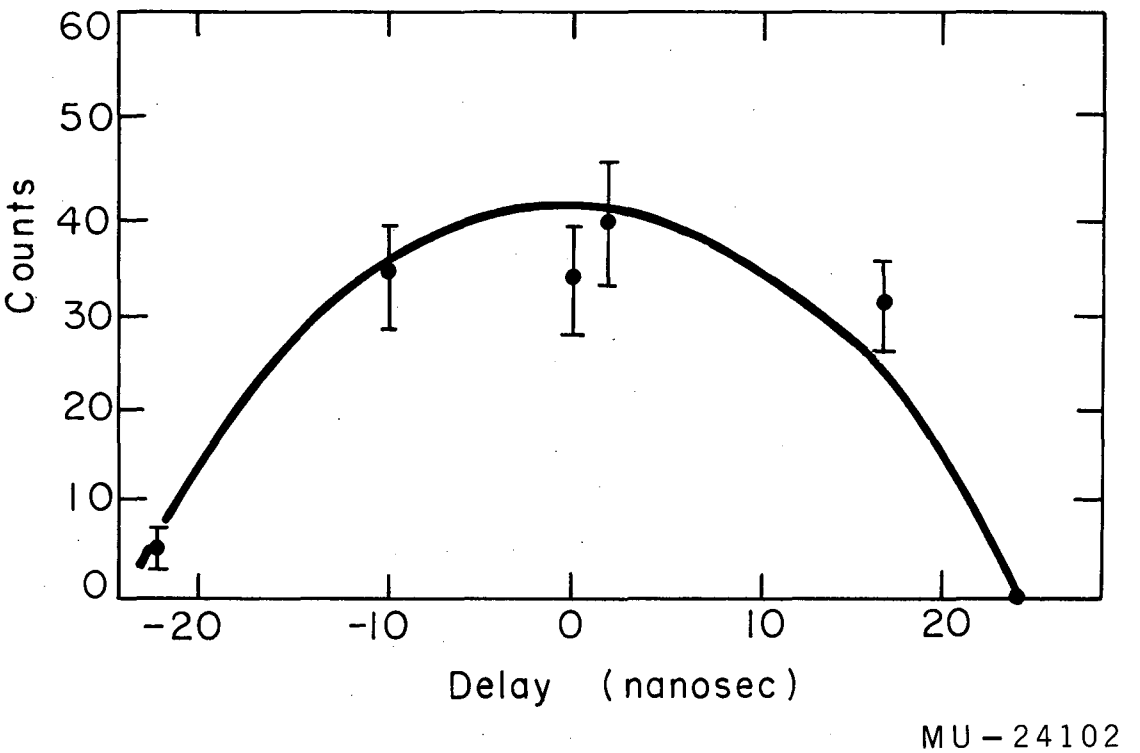

Fig. 5. Typical delay curve. The number of gamma ray counts is plotted as a function of the delay in Channel 3, with the other delays optimized with respect to that channel.

C. Development of Fast Counters

Developing a suitable fast-transmission counter for alpha particles and heavy ions presented some difficulties. Gas scintillation counters were tried first, as they had the advantages of linearity and adjustable thickness by variation of the gas pressure, and they had been successfully used in other experiments at the Hilac.[43,44] Counters used at the Hilac by other groups had consisted of a simple flow chamber through which argon passed from a tank and was vented to the air. White Tygon plastic paint, covered with evaporated quaterphenyl for a wavelength shifter, served to reflect the light into the photomultiplier. Several simple chambers 1 cm to 5 cm thick were constructed similarly and tried with argon, but none had a satisfactory resolution or pulse height for either alpha-particle or heavy-ion beams.

As xenon had been found to be a much better scintillating medium than argon,[45,46] a system was designed and built for this gas. Since xenon is rather expensive, it was necessary to recirculate it while still keeping the purity quite high. The system consisted of a manifold for filling a counting chamber with xenon and varying proportions of helium and a recirculating hot calcium gas purifier. It could be pumped out to a pressure of 10^{-5} mm of Hg or better. The valves used in the system all had Teflon seats; all gaskets were either Teflon or Kel-F O-rings, selected for low outgassing properties. While the counter was in operation, the manifold was isolated from the system and the gas circulated through the counting chamber and the purifier by convection through as short a tube as possible. Despite such precautions against contamination, the results were disappointing, with pulse heights only a few times the noise level.

All these difficulties were avoided by the use of thin plastic scintillators. As illustrated in Fig. 6, they were mounted in a parabolic framework over which was stretched a reflector of 6-μ aluminized Mylar, an arrangement which provided a large window for the beam. The plastic furnished excellent pulse height and a resolution of 10 to 15%, as estimated with an oscilloscope. A thickness of 85 μ was found best for the alpha particles, while a 25-μ thickness sufficed for carbon ions. Pulse heights of 10 v were easily obtained from the 14-state photomultipliers.

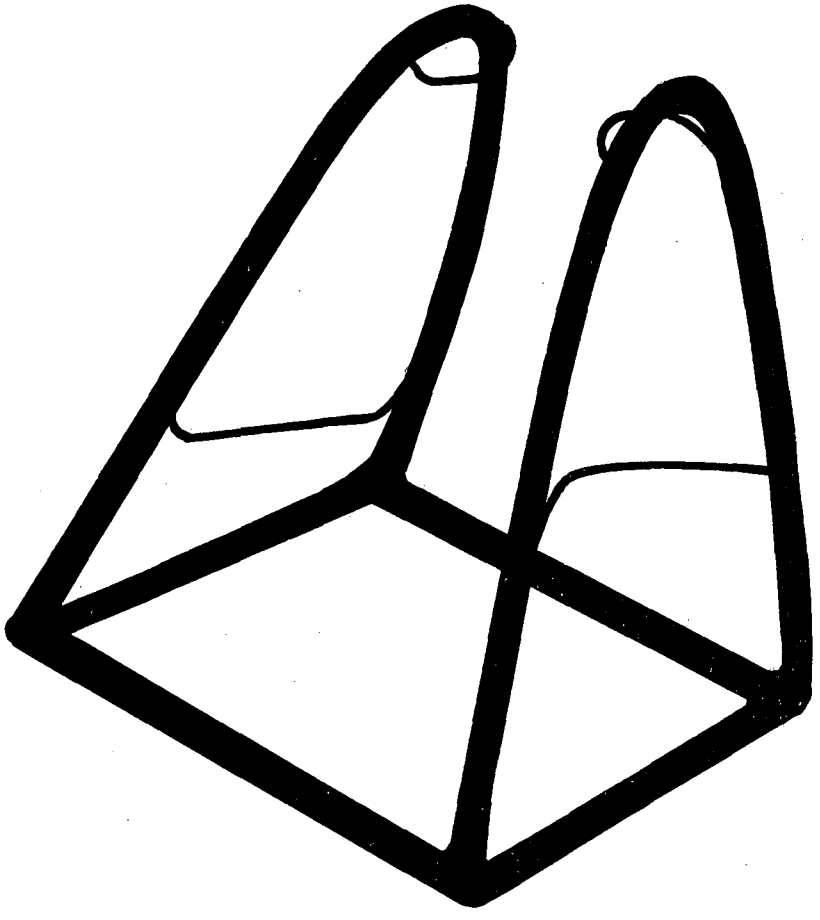

MU-24103

Fig. 6. Scintillator holder. The thin plastic is held by the inward-curving bars. In use an aluminized Mylar reflecting foil covers the frame, and the open square end rests against the face of the photomultiplier.

The width of the pulses at half-maximum amplitude was observed to be 15 nsec on a Tektronix 517A scope having a rise time of 7 nsec. The actual length of the pulses was therefore better than 10 nsec.

In order to reduce the fraction of the accelerator time used in setting up, only one collimator was used, and the target block with the collimator holder was bolted directly to the accelerator beam tube. In practice, it was found that the beam could be adjusted sufficiently with the strong focus and steering magnets to put it through the center of the target. The beam collimator was 1/8-in. in diameter while the targets were approximately 1 in. in diameter, located a little over a foot behind the collimator. After the target block was attached to the beam pipe, a 4-in.-thick lead shield containing the NaI counter was wheeled into position on a dolly.

D. Validity of the Procedures

In order to have confidence in the result of an experiment, especially when it depends on complicated techniques, one should be able to reproduce a known measurement. Although gamma-ray yields have been measured for many neutron-capture reactions,[47,48] few charged-particle reactions have been studied.[49-56] No suitable measurement has been done with alpha particles. One spectrum with heavy ions on tin has been published as a letter,[57] but the sketchiness of details inspires little confidence in the results. Attempts to duplicate a spectrum with protons did not appear feasible because the cyclotron accelerates H_2^+ ions, causing two protons to pass through counters and target simultaneously. If one proton should react, the other would still reach the third counter and cause anticoincidence. Scattering the beam from a foil into the apparatus would provide single protons, but the 10^5 times larger beam necessary would raise the background prohibitively.

For lack of a suitable reaction gamma spectrum, one from spontaneous fission of Cf^{252} was used as a check. In this case, a fast coincidence was required between a fission fragment in Counter 3 and a gamma ray in the NaI counter; otherwise the circuit was identical to that used in the bombardments.

The gamma-ray spectrum obtained after analysis of the observed pulse-height distribution is given in Fig. 7 with the spectrum of Smith, Fields, and Friedman[58] for comparison. The average gamma energy they obtained was 0.80 Mev; in this experiment the average was 0.78 Mev. Each spectrum peaks at 0.3 Mev and falls sharply at lower energies; the main difference between the two seems to be a smaller number of high energy photons in this work. This might be due to poor statistics in this region. However, the yield of compound nucleus gamma rays was found to be quite low in this energy region; hence the errors are relatively unimportant.

Another important check was necessary because of the comparison being made between runs performed at the cyclotron on the one hand and the Hilac on the other. Accordingly, a spectrum was run with 40-Mev alpha particles accelerated at the Hilac to check for systematic differences between runs at the two accelerators. The spectrum of the cobalt targets was used, being less subject to variation with bombarding energy than the other targets. Comparison of this spectrum with one from 48-Mev alphas at the cyclotron (Fig. 8) shows negligible difference; therefore we can compare spectra from two accelerators with confidence.

A rather obvious check is the reproducibility of the spectra. Two different gain settings were used with each target during a run: one to cover 0.04 to 1.04 Mev gamma rays and the other to cover the energy range 0.2 to 5.2 Mev. Agreement was required between the two spectra. The number of triggers to the analyzer for a fixed number of beam particles was never found to differ between the two by more than 6%. A better test was provided by the existence of duplicate spectra taken before the collimator was used on the gamma detector. The statistics were better on these runs because the crystal was closer to the target, thus providing a geometry four times higher. However, the existence of a very large scatter peak from 0.15 to 0.4 Mev led to the use of the collimator, cutting down the relative amount of the scatter peak by a factor of three. The shape of the spectrum above 0.5 Mev was unchanged, however.

Many of the spectra were also run with the collimator a second time, especially those run with the crystal at 45 deg to the beam, which had not been done without the collimator. Only two of the alpha-particle spectra did not have a duplicate taken at a different time, but these were run adjacent to spectra that did check, so there is little doubt of the reproducibility of any of them.

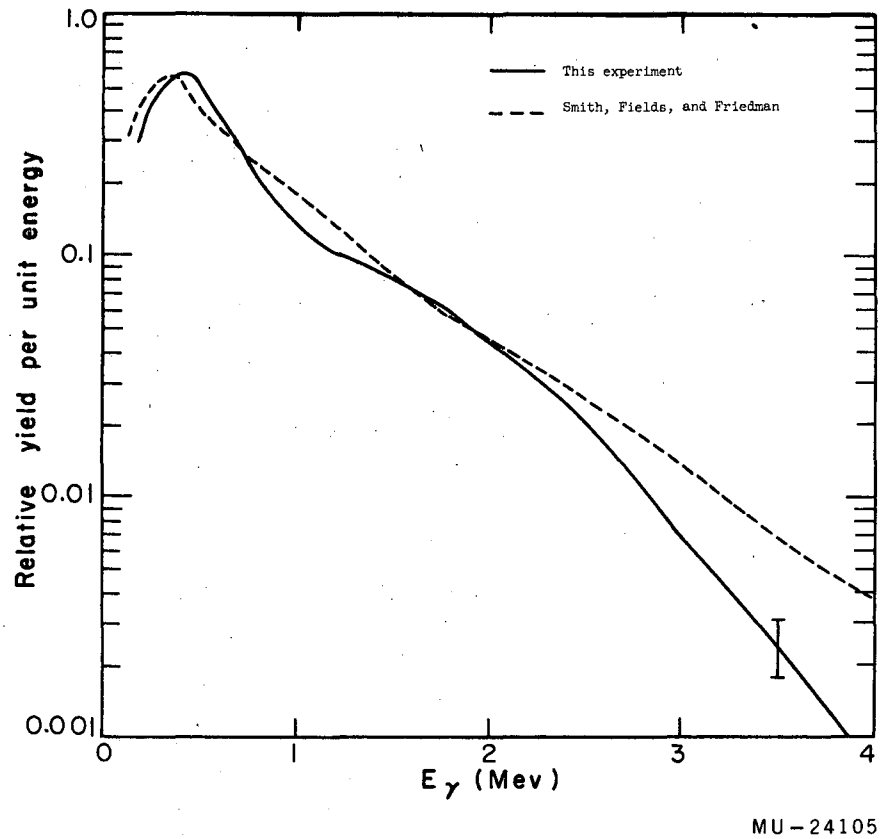

Fig. 7. Comparison of unfolded fission gamma-ray spectrum of Cf^{252} with that obtained by Smith, Fields, and Friedman (Ref. 58).

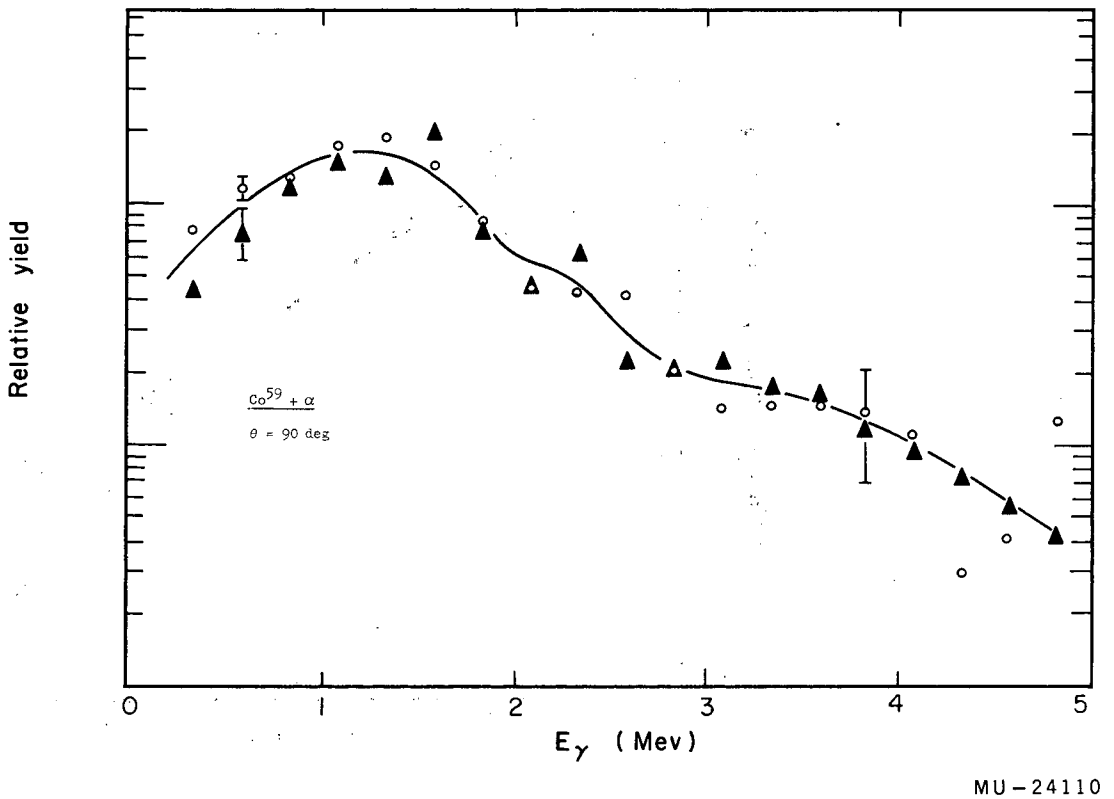

Fig. 8. Comparison of gamma spectra from alpha bombardments of cobalt at the two accelerators. Correction for detector response has been made. For $Co^{59} + \alpha$, θ = 90 deg, open circles show cyclotron points at $\overline{E}^*$ = 46 Mev; closed triangles show Hilac points at $\overline{E}^*$ = 39 Mev.

The runs with tellurium at the Hilac were the crucial ones for determining increases in gamma-ray production, and for this reason they were repeated several times. Agreement was found for different experimental conditions. On one occasion, one of the two counters preceding the target broke down and data were taken with its channel turned off. Another time, a thin stopping scintillator with a thickness equal to the carbon-ion range was used to discriminate better against charged reaction products. On a third occasion, the brass target holder was rotated so that its frame did not attenuate the low-energy gammas. In all three tests the results were in agreement within statistical errors. As a second target, holmium was bombarded with full-energy carbon ions, and a similar increase in the number of gamma rays over the yield with alphas resulted.

Differences due to fluctuation in the beam rate were checked. The runs without the gamma collimator were often done at a rate about 30% greater than later ones, yet the spectra were in agreement. Nevertheless, a momentary excursion of the beam to a higher rate occasionally occurred, particularly when the RF cavities of the accelerators were warming up. For this reason no data were taken until the beam had become stable. A monitor signal was sent to the control rooms of the accelerators and recorded, in case large fluctuations should occur. This was never seen to happen once the beam had settled down.

A more subtle form of beam fluctuation appeared in the form of bunching of the beam particles. At the cyclotron this was caused by the magnet-regulator power supply. At the Hilac, fluctuations seemed to arise in improper tuning of the Cockcroft-Walton injection system. A method was developed for detecting and evaluating the bunching before it reached significant levels. The output of the Hewlett-Packard scale of 100 on the monitor side was displayed on a Tektronix 513 or 515 oscilloscope. If the pulses were separated in time enough for the scope circuits to recover from each sweep before the next, all the traces were superimposed. However, if any pulses came in before recovery, several traces were seen at once. This was the criterion for bunching. When it was observed, the accelerator was returned until only a single trace became visible.

With the target removed, one would expect that all the beam that passed through the first two counters would enter the third. The amount scattered out by the first two counters, according to calculations done by

the method of Ashby,[59] should have been insignificant. Yet a fraction of the beam, usually about one part in 350 at the Hilac and one part in 200 at the cyclotron, did not reach the third counter. When the targets were inserted, this fraction approximately doubled. It was not likely that the target could scatter so much beam away from the third counter, which subtended an angle of about 150 deg.

The explanation for this effect seems to be in slit scattering at the collimator. Wilkins, working with a similar counting arrangment, recently found that about 0.5% of the heavy-ion beam was of lower energy after passing through the collimators in his equipment.[60] In addition, the check run with alpha particles at the Hilac was carried out with the usual collimator, which had a thickness just larger than the range of carbon ions. When alpha particles were run, a large fraction (one part in 14) did not cause anticoincidence. Since their range in the collimator material was longer than that of carbon ions, they were slowed but not stopped at the edges.

The existence of effects such as this one prevented measurement of the reaction cross section at the same time as the gamma multiplicity measurement. In this experiment, the only result was to make the number of full-energy beam particles counted appear too high by a fraction of a percent, an error that may safely be neglected.

The discrimination levels used were such that the stopping counter was not sensitive to neutrons evaporated from the target. The maximum energy of the knock-on proton (to which the scintillator is sensitive) is that of the neutron, while the average energy is less. In a test, pulses produced by 12-Mev protons were not sufficiently high to cause anticoincidence; therefore, there should have been no problem caused by protons at the energies of the evaporated neutrons.

The quality of signal at different points in the circuits is indicated in the typical discriminator curves of Fig. 9. Figure 9(a) shows the ratio of coincidences in Channels 1 and 2 to those remaining after anticoincidence with Channel 3, as a function of the setting of Discriminator 2. This ratio is just the inverse of the fraction of counts not appearing in Counter 3. Aside from the scatter of the points, the curve is quite flat over a wide range. Figure 9(b) shows the result of varying this same discriminator when the input to the coincidence unit

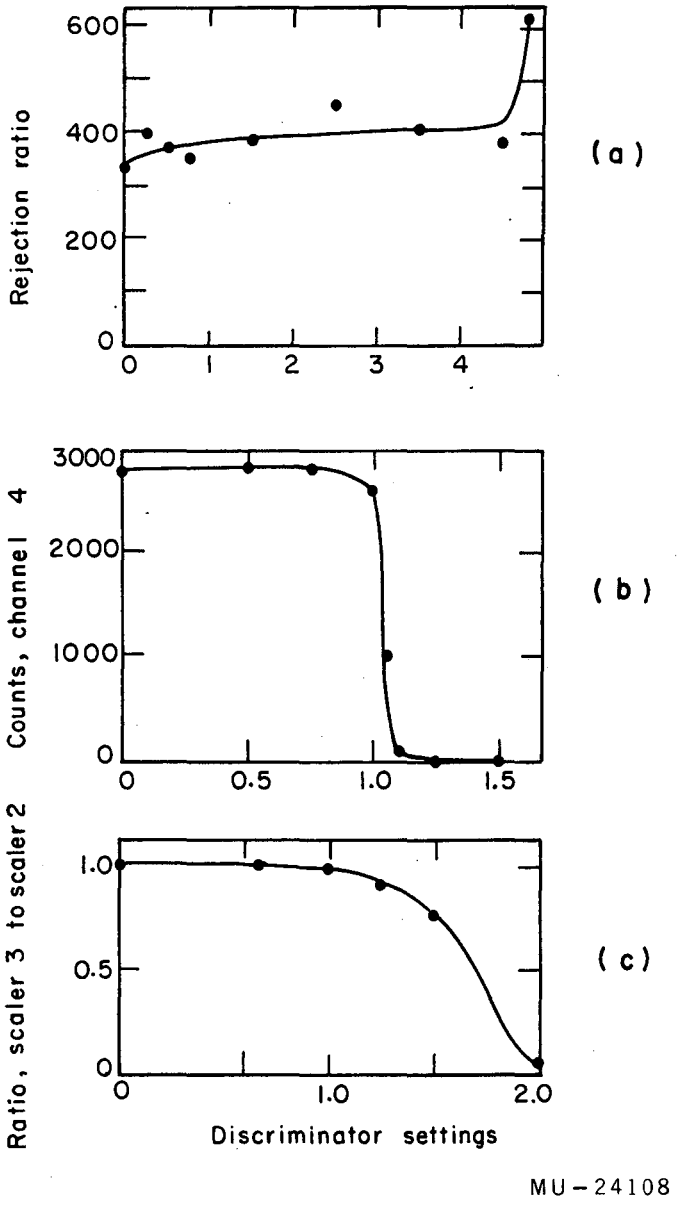

Fig. 9. Various count rates as a function of discriminator settings (see text for explanation).

was the NaI signal alone (Channels 1, 2, and 3 off). The count rate in the monitor scaler as Discriminator 3 was varied is given in Fig. 9(c). The coincidence unit had only Channels 1 and 2 turned on to serve as the monitor on this occasion.

In all these cases there was a very large plateau on which to set the discriminators. No errors were observed from pulse-height drifts in the coincidence circuits or the inputs to them.

E. Extraneous Gamma Rays

Despite the use of the anticoincidence in the third counter, there remained several sources of extraneous gamma rays: reactions in the beam stopping counter, accidental coincidences, and neutron activation of the NaI crystal. The first source was removed and the second cut down by alternating runs with a target in and a target out, and then taking the difference. If a beam particle underwent a reaction in the stopping counter after it had traveled far enough to create a pulse of the threshold size, no harm occurred, because the anticoincidence pulse would have kept the gate shut. But if it had a reaction in the early part of its range, the anticoincidence pulse would not have been of threshold size (assuming that no charged particle was emitted). Then there would appear to have been a reaction in the adjacent target. By subtracting the target-out counts, those from this source were eliminated. Background counts in coincidence with the low-energy particles mentioned above were also eliminated.

Since the target was held in a brass ring and the target-out runs were made without a dummy target holder, it was necessary to check that no beam particles were striking the target holder. No difference was observed between the target-out runs and the one with the empty target holder in position. As the tellurium target was vacuum-deposited on 6-μ Mylar, a similar piece of Mylar was run, again without any significant difference from the target-out spectra.

The case of neutrons produced in the target was different, however. They formed a background present only when the target was in the beam and could not be subtracted directly. There was no easy or accurate way to correct for the effects of the neutrons on the NaI crystal. Although the radiative capture cross sections are small, the inelastic scattering cross

sections are large enough to be significant.[61] The flux of neutrons through the counter could not be estimated too accurately because of the effect of the lead shielding in scattering neutrons into the counter.

There were some features of the situation which made the outlook more hopeful, however. While the neutron-energy spectrum may not be known for particular reactions, the inelastic cross section becomes fairly constant with energy above a neutron energy of about 1.5 Mev.[62-64] Slower neutrons were discriminated against by the fast time coincidence. At 1 Mev, a neutron required 20 nsec to reach the center of the NaI crystal. If it had an inelastic collision there, gamma rays produced were delayed long enough to reduce the probability of counting to less than one half. And equally important, in the heavy-ion bombardments where there were more neutrons produced, more gamma rays were observed also. Correction for neutron effects does not reduce the difference between the photon yields in the two cases. Hence we cannot ascribe any major differences that may appear between the carbon-ion and alpha-particle bombardments to the effects of neutrons. Additional proof may be seen below in the comparison of the 45- and 28-Mev alpha bombardments— there is no increase in the gamma spectra for 45 Mev, though the number of neutrons should average 40% more.

One may set an upper limit for the correction factor by considering the inelastic scattering cross sections for sodium and iodine. The actual number of counts produced should have been less than this cross section would predict, due to the elastic scattering of neutrons out of the crystal, to the escape of gamma rays without interaction in the crystal, and to the time discrimination of the coincidence. On the other hand, neutrons scattered into the crystal by the shielding were delayed and discriminated against because they took a longer path to the crystal. Using the cross sections for 2.5-Mev neutrons given by Howerton, 1.96 b for iodine and 0.47 b for sodium,[61] approximately 25% of the incident neutrons interact with the crystal.

A better correction can be obtained by examining the data for peaks known to be caused by effects of neutrons on the NaI crystal. Several authors have reported the spectra from neutrons on their NaI crystals: Van Loef and Lind with 640-kev neutrons,[63] Kiehn and Goodman with neutrons up to 1 Mev,[65] and Rothmann and Mandeville with 3.9-Mev neutrons.[66] All these spectra show peaks at 210, 410, and 630 kev, and

a much less intense continuum above 640 kev. Grace and associates report that this distribution cuts off at 2.5 Mev.[67] The gamma spectrum from inelastic neutrons on iodine at 3.2 Mev has been observed by Scherrer and his colleagues, showing peaks at 210, 400, and 610 kev.[68] Likewise, the spectrum from sodium has been shown by Morgan to consist mainly of a peak at 440 kev.[69]

Examination of the low-energy spectra obtained for both carbon and helium-ion bombardments uncovered no peaks that could be unambiguously attributed to the neutrons. An example is given in Fig. 10. The rather large backscatter peak in the vicinity of 200 kev, and statistical fluctuations elsewhere, apparently mask peaks from the inelastic events. Though the continuum from 0.6 to 2.5 Mev may contain half the gamma counts, the correction factor still should not be over 10%.

F. Preparation of Targets

Because of the very low beam rates, it was necessary to use fairly thick targets in order to provide a reasonable gamma count rate. The resulting energy spread of the beam in the target, especially at the Hilac, was quite large. However, this had the beneficial effect of averaging over the excitation functions for neutron emission. Differences at various excitation energies with respect to the peaks of the neutron-emission cross sections were thus minimized.

1. Barium Target

Natural barium was rolled to an approximate thickness of 125 μ and stored under kerosene. Oxidation of the targets in air was minimized by allowing a slight film of oil to remain on the target while it was being inserted into the target block. The kerosene evaporated under vacuum. The thickness of the target was 42.6 ± 1.0 mg/cm^2.

2. Holmium Target

Three unsupported foils of vacuum-deposited holmium were used in series in the alpha bombardments. Their combined weight was 40.57±0.06 mg/cm^2. One foil weighing 14.06±0.02 mg/cm^2 was used as the target with carbon ions.

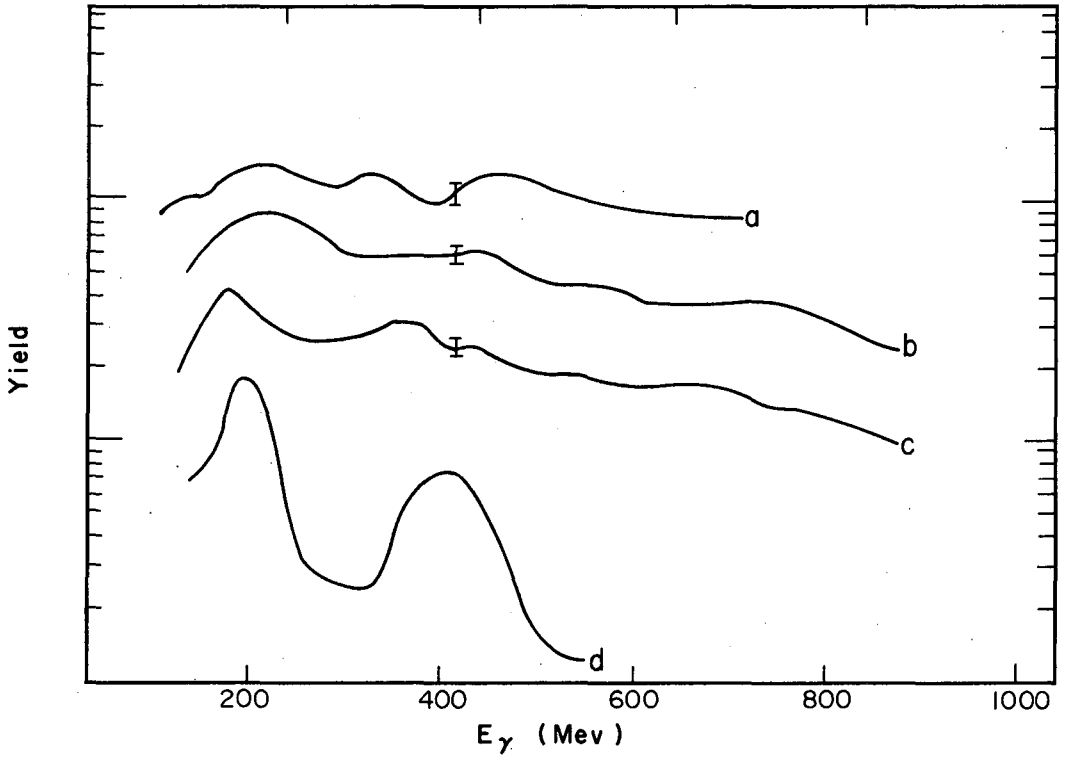

Fig. 10. Comparison of spectrum obtained with 617-kev neutrons on NaI (Ref. 65) with experimental gamma spectra. The experimental curves, not corrected for target-out counts, are: (a) α on Co, 90 deg; (b) α on Ba, 45 deg; (c) α on Ba, 90 deg; and (d) neutrons on NaI.

3. Tantalum Target

The tantalum target was rolled to a thickness of 66 ± 2.5 μ or 109 ± 4 mg/cm^2.

4. Cobalt Target

This target was rolled of iron-free cobalt to a weight of 46.6 ± 0.4 mg/cm^2.

5. Vanadium Target

The vanadium was rolled with some difficulty to a thickness of 25 μ. It weighed 14.3 ± 0.2 mg/cm^2.

6. Tellurium Target

Natural tellurium was vacuum-deposited on a backing of quarter-mil Mylar, from which it was not removed. The two targets used had net weights of 7.05 ± 0.07 mg/cm^2 and 6.99 ± 0.07 mg/cm^2.

G. Analysis of the Gamma Spectra

While a single NaI crystal used as a gamma detector has the advantage of high efficiency, its response to radiation is complicated by the presence of the Compton tail on the spectrum and other nonlinear effects. Discrete gamma lines can be resolved fairly quantitatively by inspection, but a continuous spectrum cannot. An efficiency correction cannot be applied separately to each interval of the spectrum because each contains Compton events from higher-energy rays.

A stripping technique is the simplest method for unfolding a complex spectrum. Pulses in the highest channel or group of channels in the analyzer spectrum are assumed to constitute a photopeak. Then the remainder of the pulse-height distribution associated with a photopeak of that area and energy is calculated. This distribution is subtracted from the first spectrum, and the process is repeated with the remainder until all the channels have been treated. A disadvantage of this method is that it accumulates errors and deposits them in the lowest-energy channels.

Accordingly, matrix methods have been developed to unfold gamma spectra.[70,71] A matrix is prepared that represents the response of the crystal to the gamma rays. One dimension provides the energy intervals and the other the pulse-height intervals. The rows denote the pulse-height distributions corresponding to the incident energies. This response matrix is inverted and multiplied by the observed pulse-height distribution to obtain the incident energy distribution. Details of this method are given in Appendix B. Hubbell and Scofield found it satisfactory in analyzing continuous brehmsstrahlung spectra.[71]

This method was followed in analyzing gamma spectra obtained in this experiment, with poor results. While the matrix method is exact if one has perfect accuracy in the response matrix and no statistical fluctuations in the experimental spectra, under experimental conditions it failed completely. Presumably because of the poor statistics at the high-energy and of the spectra and the presence of separate peaks there, large fluctuations between positive and negative values were seen in the unfolded spectrum.

Scofield, however, had similar troubles in unfolding spectra containing large peaks. He then developed an iterative method for using the response matrix to obtain the incident spectrum.[72] His procedure was applied to this experiment and found to work quite well (Appendix B).

Although the crystal response to gamma rays may be calculated theoretically, it was considered better to take a strictly empirical approach because of the effect of the shield. The pulse-height spectra of a number of standard sources were taken with the sources mounted in the target block, and with the crystal in the same lead shield used in the bombardments. Checks showed that the geometry of the runs was reproducible within 2 or 3%. The sources used and their gamma energies are listed in Table I.

In generating the response matrix, it was necessary to interpolate between the standard gamma energies to obtain the response at even intervals. This was done by resolving the standard spectra into several components and fitting the height, width (or area), and position of these components with functions of the gamma-energy. The components used were the photopeak, two escape peaks, Compton distribution,

Table I

Sources used in crystal calibration

Source	E_γ (Mev)
Am^{241}	0.060
Co^{57}	0.122
Na^{22}	0.51 (1.28 Mev not used)
Rb^{86}	1.08
Na^{24}	1.38
	2.75
Po - Be	4.45

scatter peak, and annihilation peak. The response matrix was generated by selecting a gamma energy in the center of an energy interval and then choosing a pulse-height interval. The response was then calculated for 10 sub-intervals over the pulse-height interval, and averaged. The result was one element of the response matrix. Calculation of the matrix and its use in analyzing the incident spectra were done on an IBM 704. The Fortran listing of the program appears in Appendix B.

The parameters used in calculating the response matrix are shown in Table II, along with their functional dependence on the gamma energy. The response was measured also when the crystal was set at 45 deg from the beam direction. The pulse-height spectra were essentially the same; the ratio of the geometries of 90 deg to 45 deg was 2.25 ± 0.02 on the basis of four sources.

Figure 11 compares the experimental spectrum from the Na^{24} source with the spectrum generated in the appropriate row of the response matrix. Figure 12 presents a complex spectrum before and after analysis by a 50-by-50 matrix. All the lines but those at 1.55 and 1.38 Mev are well resolved with fifty channels. The most evident error lies in the failure of the matrix to allow sufficiently for the first escape peak of Na^{24}. The remainder is about 5% of the unfolded photopeak. The accuracy of the matrix is fair— all the unfolded peaks seem to be about 10% high. With more complex functions fit to the curve parameters, this figure could undoubtedly be improved.

Since the statistics, at least at the high-energy end of the observed spectra, were very poor, several methods of smoothing were tried. Both a 50-by-50 and a 20-by-20 response matrix were used; because of statistical fluctuations, the unsmoothed 50-channel analysis gave spurious peaks, while a smoothed spectrum was handled adequately by 20 channels. The methods of smoothing included machine smoothing according to the formula

$$y_k' = \frac{1}{4} y_{k-1} + \frac{1}{2} y_k + \frac{1}{4} y_{k+1} \tag{58}$$

before and after unfolding of the spectra, and hand smoothing allowing for the better statistics at the low-energy end. All combinations of

Table II

Dependence of spectrum components on gamma energy E and pulse height x: E and x in Mev

Component	Condition		Height of component	Half-width
Photopeak height $P_1(E)$	$E< 0.65$		$P_1=4.59\times10^{-3}E^{-0.033}$	$0.0815\sqrt{E}$
	$E> 0.65$		$P_1=2.53\times10^{-3}E^{-1.46}$	(10% of E at E=0.66)
1st escape peak height $P_2(E)$	$E< 1.75$		$P_2=0$	Same as photopeak
	$E> 1.75$		$P_2=0.623P_1 \ln(E/1.75)$	
2nd escape peak height $P_3(E)$	$E< 1.75$		$P_3=0$	Same as photopeak
	$E> 1.75$		$P_3=0.247\ P_1 \ln(E/1.75)$	
Annihilation peak height A(E)	$E< 1.75$		$A=0$	
	$E> 1.75$		$A=1.2\ [P_2(E)+P_3(E)]$	
Position of Compton edge c(E)	$E< 0.5$		$c = 0.6E$	
	$0.5< E< 1.0$		$c = 0.9E-0.15$	
	$E> 1.0$		$c = E-0.25$	
Basic Compton height H(E)			$H = \frac{7.7\times10^{-3}(E+0.235)-1.806\times10^{-3}}{10(E+c)\ (E+0.235)}$	
Compton distribution height D(E,x)	$E< 1.75$	$x<c$	$D=H$	
		$c<x< E$	$D=H(E-x)/(E-c)$	
		$x> E$	$D=0$	

Table II (continued)

Dependence of spectrum components on gamma energy E and pulse height x: E and x in Mev

Component	Condition	Height of component	Half-width
Compton distribution height D(E,x)	$E > 1.75$; $1.22 < E-x$	$D=x$	
	$0.87 < E-x < 1.22$; $P_2 < H$	$D=x$	
	$P_2 > H$	$D=H+(P_2-H)(x-E+1.22)/0.35$	
	$0.51 < E-x < 0.87$	$D=P_2$	
	$E-c < E-x < 0.51$	$D=P_2+0.1H(x-E+0.51)/(c-E+0.51)$	
	$0 < E-x < E-c$	$D=(P_2+0.1H)(E-x)/(E-c)$	
	$E-x < 0$	$D=0$	

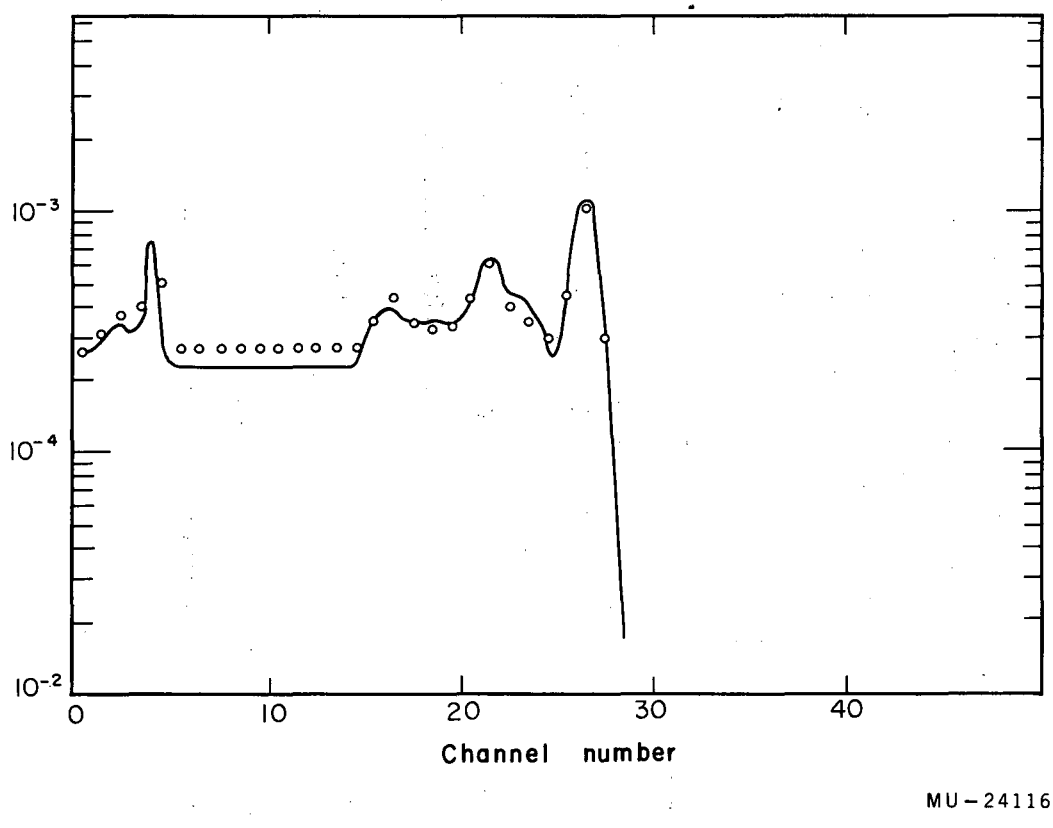

Fig. 11. Comparison of the experimental spectrum of the 2.75-Mev gamma ray of Na^{24} with the appropriate row of the 50-channel response matrix. The spectrum of the 1.38-Mev gamma ray in Na^{24} has been subtracted from the experimental spectrum shown. With $\overline{E}$ = 2.75 Mev, the open circles are Row 27, and the solid curve is the Na^{24} source.

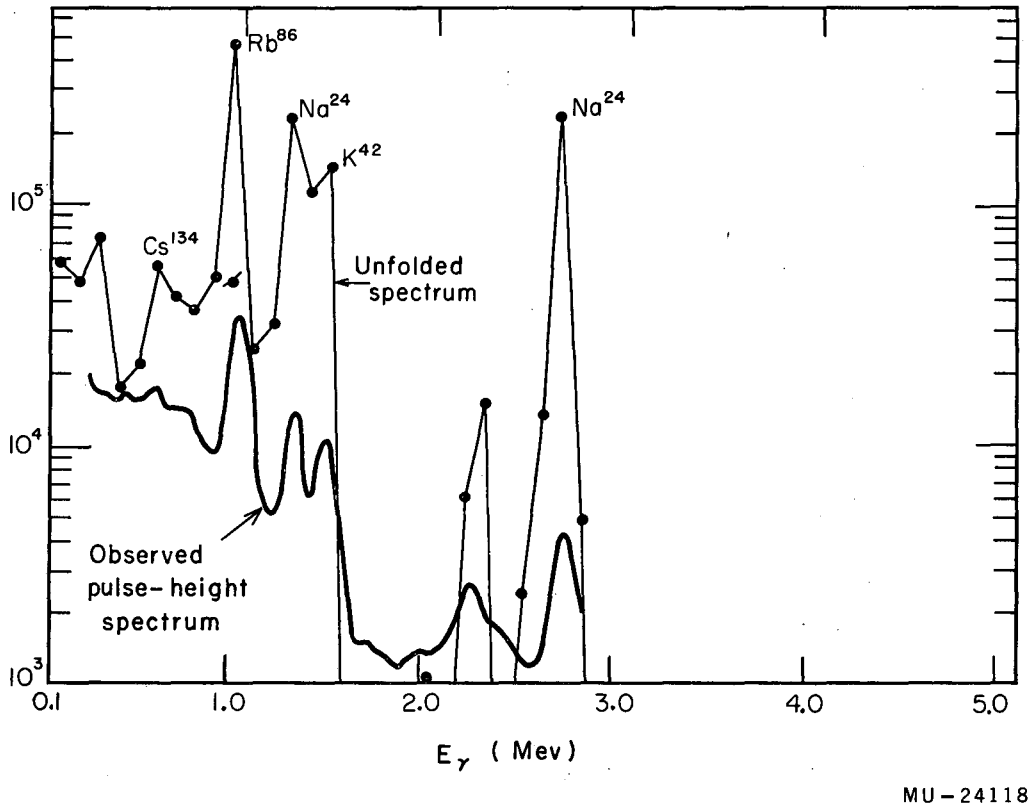

Fig. 12. Comparison of observed and unfolded spectra for a mixture of several sources: Rb^{86} at 1.06 Mev; Na^{24} at 1.38 and 2.75 Mev; K^{42} at 1.55 Mev; and Cs^{134} at 0.60 Mev.

the smoothing methods were tried, and all resulted in average energies for the test spectrum within 3% of each other. Hand smoothing alone was selected for use since it took best account of the statistics and did not eliminate structure where the statistics were good. An example of a raw spectrum and the smoothing line drawn through it is shown in Figure 13. While such a method is not exactly reproducible, the agreement in the average energy with other methods indicates that there are no significant errors involved.

IV. RESULTS AND INTERPRETATION

A. Calculations of Cross Sections and Angular Momenta

The total capture cross sections for both the alpha- and carbon-ion bombardments were calculated with the diffuse-edge program of Thomas for the IBM 650.[8] Although it was written for heavy ions, the use of a radius of 1.61 fermis for the alpha particle gave very good agreement with optical-model calculations of Huizenga and Igo.[73]

The results of the calculation are presented in Table III. The cross section σ and average angular momentum $\overline{\ell}$ were found for the average energy of the beam particle in the target for all cases except carbon on vanadium at low energy. In the latter case, the large energy spread and the presence of the barrier made it necessary to take weighted averages over the energy intervals.

The cross sections were calculated with the assumption that direct reactions are negligible. This is far from the actual case for heavy ions, especially with light targets. In the more extreme case of 160-Mev O^{16} on Ni^{58}, Knox[74] has seen as high a yield of alpha particles as of neutrons. However, part of this high charged-particle yield may be ascribed to the relative proton excess of Ni^{58}. In the bombardment of gold with carbon ions, a case that corresponds better to the tellurium bombardment, Britt and Quinton found nearly a barn of alpha-production cross section at 126 Mev.[75] Of this, 85% was estimated by its angular distribution to result from direct processes. This alpha cross section fell off rapidly with lower beam energy. In the comparable case of oxygen on bismuth, it decreased from one barn to half that when the energy of the beam was lowered to 105 Mev,

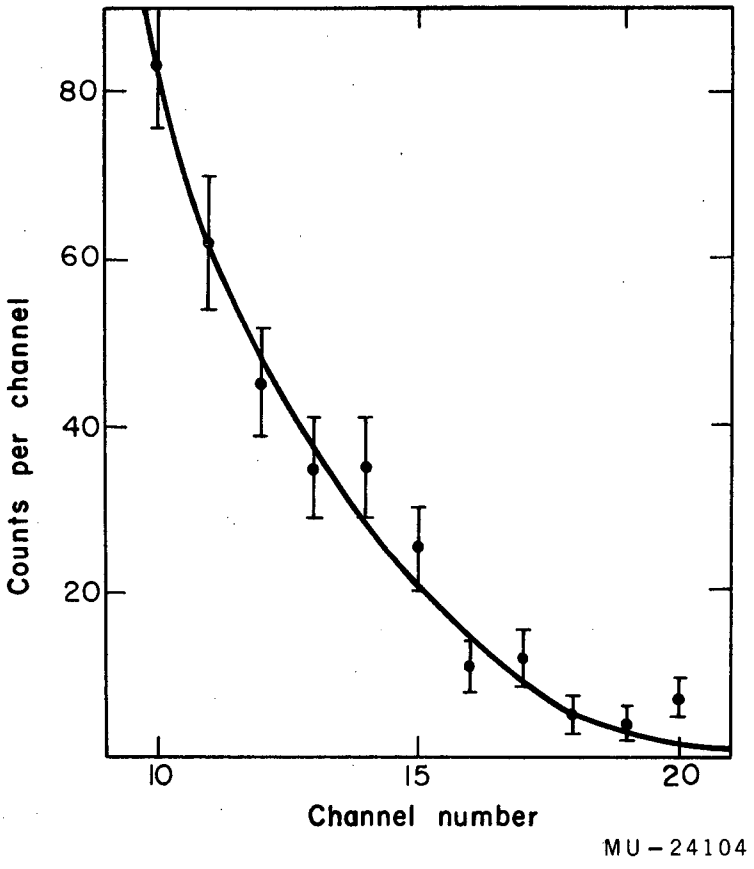

Fig. 13. Typical hand smoothing of the high-energy end of a spectrum. The example is given for alpha particles on tantalum at θ = 90 deg, $\overline{E}^{*}$ = 38 Mev.

Table III

Calculated total-reaction cross sections and angular momenta

Target	Projectile	Energy range (Mev)	Total cross section $\sigma(\bar{E})$ (barns)	Average Angular Momentum $\bar{\ell}$
Ba	α	45 - 41.7	1.84	13.8
	α	28.4-24.9	1.27	9.0
Ho	α	45 - 42	1.81	13.9
	α	28.4-25.5	1.11	8.1
	C^{12}	115 - 103.5	1.76	36.2
Ta	α	45 - 37	1.72	13.2
Co	α	45 - 41	1.61	12.3
	α	28.4-24.4	1.45	9.4
	α	37 - 33	1.57	11.0
Te	C^{12}	115 - 107	2.00	38
V	C^{12}	115 - 102	1.72	31
	C^{12}	58 - 26	0.91	16.5

while the proportion of direct processes in the total remained the same. In the present experiment, therefore, direct processes should have been negligible in the low-energy carbon bombardment of vanadium, as well as in the alpha bombardments.

The diversion of a part of the cross section into direct reactions has several effects on the gamma yield per reaction. First, heavy particles from the breakup of the projectile trigger the anti-coincidence, and the gammas seen correspond to a smaller number of reactions than calculated; second, the excitation left in the compound nucleus after the departure of any direct particles that do not trigger the anticoincidence is less than the full amount; and third, the greater probability of direct reactions in high-angular-momentum collisions lowers the average angular momentum.[74,76]

In order to estimate the effects of charged particles, two thicknesses of stopping scintillator were tried. One thickness sufficed to stop all charged particles, and the other was just thick enough (approx 0.6mm) to stop the carbon ions. Calibration at various energies at the 60-inch cyclotron indicated that the thick scintillator provided pulses with 45-Mev alpha particles nearly as high as with 110-Mev carbon ions. Alpha particles with energies above about 15 Mev, including all those from direct reactions, should have given pulses high enough to trigger the anticoincidence and thereby reject coincident gammas. On the other hand, the thin scintillator provided pulses no higher than half the threshold of the anticoincidence either with alpha particles or protons at any energy.

Gamma spectra were run consecutively with the two scintillators using the full-energy carbon beam on the tellurium target. The spectra obtained were identical within statistics. This observation indicates that the yield of gamma rays coincident with direct alpha particles and protons was probably small. The case of evaporated alpha particles, which have a probable energy closest to the Coulomb barrier (in this case 16 Mev), was not so clear-cut. Approximately half should have been able to trigger the anticoincidence with the thick scintillator. They were not peaked forward,[75] however, and only about a third should have entered the stopping scintillator.

By this estimate, one in six should have caused rejection of the accompanying gamma rays.

Preliminary cross section measurements by Choppin, using chemical means,[77] indicate that charged-particle emission is quite large. For Te^{128}, he has found that the $(C^{12}, p4n)$, the $(C^{12}, \alpha 3n+p5n)$, and the $(C^{12}, \alpha n+p3n)$ cross sections are as large as the $(C^{12}, 6n)$ and the $(C^{12}, 8n)$ cross sections. The bulk of the charged-particle evaporation probably goes by emission of two protons rather than one alpha particle, since the barrier for protons is lower.[75] The chance of both protons going into the thick stopping counter simultaneously was relatively low and the counter should not have been sensitive to single protons. Assuming that the gamma rays associated with direct alpha particles were in small yield, we have a possible explanation of the lack of difference between the two scintillator thicknesses.

Other direct processes are not differentiated by the use of the two stopping scintillators. As indicated by momentum transfer, absorption of an alpha particle has been found more probable than absorption of Be^8 from a C^{12} projectile, in the fission of uranium.[78] If such a process occurred with tellurium, the Be^8 would probably have given a pulse exceeding the threshold in both the thick and thin stopping scintillators. Consequently, one cannot estimate directly the contribution to the cross section from such events.

Nor could the portion of the cross section that goes into nucleon-transfer reactions be determined directly in this experiment. Barrier-tunneling cross sections are not included in the one calculated by Thomas' method; however, their cross sections are only a few millibarns. Multi-nucleon transfer by a grazing-incidence mechanism is estimated by Kaufman and Wolfgang[76] to be on the order of several hundred millibarns, including unobserved stable products. Since the remainder of the projectile proceeds into the third scintillator, such reactions were not detected by the coincidence system.

Fission should not have occurred in any of the bombardments except for carbon ions on holmium. In that case, however, the cross section is relatively small. Gilmore measured the cross section for oxygen ions on holmium;[5] at the same excitation energy it was 10% of the calculated compound-nucleus value. With carbon ions it should be less.

Since the angular distribution of the fission fragments goes as $1/\sin\theta$, very few of the fission events resulted in both fragments missing the third scintillator. Fragments from the fission of Cf^{252} gave pulses quite adequate to trigger the anticoincidence. Therefore very little of the gamma-ray spectrum measured was associated with fission events.

The best available estimate of the actual compound-nucleus cross section for tellurium comes from Choppin's preliminary data. Even when allowance is made for unobserved reactions such as $(C^{12},\alpha 2n)$, the sum of the upper limits of the evaporation cross section is barely one barn at 110 Mev. The calculation predicts two barns. Though this procedure is crude, it does indicate that the calculated cross section is much too high.

Nevertheless, a low compound-nucleus cross section does not seem to be typical of all heavy-ion reactions. Using several different projectiles, Alexander[3] has found that reactions going through the dysprosium and holmium compound nuclei have cross sections that add up to about 80% of the calculated value. Therefore, the cross section for carbon on holmium may be fairly good. Knox's work with oxygen on nickel[74] suggests that the cross section on vanadium is too high at 101 Mev, while it should be more accurate at 49 Mev. Even considering the results of Alexander when heavier targets were used, it appears very unlikely that the compound nucleus cross section for tellurium should be more than 65% of that calculated.

In the classical approximation, the partial-wave cross sections go as $\ell + \frac{1}{2}$. Therefore, if we assume that the direct processes are predominantly high angular-momentum reactions occurring at the nuclear surface, the average compound-nucleus angular momentum is closer to 20 or 25 units than to 35 or 40 units. It is assumed that the target spin is small compared to ℓ; then for the compound system, we have $J \sim \ell$. The angular momentum carried off by neutrons as a function of angular momentum and temperature has been calculated by Pik-Pichak.[12] For angular momenta on the order of those brought in by the carbon-ion bombardment of tellurium, the average removed is about $\frac{1}{3}\hbar$ at a temperature of 4 Mev and $\frac{2}{3}\hbar$ at 1 Mev.

This decrease with increasing temperature is plausible from the standpoint that the cutoff of the level density with increasing spin is not so sharp at a higher temperature. Therefore, the transition is less

constrained to go to a lower spin state. The amount of angular momentum removed goes as the ratio of the spin to the moment of inertia; for the low-energy bombardment of vanadium the average carried off at a temperature of 1 Mev is about one unit. It should be mentioned that the temperature used by Pik-Pichak is based on the thermal excitation left after the rotational energy is subtracted from the total. In the derivation of the spin-dependent level-density formula, the temperature used is that of a nonrotating system with the same total excitation energy.

Deformation of the target nucleus results in a higher average ℓ value than calculated here because of the possibility of larger impact parameters. Gilmore calculated the effects of deformation in the classical approximation and found $\bar{\ell}$ about 20% higher for nuclei in the vicinity of holmium and tantalum.[5]

B. Experimental Results

1. Total Gamma Yields

The gamma-ray yields for the various targets are given in Table IV. The excitation energies were either derived using the table of Q values of Ashby and Catron,[79] or if unavailable there, were taken from Cameron's mass tabulation.[80]

The correction for neutron effects in the gamma detector, and for the slightly high result obtained in testing the unfolding program, is 15% for the alpha bombardments and 10% for the heavy-ion bombardments where the ratio of gamma rays to neutrons was higher. A correction is also applied for coincidence summing in the gamma detector. With an average absolute efficiency of E, the correction added to n_γ is $En_\gamma(n_\gamma-1)$ assuming isotropic emission. The value of E was about 1% at 90 deg and 0.5% at 45 deg. These corrections are rather arbitrary, but they should serve to correct the data in the right direction.

The tabulated total gamma energy is based on the corrected number of photons. Considering both the solid angle of the detector and the anisotropy, the average gamma yield should be equal to that measured at 55 deg to the beam direction. If the quadrupole angular distribution includes significant terms in $\cos^4\theta$, the proper angle will be closer to 50 deg. The measurement made at 45 deg should be a good approximation

TABLE IV

Photon yields per reaction n_γ, based on calculated cross sections

Target	Beam	σ_{calc} (barns)	$\bar{E}^*$ (Mev)	$\bar{\ell}_{calc}$	n_γ uncorr.	n_γ corr.	$\bar{E}_\gamma$ (Mev)	Total gamma Energy (Mev)
Ba	α	1.84	42	13.8	6.2	5.4	1.2	6.5
	α	1.27	26	9.0	5.6	4.9	1.3	6.4
Ho	α	1.81	42	13.9	7.1	6.2	1.1	6.8
	α	1.11	26	8.1	6.7[a]	5.8	1.1	6.4
	C^{12}	1.76	90	36	14.8	14.1	1.2	17.0
Ta	α	1.72	38	13.2	5.4	4.7	1.0	4.7
Co	α	1.61	46	12.3	4.0	3.4	1.5	5.2
	α	1.45	30	9.4	4.1	3.5	1.4	5.0
	α	1.57	39	11.0	2.9[a]	2.5	1.6	4.0
Te	C^{12}	2.00	99	38	11.8	11.1	1.1	12.2
V	C^{12}	1.72	101	31	8.5	7.9	1.5	11.8
	C^{12}	0.91	49	16.5	6.8	6.3	1.5	9.4

[a] No data were taken at 45 deg; the value given is that for 90 deg, assuming isotropic distribution.

to the average gamma yield. For gamma rays, the center of mass and laboratory angles are essentially identical.

It is immediately evident that the heavy-ion bombardments yield a total photon energy in excess of the neutron binding energy in all cases. This result disagrees with the assumptions made in statistical evaporation theory. The predicted level widths for neutron emission are greater than for gamma emission. It is then assumed that neutron emission predominates when energetically possible.[9]

2. Agreement with Other Experiments

These results agree well with the observed energy shifts in excitation functions, indicating that most of the displacement can be attributed to gamma emission. Karamyan and associates found the peak of the excitation function for the V^{51} (C^{12},2n) reaction moved upward about 7 or 8 Mev from the peak of the Cu^{65} (p,2n) reaction.[3] If we assume that some of the shift is due to the Coulomb barrier, it is consistent with the observed 9 Mev of gamma rays, which is about 4 Mev more than would be expected without angular-momentum effects. The yield of 11.8 Mev of gamma rays at 107 Mev is consistent with Pik-Pichak's prediction of an 8-Mev excess at 80 Mev bombarding energy.[12]

However, the observed yield of 12.2 Mev in the case of tellurium is not sufficient to account for the shifts observed by Choppin.[2] At comparable bombarding energies, the displacement in the peaks of the cross sections was 23 Mev with respect to Jackson-model calculations, assuming a temperature of 2 Mev. If one makes the rough assumption that the calculated cross section is twice the effective cross section, this shift can also be accounted for. The agreement is within the accuracy of the estimate of the gamma yield, or of the Jackson calculation.

Though Morton's results[4] were obtained by quite a different method, namely measurement of angular distributions of recoil nuclei, they agree with the gamma yields. He fit his data with Monte-Carlo calculations using temperatures of 1.5 and 2.5 Mev, but 2 Mev is more consistent with Broeck's evaporation spectra. Interpolating in T and extrapolating from 87.5 to 100 Mev, one finds the value of Morton's excess-gamma-energy parameter E_γ to be about 16 Mev. This figure is quite consistent with a total gamma yield of 20 to 24 Mev.

The number of gamma rays found here agrees with the results of Karnaukhov and Organesyan[57] for 78-Mev carbon ions on tin. By observing the variation in the amount of pileup in the gamma spectrum as the geometry was changed, these authors estimated that the number of gamma rays was greater than ten.

An exception to the general observation of energy shifts has been observed by Alexander[3] in the reaction $Pr^{141}(C^{12},4n)Tb^{149}$. Morton has fit recoil data for this reaction with $E_\gamma = 0$. However, the cross section is very small, only 4% of the calculated total at its peak. Alexander points out that most of the cross section for the praseodymium target goes to even-Z products in which a shift is observed in the excitation function.

While carbon ions on tellurium and alpha particles on barium both go to cerium compound nuclei, the excitation energies are different. For these targets, it cannot be proved that the difference in gamma-ray yields is the result of angular momentum effects alone. However, the comparison may be made directly in the bombardment of Co^{59} with alpha particles and V^{51} with carbon ions since the excitation energies are nearly the same although the angular momenta are different. The gamma yield in the heavy-ion bombardment is more than twice as great with an angular momentum increase of about 50%, assuming that three units are carried off by neutrons before gamma emission.

Since the energy spread of the carbon beam in the vanadium target was quite large, it might be argued that a yield proportional to the square or higher power of the excitation energy would give the same effect. The bombardment of vanadium with carbon ions of about twice the energy shows that this is not likely. The yield is increased only 20%, and consequently angular momentum must be held responsible for the difference between the vanadium and cobalt bombardments. The smallness of the increase here, compared to that of carbon ions over alpha particles, may be the result of the larger proportion of direct processes at higher energies.

In Figs. 14 and 15 the effect of angular momentum with the same original compound nucleus is shown. In both cases, the yield of gamma rays for the higher angular momentum is higher below 3 Mev. A peak centered at Channel 19 (4.95 Mev) appears in many of the spectra, but

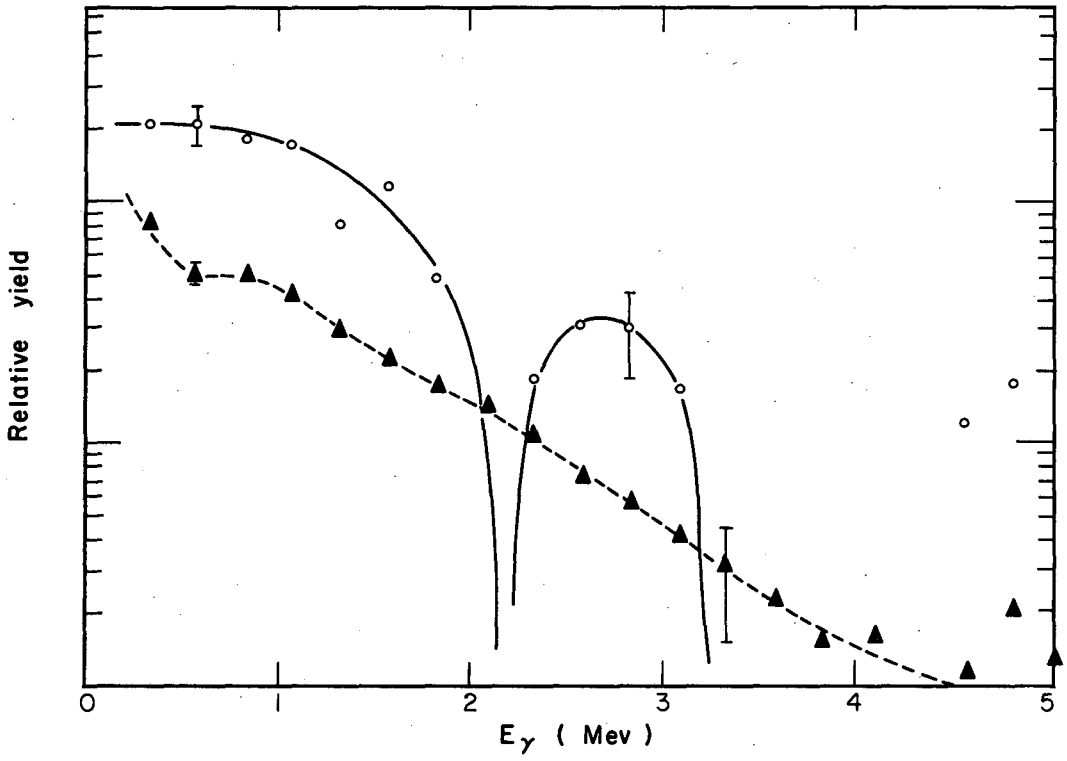

Fig. 14. Gamma spectra from reactions going to a Ce compound nucleus. The curve with open circles shows Te + Ce^{12}, $\bar{E}^*$ = 99 Mev, θ = 90 deg; with closed triangles, Ba + α, $\bar{E}^*$ = 42 Mev, θ = 90 deg.

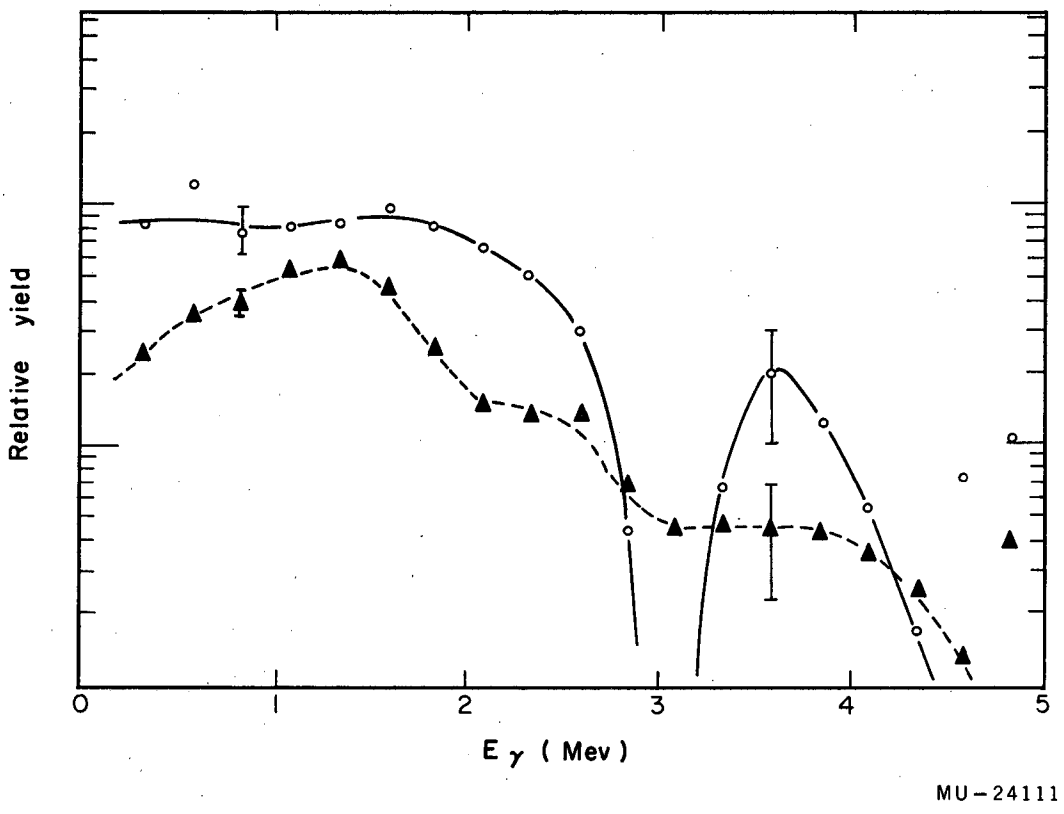

Fig. 15. Gamma spectra from reactions going to a Cu compound nucleus. The curve with open circles shows V^{51} at $\overline{E}^{*}$ = 49 Mev, θ = 90 deg; with closed triangles, Co^{59} at $\overline{E}^{*}$ = 46 Mev, θ = 90 deg.

it is probably not real. It may result from end effects in the unfolding process and the occasional tendency of the DD2 amplifier to pile pulses up at about 95 volts. Spectra covering 0.4-10.4 Mev did not show this peak. Other details of the spectra will be discussed later.

3. Anisotropy of the Gamma Emission

Anisotropy of the gamma radiation was measured by comparison of the yield at 90 deg and 45 deg to the beam direction. Angles closer to the beam were not practicable because of the distance between crystal and target. The yields at these two angles are summarized in Table V. Spectra of these runs are provided in Figs. 16 through 20. Figures labeled A, B, and C with the same number are normalized to the same calculated number of reactions and Figs. 16A through C are also normalized to Fig. 15; otherwise the scale is arbitrary.

The magnification of statistical fluctuations by the unfolding program makes it difficult to estimate errors at all accurately. On the basis of the reproducibility of the spectra, the errors in individual channels may be very roughly ± 10% at the low-energy end for the alpha runs, or 20% for the Hilac runs where the number of counts was fewer. At 4 Mev the errors were ± 50% or more. Structure at the high-energy end of the spectra cannot be located better than ±1 channel because of the poor statistics. Statistics of the total yield are much better. Including all experimental factors except the calculation of the cross section, the data should be accurate within about 15%.

C. Multipolarity of the Radiation

If we denote the yields of photons observed at 90 deg and 45 deg to the beam by W(90) and W(45), respectively, a measure of the anisotropy is given by b, where

$$b = \left(\frac{W(90)-W(45)}{W(90)}\right) \Bigg/ \left[1 - 2\left(\frac{W(90)-W(45)}{W(90)}\right)\right] . \qquad (58)$$

According to Eq. (43), b is positive for dipole emission and negative for quadrupole emission. The angular distribution is

$$W(\theta) = 1 + b \sin^2\theta . \qquad (59)$$

Table V

Comparison of gamma yields at 90 deg and 45 deg
(data in parentheses may be less reliable than the rest)

Target	Beam	$\overline{E}^*$ (Mev)	$\overline{\ell}_{calc}$	W(90 deg) (ster^{-1})	W(45 deg) (ster^{-1})	Anisotropy[a] b
Ba	α	42	13.8	0.30	0.43	-0.46
	α	26	9.0	(0.38)	0.39	+0.05
Ho	α	42	13.9	0.34	0.49	-0.47
	α	26	8.1	(0.47)	-	-
	C^{12}	90	36	-	1.12	-
Ta	α	38	13.2	0.24	0.37	-0.52
Co	α	46	12.3	0.21	0.27	-0.36
	α	31	9.4	(0.28)	0.28	0
	α	39	11.0	0.27	-	-
Te	C^{12}	99	38	1.09	0.88	+0.63
V	C^{12}	101	31	-	0.63	-
	C^{12}	49	16.5	0.42	0.49	-0.25

[a] See Eq. (58).

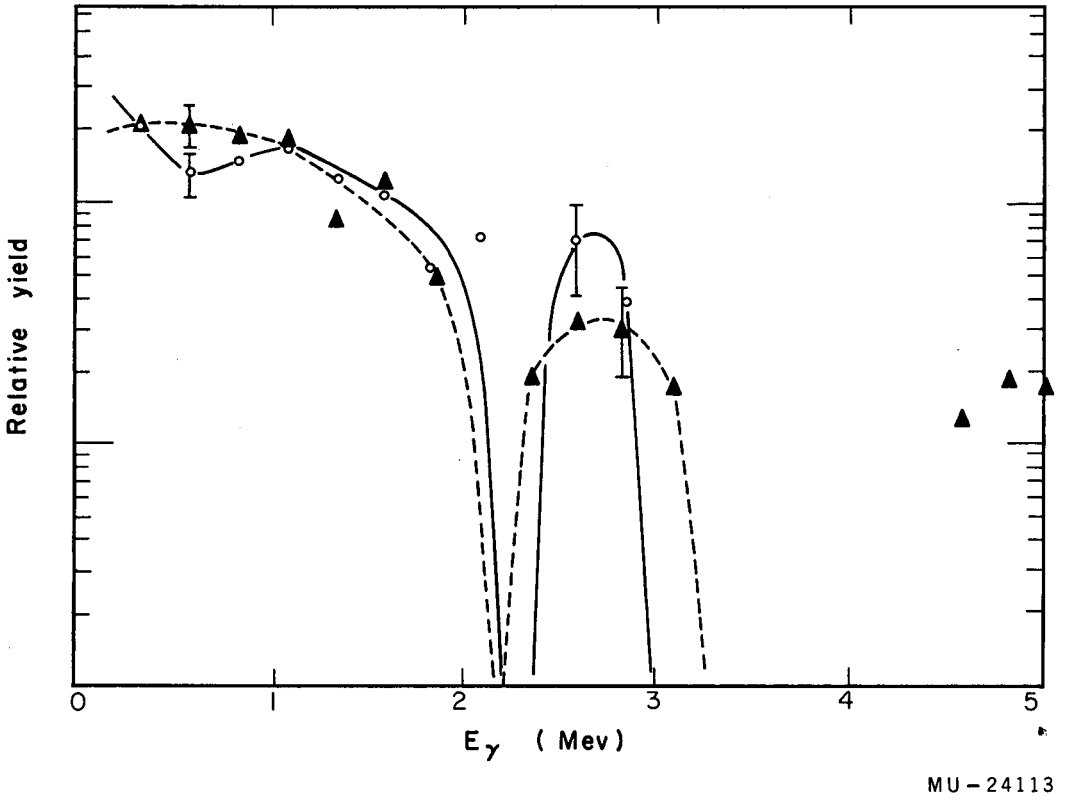

Fig. 16A. Comparison of gamma spectra for C^{12} on Te, with $\bar{E}^*$ = 99 Mev. On curve with open circles, θ = 45 deg; with closed triangles, θ = 90 deg.

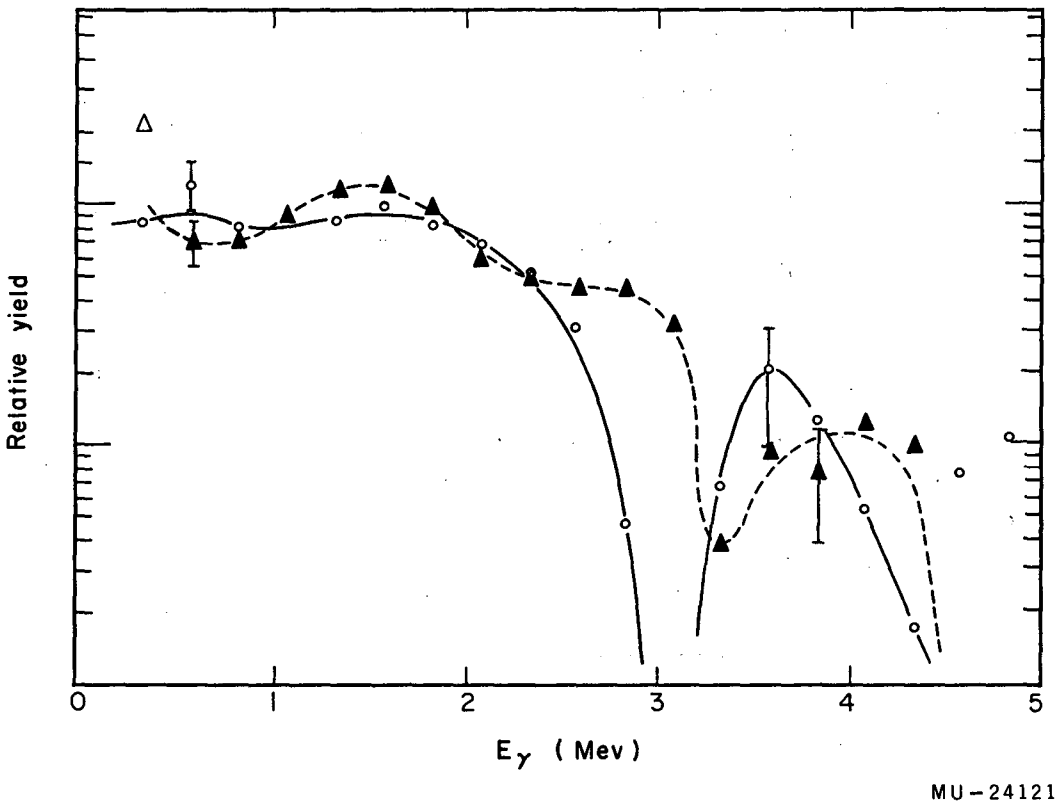

Fig. 16B. Comparison of gamma spectra for C^{12} on V^{51}, with $\bar{E}^*$ = 49 Mev. On curve with open circles, θ = 90 deg; with closed triangles, θ = 45 deg.

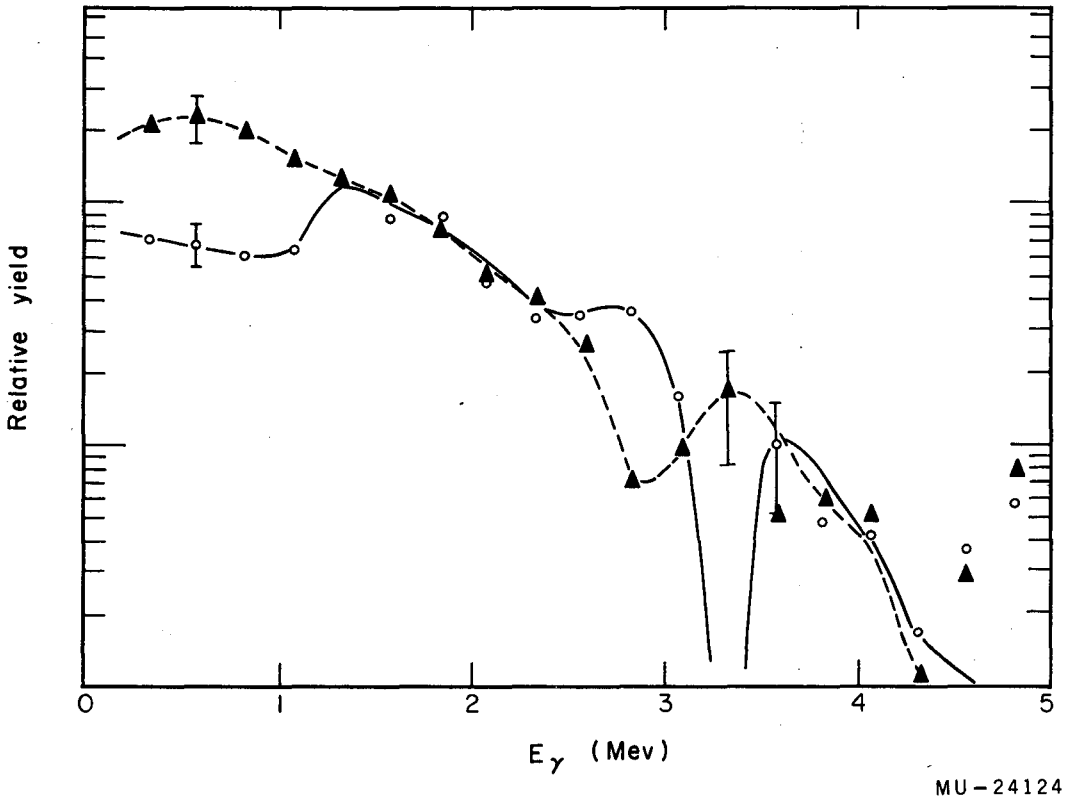

Fig. 16C. Gamma spectra for C^{12} on V and Ho at full energy. Curve with open circles shows V + C^{12} at $\bar{E}^*$ = 101 Mev, θ = 45 deg; with closed triangles, Ho + C^{12} at $\bar{E}^*$ = 90 Mev, θ = 45 deg.

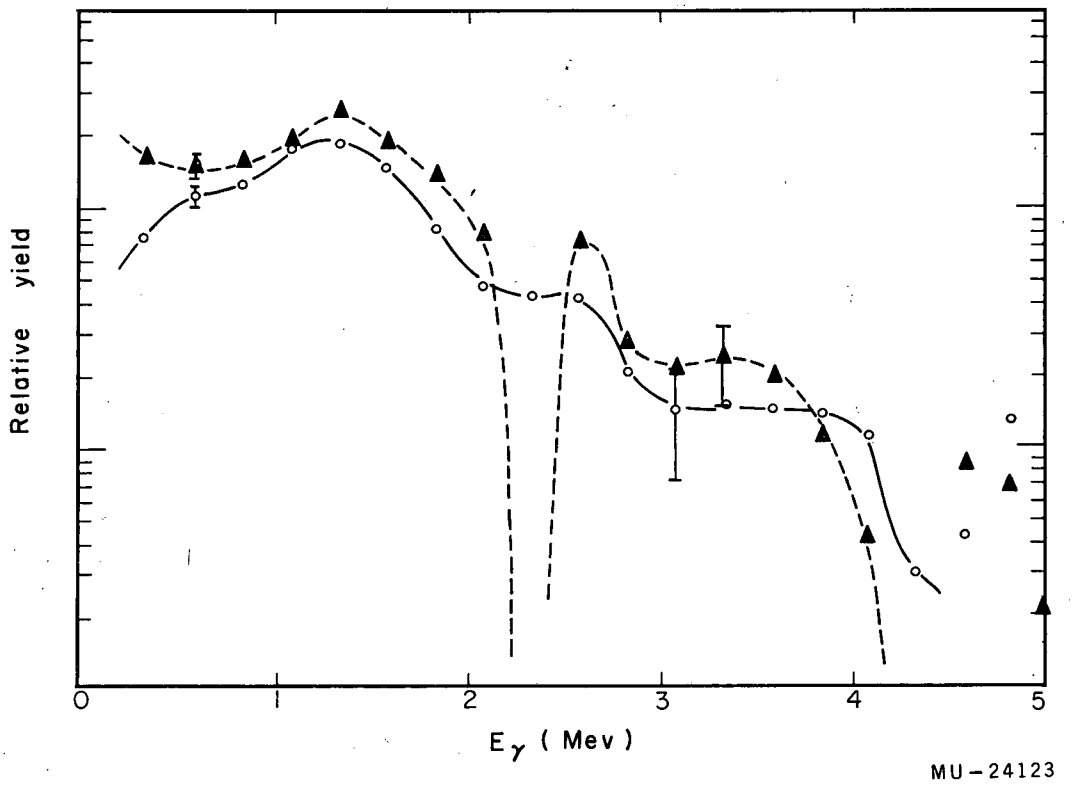

Fig. 17A. Comparison of spectra for alpha particles on Co with $\overline{E}^*$ = 46 Mev. On curve with open circles, θ = 90 deg; with closed triangles, θ = 45 deg.

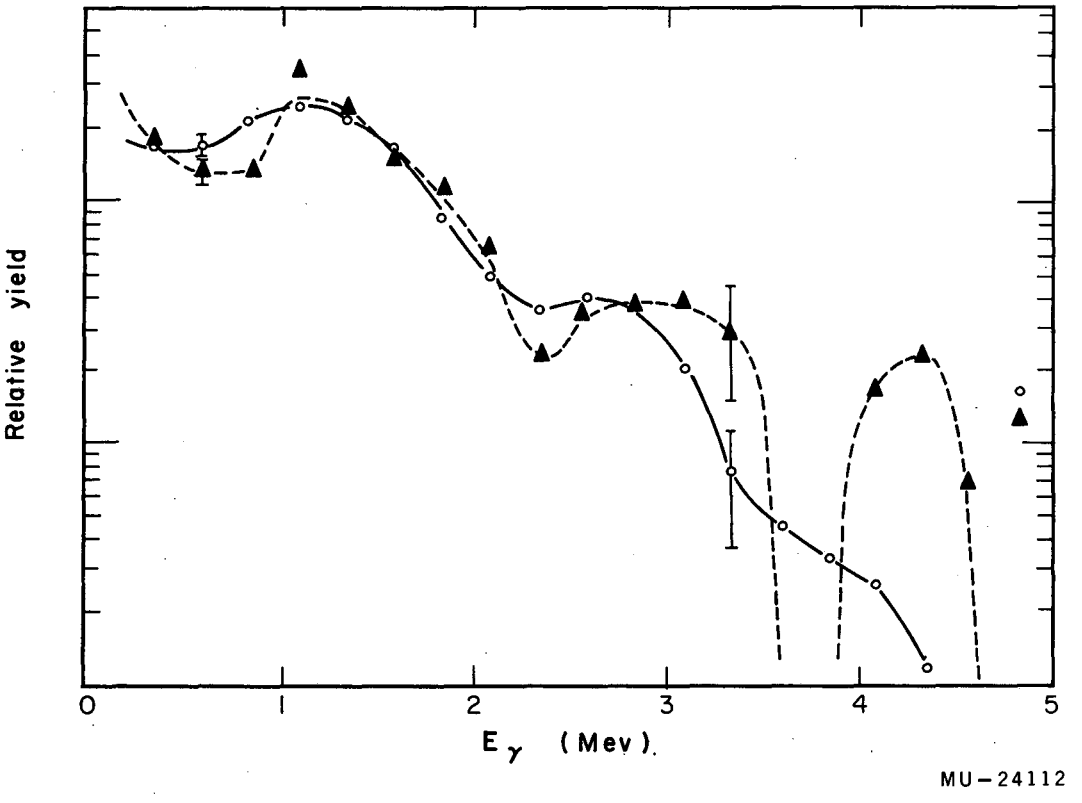

Fig. 17B. Spectra for alpha particles on Co with $\bar{E}^*$ = 30 Mev. On curve with open circles, θ = 90 deg; with closed triangles, θ = 45 deg.

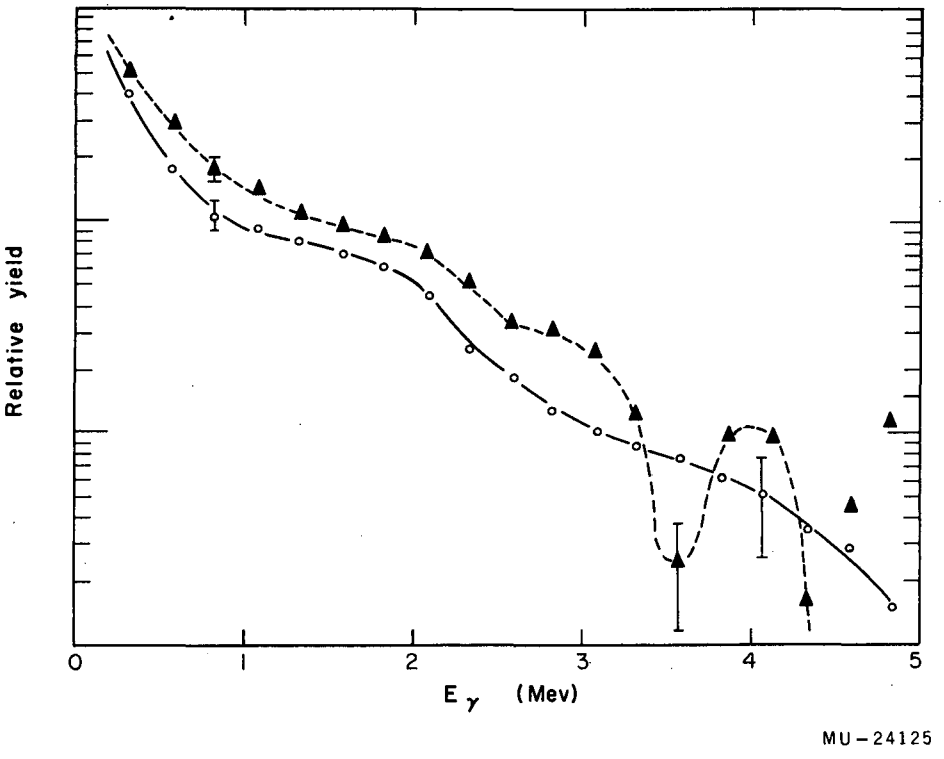

Fig. 18. Spectra for alpha particles on Ta with $\overline{E}^*$ = 38 Mev. On curve with open circles, θ = 90 deg; with closed triangles, θ = 45 deg.

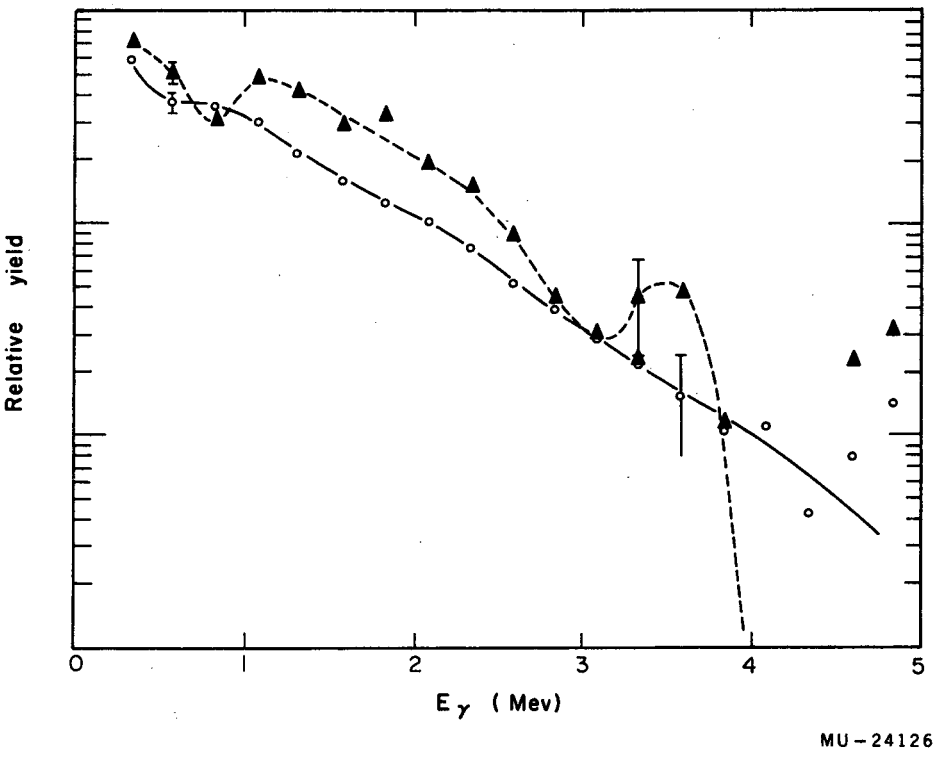

Fig. 19A. Spectra for alpha particles on Ba with $\overline{E}^*$ = 42 Mev. On curve with open circles, θ = 90 deg; with closed triangles, θ = 45 deg.

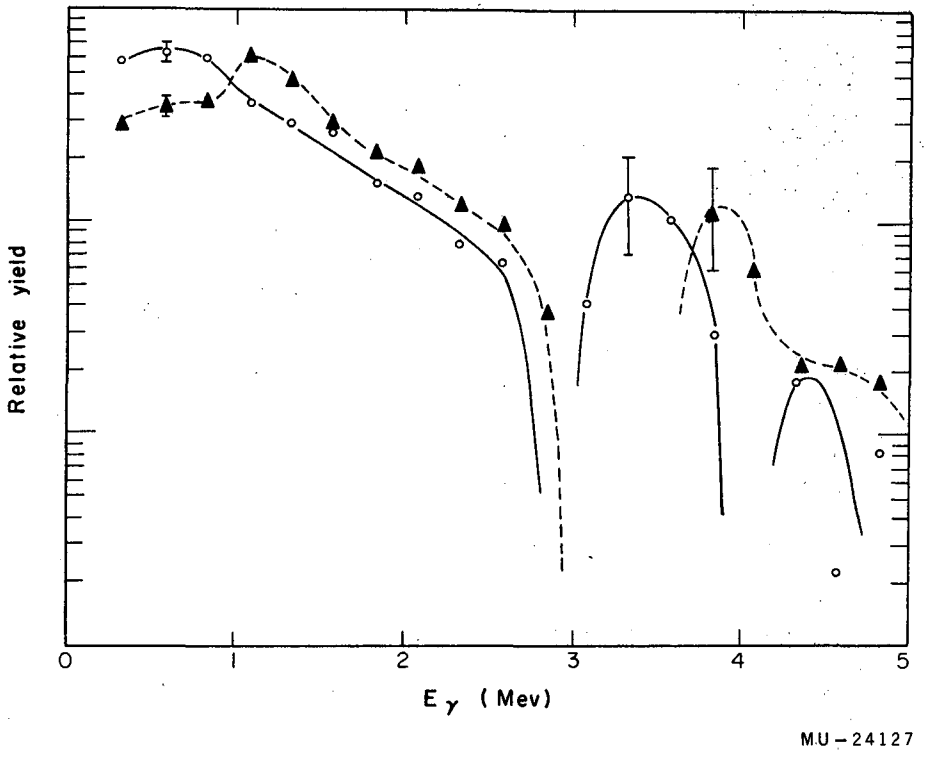

Fig. 19B. Spectra for alpha particles on Ba with $\overline{E}^*$ = 26 Mev. On curve with open circles, θ = 90 deg; with closed triangles, θ = 45 deg.

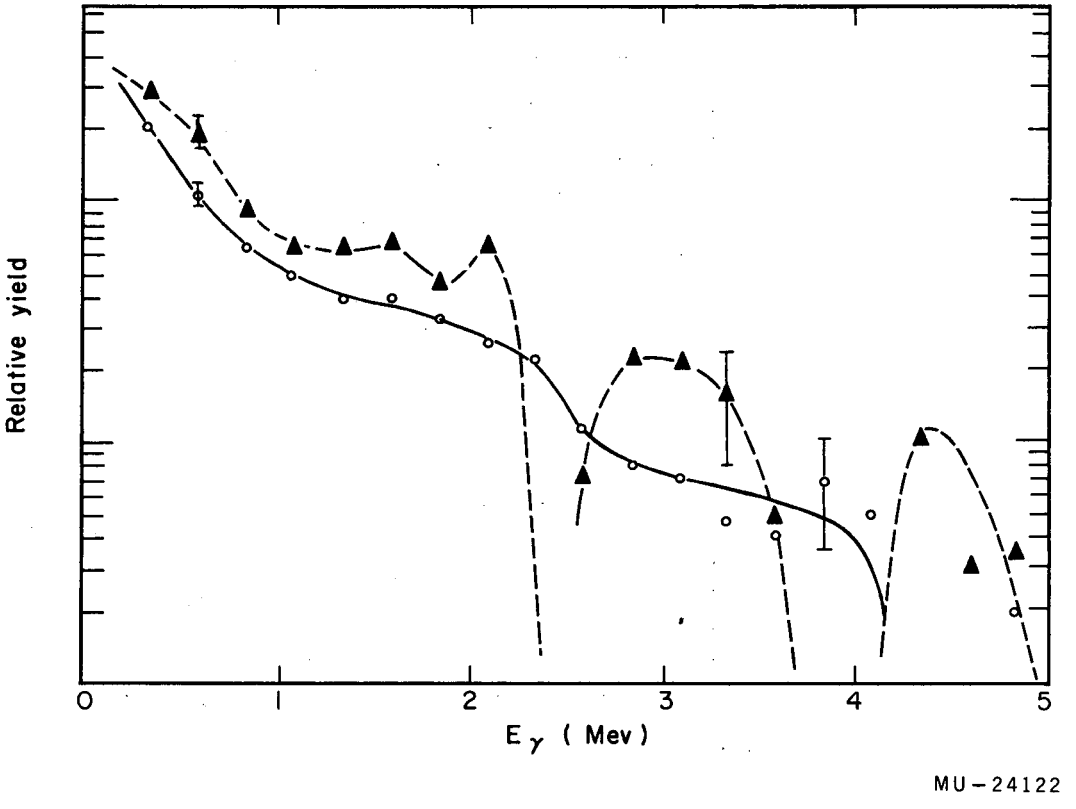

Fig. 20A. Spectra for alpha particles on Ho with $\overline{E}^*$ = 42 Mev. On curve with open circles, θ = 90 deg; with closed triangles, θ = 45 deg.

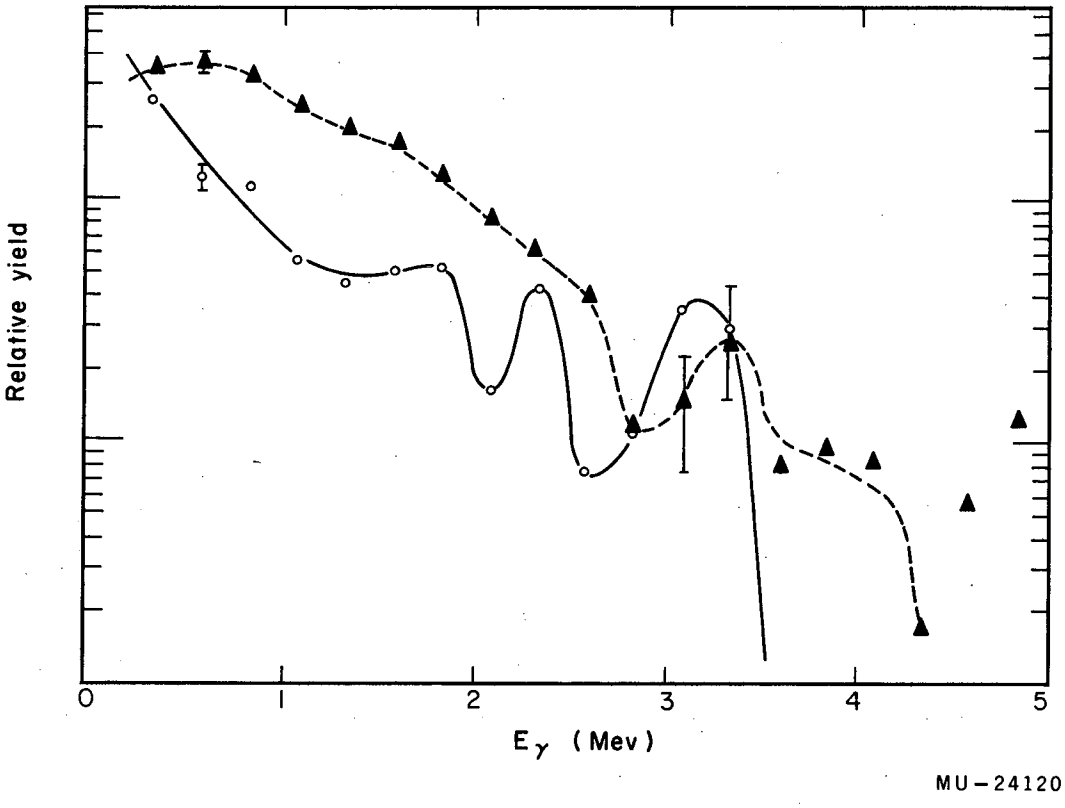

Fig. 20B. Comparison of spectra for Ho target bombarded with alpha particles. Curve with open circles shows Ho + α at $\overline{E}^*$ = 26 Mev, θ = 90 deg; with closed triangles, Ho + C^{12} at $\overline{E}^*$ = 90 Mev, θ = 45 deg.

Mixtures of quadrupole and dipole radiation are weighted by the coefficients k_L; equal numbers of photons with L = 1 (dipole) and L = 2 (quadrupole) have the angular distribution of quadrupole emission, but with smaller anisotropy.

Reference to Table V indicates that the full-energy alpha bombardments of barium, holmium, and tantalum produce strong evidence of predominantly quadrupole radiation, while the anisotropy is less marked in cobalt. At lower bombarding energy, the emission is nearly isotropic. On the other hand, tellurium, which has received more angular momentum and might be expected to emit high multipoles,exhibits more dipole emission. The vanadium target does not show this effect, however; at a higher angular momentum than cobalt its radiation has essentially the same anisotropy. The contribution of octupole and higher orders to the radiation is expected to be negligible on the basis of the very long lifetimes predicted and observed for such transitions.

The magnitude of the anisotropy is surprisingly great. A discussion of this subject and its relation to the de-excitation mechanism is deferred to Section D below.

As a rough guide, the multipolarity of the radiation would be approximated by the ratio of the angular momentum at the beginning of gamma emission to the number of photons emitted. The photon yield is plotted in Fig. 21 against the estimated angular momentum at the beginning of gamma emission. The results here are consistent with the angular distribution in most cases. Yet the points corresponding to the tellurium and cobalt bombardments fall more in the direction of higher multipoles than the angular distribution indicates.

For tellurium this is no doubt the result of the large cross section for direct processes. As a limiting case, if the partial-wave cross sections are divided so that the direct processes go only through the states of highest angular momentum ℓ, the average compound-nucleus cross section will decrease, and the average ℓ will decrease in the same ratio. Points are plotted for various probabilities of direct processes. In the opposite limit of equal probability for direct processes at all angular momenta, a doubling of the apparent gamma yield would still be consistent with a mixture of dipole and quadrupole emission. The actual case probably falls between these limits, and a doubling of the apparent

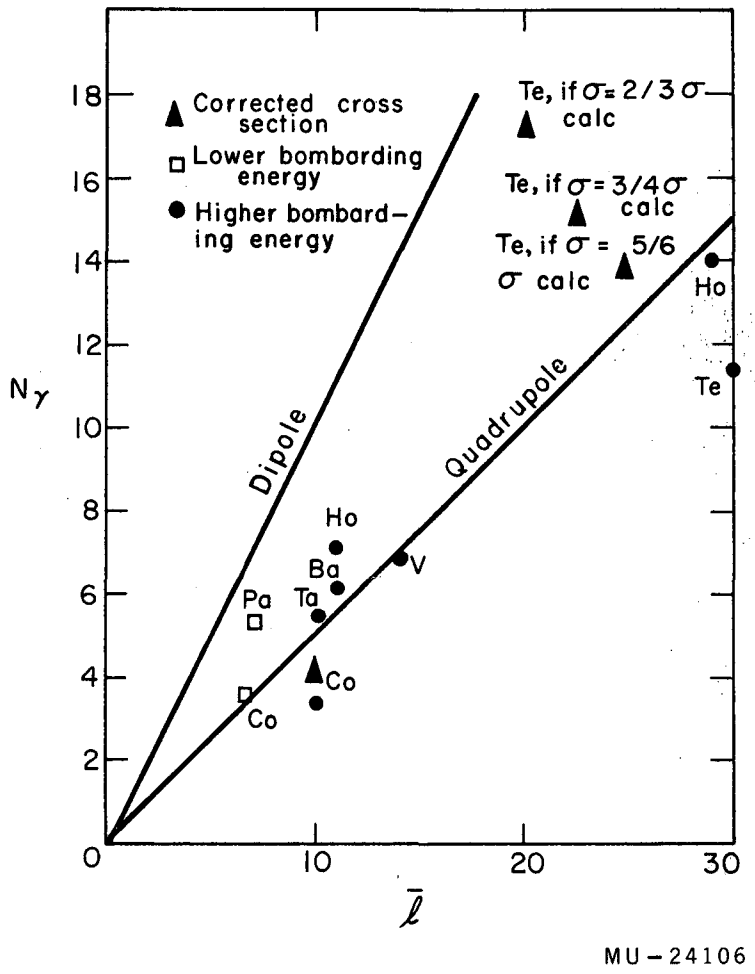

Fig. 21. Gamma ray yields n_γ as a function of the estimated average angular momentum $\bar{\ell}$ at the start of the cascade. The dipole and quadrupole lines represent $n_\gamma = \bar{\ell}$ and $n_\gamma = 1/2\ \bar{\ell}$, respectively.

yield would result in a point somewhere near the dipole line.

For a nucleus as small as cobalt, the cross-section program may be inaccurate. While the calculated cross section at a bombarding energy of 32 Mev is 1.5 b, the sum of the measured cross sections for nickel[81] is 1.25 b. An appropriate correction brings the 46-Mev cobalt point closer to the quadrupole line, and the lower energy one to an intermediate position.

The position of the low-energy points for barium in a region corresponding to a mixture of quadrupole and dipole emission is not necessarily to be expected on the basis of the average anisotropy. Reference to Fig. 19B indicates that dipole and quadrupole emission predominate over different energy ranges; fact is consistent with the expected mixture. Differentiation of the spin-dependent level-density formula (Eq. 22) indicates that the most probable spin, assuming an equal probability of populating all states, is 5.5 at a temperature given by $T = (10U/A)^{1/2}$. At the beginning of the gamma cascade, the spin is estimated to be quite close to this value— about 7 units. Therefore, in the independent-particle approximation we should not see large effects due to a scarcity of final states of the proper spin. In the low-J limit of a level density going as (2J+1), the emitted radiation should be isotropic.[7]

D. The Role of Collective Effects

1. Evidence for Collective Transitions

The observation of quadrupole emission strongly suggests collective effects in the de-excitation. The independent-particle model predicts for a single proton transition of 1 Mev at A = 100 that dipole transitions should be on the order of 10^4 times faster than quadrupole transitions.[82] Experimentally, the electric-dipole transitions are found to be several orders of magnitude slower than predicted, while the magnetic-dipole transitions are slower by a factor of about 20. Despite these effects, dipole emission should still be preferred. Any large quantity of quadrupole emission must be due to the enhancement found in collective transitions.

If the photon emission can be described in terms of the statistical model, Eq. (57) should give the average yield of photons, starting with a given excitation energy and angular momentum. The term for angular-momentum effects amounts to about 10% for the carbon-ion bombardments and 2% for the alpha particles. It is assumed that the actual cross section is half the calculated value for tellurium and vanadium at 100 Mev, but equal to it in the other bombardments. Table VI compares the calculated and experimental values of the photon yield n_γ.

Although the initial excitation energy U_o is taken as the experimental total gamma energy, the numbers of photons predicted for the given initial excitation and spin are not consistent with the experimental values. Nor are they consistent for tellurium and vanadium if the calculated cross sections are used. This disagreement constitutes good evidence for collective effects, as the approximation of a large number of gamma rays should be valid at least for the heavy-ion bombardments.

The gamma-ray spectra from thermal-neutron capture are held by Strutinsky and co-workers to have a shape consistent with dipole but not quadrupole radiation.[39] Comparison of typical neutron-capture spectra from Groshev's compilation[83] with spectra from this experiment in Fig. 22 shows considerable difference in shape. The neutron-capture spectra in general have very broad maxima in the vicinity of 2 or 3 Mev for the heavier elements, while the lighter elements such as copper show a greater number of discrete peaks and a more or less flat distribution.

Examination of the spectra indicates that the relative amounts of dipole and higher-order gamma emission are not the same at all energies. For tellurium (Fig. 16A) the spectra taken at 90 deg and 45 deg are fairly even in heights above 1 Mev. Below that point the spectrum at 90 deg has a greater intensity. Apparently quadrupole emission is competing more favorably with dipole emission at higher gamma energies.

For barium at both energies (Figs. 19A and 19B), the quadrupole strength is increased: above 1 Mev the 45 deg yield is higher, while the 90 deg yield is greater below 1 Mev. This effect is stronger above 1 Mev in the 42-Mev bombardment, an observation consistent with increased collective effects at higher angular momentum. Cobalt at 30 Mev (Fig. 17B) shows neither angle with a significantly higher yield, but at 46 Mev the 45 deg yield is slightly higher in almost every channel. Again, there

Table VI

Calculated values of the gamma-ray yield based on Eq.(57)[a]

Target	Beam	U_o (Mev)	J_o	N_γ, calc	N_γ, exp
Te	C^{12}	20	25	8.6	~18
V	C^{12}	16	20	6.7	~15 (est)
V	C^{12}	9	13	3.0	6.3
Ba	α	6.4	11	3.1	5.4
Co	α	6	10	2.2	3.4

[a] U_o is the excitation energy assumed at the beginning of the cascade and J_o is the initial spin used. A cross section smaller than calculated was assumed in the first two cases.

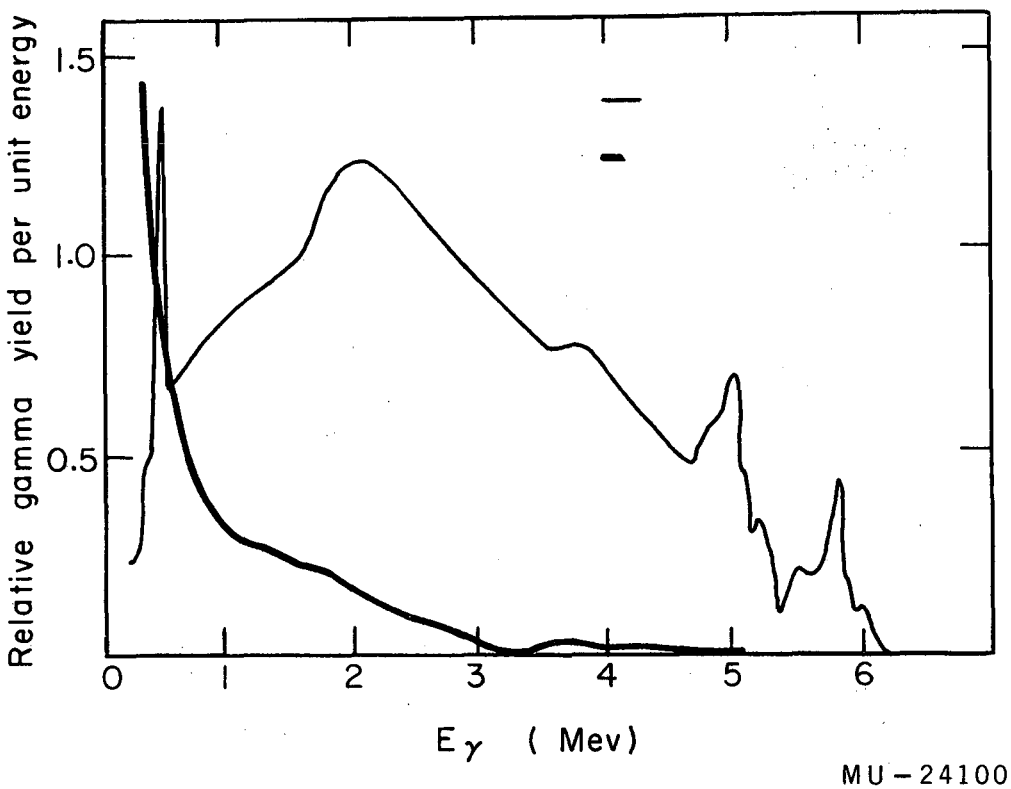

Fig. 22A. Comparison of gamma spectra for this experiment with spectra from thermal-neutron capture. Typical deformed-nucleus spectra are plotted, in this case for rhenium. The light curve represents thermal neutrons on rhenium; the heavy curve, α on Ta at $\overline{E}^* = 38$ Mev.

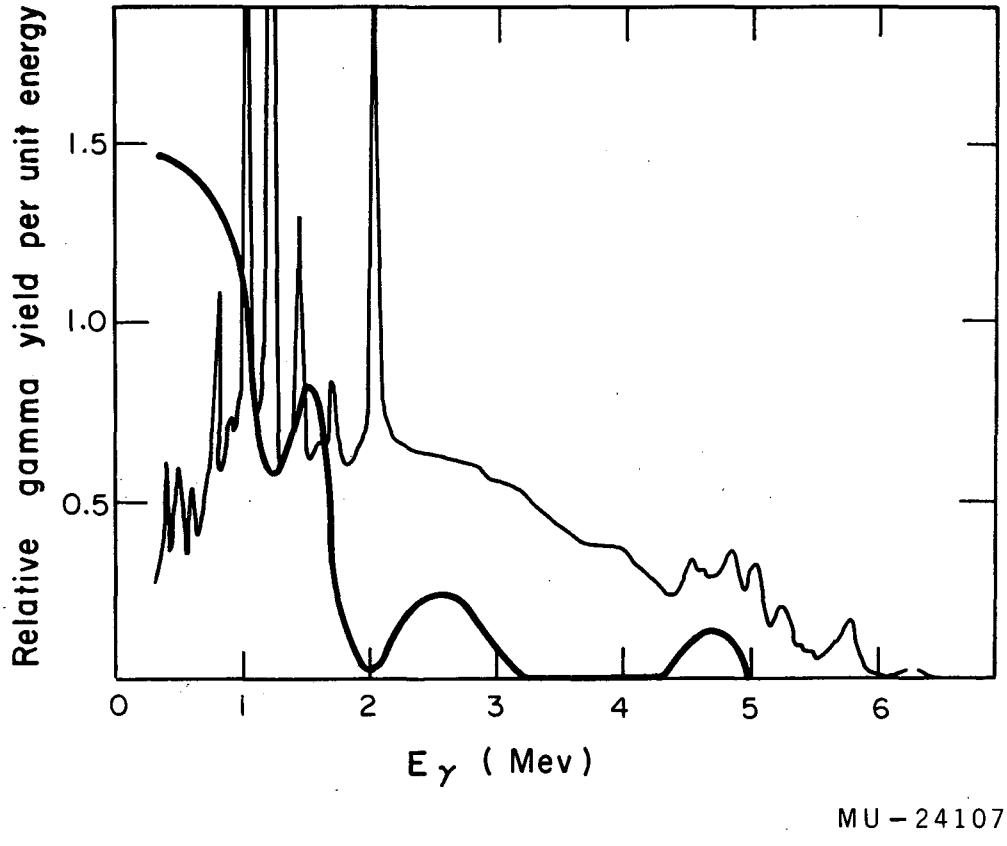

Fig. 22B. Comparison of gamma spectra for this experiment with spectra from thermal-neutron capture. As spherical nuclei, Te + C^{12} at $\bar{E}^{*}$ = 99 Mev (heavy line) is compared with thermal neutrons on tin (light line), since thermal neutron data for cerium are not available. Neutron capture data are from Groshev et al. (Ref. 84).

is a correlation between higher angular momentum or excitation energy and increased quadrupole strength.

However, the spectra for C^{12} on vanadium (Fig. 16B) do not show an increase in the anisotropy over cobalt (Fig. 17A) though the angular momentum is greater. The lowest energy point for 45 deg and the next to lowest for 90 deg are not believed to be as accurate as the others. At 45 deg the spectrum is from a single run on the analyzer rather than from a composite of low- and high-energy spectra; nonlinear effects were sometimes observed in the lowest few channels out of 100. At 90 deg, the high- and low-energy spectra did not match up so well, probably due to rather poor statistics; this region was not smoothed before unfolding.

The spectra for tantalum (Fig. 18) and holmium (Fig. 20A) indicate a preference for quadrupole transitions over the whole energy range. This may be due to the deformation of these nuclei, which enables them to undergo rotational quadrupole transitions up to several hundred kilovolts in energy.

2. Dipole Emission at High J

Despite the higher spin produced in the carbon bombardment of tellurium, there is relatively less quadrupole emission although the initial angular momentum is higher than in the other bombardments. Below 1 Mev (Fig. 16A), dipole emission appears to predominate strongly, with a greater gamma yield at 90 deg. The magnitude of the excess at 90 deg for low gamma energy may be due to experimental error since the statistics are rather poor. The data at 45 deg were taken only once; there was no check in the form of a duplicate run. It still seems safe to observe that anisotropy characteristic of quadrupole emission is considerably lower than in the other alpha bombardments.

A possible explanation for the reduced quadrupole emission is illustrated in Table VII. Here the spin at the start of the gamma cascade is compared with three critical values: J_{mp}, the most probable spin if the states are populated at random without spin restrictions; $J_{rb_{off}} \sim cT$, the spin at which the level density may be expected to fall off[26] from the values given by the equation

$$\omega_J = \omega_o \exp [- (J+ 1/2)^2/2cT];$$

Table VII

Comparison of the spin J_o at the beginning of the gamma cascade with various critical values (see text)

Target	Beam	$\bar{E}^*$ (Mev)	J_o	J_{mp}	J_{rb}	J_c
Te	C^{12}	99	25	7.2	50	10
Ba	α	42	11	5.5	50	10
		26	7	5.5	50	10
V	C^{12}	49	13	3.5	13	7
Co	α	46	10	2.9	13	7
		31	7	2.9	13	7
Ta	α	38	10	5.9	82	12
Ho	α	42	11	6.0	71	12
		26	6	6.0	71	12
Ho	C^{12}	90	25	8.1	74	12
V	C^{12}	101	20	3.8	13	7

and J_c, the spin beyond which correlations between nucleons are predicted to disappear. J_c is interpolated from values given by Mottelson and Valatin[13] and by Pik-Pichak.[29] The values of J_{rb} and J_c are approximate.

Comparison of the barium and tellurium bombardments shows that the spin for the carbon bombardment exceeds J_c by a large margin, while the alpha bombardment gives a spin about equal to it. Quadrupole emission in the heavy-ion case may not be collectively enhanced until the spin has fallen below J_c through dipole emission.

However, the carbom bombardment of vanadium exceeds J_c and yet quadrupole emission still predominates. This result might follow from the closeness of J_o to J_{rb} and consequently the greater angular-momentum restriction on the level density in this case, or to inaccuracy in the value of J_c at low Z.

The tantalum and holmium bombardments at full energy, which showed strong quadrupole characteristics, fall within the limit of J_c. The low-energy bombardment of barium results in a J_o close to the most probable value; the observed gamma distribution being nearly isotropic. Although the low-energy alpha bombardment of cobalt gave a J_o larger than the most probable spin, a mixture of dipole and quadrupole (see Fig. 21) would still be fairly isotropic.

3. The Alignment Model

Equation (43) for the angular distribution of the gamma radiation assumes that all product levels of proper J are selected with equal probability and that the level density is proportional to $\exp[-\hbar^2(J+1/2)^2/2\Im T]$. The failure of this equation to predict the surprisingly large observed anisotropy, when reasonable values of the temperature and moment of inertia are used, suggests that the decay cascade does not proceed through random levels.

Table VIII compares the values expected for b, using a rigid-body moment of inertia and $T = (10\ U/A)^{1/2}$, with the experimental values. Use of a moment of inertia equal to about 0.4 of the rigid-body value, which fits the rotational spectra of the deformed nuclei around holmium and tantalum, would still not give agreement. It is assumed here that the radiation is pure quadrupole; assumption of any mixture of dipole quanta would make the agreement even worse.

Table VIII

Comparison of the experimental values of the anisotropy parameter b with those given by Eq. (43)

Target	$\overline{J^2}$	$T=(10\ U/A)^{1/2}$	b_{calc}	b_{exp}
Ba	44	0.47	-0.029	-0.46
Ho	53	0.42	-0.021	-0.47
Ta	44	0.33	-0.023	-0.52
Co	44	0.71	-0.14	-0.36
V	80	0.74	-0.23	-0.25

If we let $A = -\frac{\hbar^2 J}{\Im T}$, Eq. (43) may be derived to a better approximation as

$$\omega_1(\theta) = 1 + \frac{1/8\ A^2}{1 + 1/4\ A^2} \sin^2\theta \tag{60}$$

for dipole radiation, and

$$\omega_2(\theta) = 1 - \frac{3/8\ A^2}{1 + 5/4\ A^2} \sin^2\theta \tag{61}$$

for quadrupole emission. The limiting value of b for high A in the quadrupole case is -3/10. Because the experimental magnitudes of b are usually even larger, approximations made in the derivations are not valid. A high value of A implies that the density of final states is considerably below that given by Eq. (22).

The large values of anisotropy suggest an alternative analysis that provides limiting values for the anisotropy. One may calculate the anisotropy that would be observed in the gamma radiation from a nucleus of initial angular momentum J_i aligned perpendicular to the beam axis ($M_J = 0$). The cascade of gamma rays is assumed to proceed to J= 0 entirely via the lowest spin states consistent with the multipolarity ($J_i \rightarrow J_i\text{-}L \rightarrow J_i\text{-}2L \cdots L \rightarrow 0$). While J_i may fall at all azimuthal angles about the beam axis with equal probability, it is not necessary to average over them. Quantization about the beam axis leaves the azimuthal angle undefined. In terms of the vector model, one may say that J_i precesses about the beam axis with projection 0; in doing so it passes through all azimuthal positions that may be reached in the experiment.

The angular distribution is given by the equations derived in the study of aligned nuclei:[84]

$$\omega_1(\theta) = 1 + B_2 F_2 P_2 (\cos\theta) \tag{62}$$

for dipole emission, and

$$\omega_2(\theta) = 1 + B_2 F_2 P_2 (\cos\theta) + B_4 F_4 P_4 (\cos\theta) \tag{63}$$

for quadrupole radiation. Here $P_k(\cos\theta)$ is the Legendre polynomial of order k, F_k is a constant whose value depends on the multipolarity of the radiation and the spins of the states involved, and for $M_j = 0$, we have

$$B_2 = - \frac{J(J+1)}{\sqrt{\frac{1}{5} J(J+1)(2J-1)(2J+3)}} ,$$

and

$B_4 = 3\, C^{J4J}_{000}$, where C^{J4J}_{000} is a Clebsch-Gordan coefficient.

A surprising feature of the model is that the angular distribution of the subsequent photons is identical to that of the first. While the J value changes, the magnetic substates are populated in such a way that the angular distribution remains constant. Thus only the angular distribution of the first gamma ray need be calculated explicitly.

Table IX compares the experimental values of $a = W(45)/W(90)$ with those calculated from the alignment equations. Pure quadrupole radiation is assumed. The agreement is very good except for the vanadium target. The experimental values of the anisotropy are lower than those calculated; this is consistent with the alignment model as a limiting case.

For the reactions going to the copper compound nucleus, the observed anisotropy is in better agreement with Strutinsky's prediction than with the alignment model. Since the parameter b is a difference between two observed quantities, the agreement in Table VIII should be considered fairly good for the cobalt as well as the vanadium bombardment. The agreement with the alignment model given in terms of the ratio a in Table IX is not so good. In a nucleus as light as copper, it is reasonable to assume that collective effects will be less prominent than in heavier nuclei.

Table IX

Comparison of experimental values of the parameter a with predictions of the alignment model

Target	Beam	$J_{assumed}$	a_{calc}	a_{exp}
Ba	α	$12 \rightarrow 10 \rightarrow 8 \ldots 0$	+1.57	+1.46
Ho	α	$12 \rightarrow 10 \rightarrow 8 \ldots 0$	+1.57	+1.45
Ta	α	$12 \rightarrow 10 \rightarrow 8 \ldots 0$	+1.57	+1.55
Co	α	$10 \rightarrow 8 \rightarrow 6 \ldots . 0$	+1.58	+1.29
V	C^{12}	$14 \rightarrow 12 \rightarrow 10 . . 0$	+1.56	+1.23

4. Evidence for Vibrational Transitions

The energies of the observed gamma rays are inconsistent with an origin in rotational transitions. For the deformed nuclei, the gamma-ray energies are greater than the distance between levels in the rotational bands. In the vicinity of holmium, the experimental transition energy is approximately $60(J-1/2)$ kev for even-even nuclei. For high J, second-order effects tend to lower the energies. Even if a moment of inertia considerably lower than the experimental rotational value is used, the greater amount of quadrupole emission above 1 Mev is unexplained by rotational transitions.

The liquid-drop calculation shows that at the rotations considered here the equilibrium shape of a nucleus spherical in the ground state is oblate. Deviations from cylindrical symmetry occur only at high rotations. Since the rotation is about the axis of symmetry, the probability of rotational transitions vanishes, according to this model. The energy of rotation is also less than the observed excitation function displacements or excess gamma yields unless one assumes a low moment of inertia. With the rigid-body value, the cerium nucleus has a rotational energy of 6.3 Mev with $J = 25$, while the gamma yield is about 20 Mev.

Transitions between vibrational levels may provide an explanation for the quadrupole emission. The vibrational motion of both spherical and spheroidal nuclei is associated with an angular momentum.[85] The lowest-order motions are the even-parity quadrupole vibrations, whose quanta each carry two units of angular momentum. In the approximation of a three-dimensional isotropic harmonic oscillator, the energies of all the quanta, or phonons, are equal. Therefore, a state with n phonons will have an energy of $(n + \frac{3}{2})\hbar\omega$, where $\omega/2\pi$ is the frequency of the oscillation. The harmonic-oscillator approximation is fairly good; the experimentally measured ratios of the energies of the first two vibrational states range from 1.9 to 2.7.

In spheroidal nuclei, the quadrupole vibrations may be subdivided into β and γ vibrations. The β vibrations carry no component of angular momentum along the symmetry axis, while the γ vibrations have a projection of two units per phonon. Reference to Fig. 1 illustrates the distinction between these two modes. In the β-γ

coordinate system, β vibrations simply correspond to oscillation in the value of β at constant γ, and γ vibrations are described by oscillation in γ at constant β. Since the γ vibrations carry a component of angular momentum about the symmetry axis, it is most probable that these are the vibrations involved in the de-excitation.

The experimental values for the energies of the low-lying vibrational excitations are fairly close to the energies of the observed gamma spectra. Alder and colleagues list the quadrupole vibrational energies of even-even spherical nuclei.[85] Near closed shells, as in the case of isotopes of cerium after neutron evaporation, the energies are nearly 1 Mev. In the region of nickel, they are higher, approximately 1.4 Mev. For deformed nuclei the energies also appear to be above 1 Mev, with Er^{166} at 1.46 Mev and W^{182} at 1.22 Mev. Cohen and Price report a vibrational peak at 1.4 Mev in the inelastic scattering of deuterons on tantalum.[86] This energy corresponds to the peak in the gamma spectrum of Fig. 16C, in which the reaction goes to the tantalum compound nucleus.

The observation of quadrupole photons with energies up to about 2.5 Mev may result from the breakdown of the harmonic-oscillator approximation. The transitions between vibrational levels may not all be equal in energy to the difference between the ground state and first vibrational excitation. Moreover, the selection rule requiring single-phonon transitions may break down, permitting higher-energy transitions.

While the independent-particle equation (57) did not provide gamma-ray yields in agreement with experimental values, addition of a weighting factor to the transition probability enables it to do so. We may choose one peaked at the single-phonon energy of approximately 1 Mev, and fit its width to the experimental gamma yields. A broad function is sufficient. For ease of integration, a function of the Poisson form $E^{\lambda} \exp(-E/\nu)$ was used, with $\lambda\nu = 1$ Mev. Substituting in Eqs. (44) and (45), we have

$$\omega_L(U,E)dE = E^{2L+1}\,\rho(U-E)E^{\lambda}\;e^{-E/\nu}dE/N_L(U);$$

$$N_L(U) = \int_0^{K} E^{2L+1}\,\rho(U-E)E^{\lambda}\,e^{-E/\nu}dE. \qquad (64)$$

The yield from the barium target, for example, can be fit with $\lambda = 1.1$ and $\nu = 0.9$. This function has half-maxima at about 0.2 and 2.7 Mev.

De-excitation through vibrational levels would provide the limited number of states indicated by the agreement with the alignment model. Final states differing only in the number of vibrational quanta may be preferred at each step of the gamma cascade. While branching in the decay is probably present, the agreement of the alignment prediction with the experimental results shows that final states are not populated in a random manner.

Figure 23 illustrates a possible mode of de-excitation in the case of a spheroidal nucleus. The energy-level diagram of the product nucleus is resolved into groups of states, each with the same numbers of γ-vibrational phonons. Neutron emission may carry the nucleus to levels of the vibrational group with m phonons at right. Single-particle transitions, being quite fast, may occur first and take the nucleus to the lowest state of this group. Henceforth, it may proceed by vibrational transitions through the lowest states of the other groups to the ground state.

4. Octupole States

While the simplest nuclear vibrations are of the even-parity quadrupole form, odd-parity octupole vibrations have also been seen.[87] The so-called anomalous inelastic-scattering peaks are generally attributed to such vibrations, which occur at an energy of 2 or 3 Mev throughout the periodic table.[87] Peaks at the same energies are also seen in the gamma spectra of this experiment. Although the statistics are generally poor in that energy range, the presence of the peaks in most of the spectra must be more than coincidence.

The correspondence between the peaks in the gamma spectra and the inelastic peaks is illustrated in Table X. Both fall within the energy resolution in all cases except rhenium (Ta + α), in which the gamma peak is rather small. While no data are available for cerium, lanthanum and praseodymium have inelastic peaks at 2.5 Mev. These data are consistent with the 2.7-Mev peak in the gamma spectrum of the intermediate cerium.

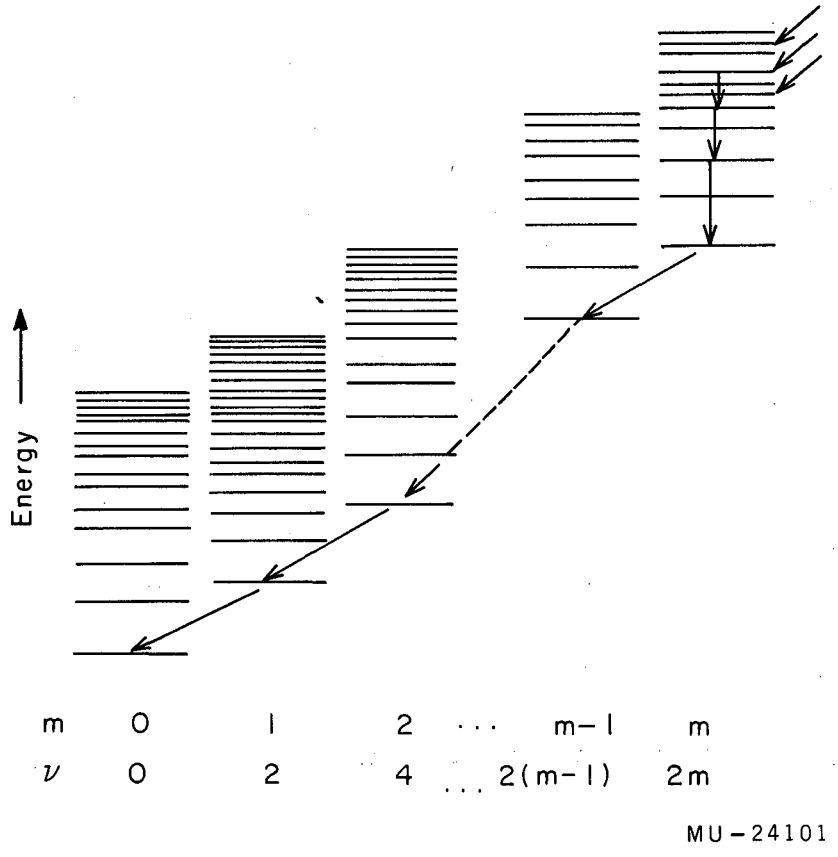

Fig. 23. Schematic de-excitation. Levels of the product nucleus are grouped according to n, the number of γ-vibrational phonons. Symbol ν is the maximum component of vibrational angular momentum on the symmetry axis.

Table X

Energies of gamma peaks compared with energies of anomalous inelastic peaks

Compound nucleus	See fig. no.	Gamma peak energy (this work)	Anomalous peak energy (scattering studies)	See ref. no.
Cu	16B, 16C, 17A, 17B	3.3, 2.6	3.2, 2.5	86, 87
Te			3.0, 2.0	88
Ce	16A	2.7		
La			2.5	89
Ba			3.0	89
Ta	16C	3.3	3.0	90
		no peak at	3.0	86
Re	18	4.0	none	89

In all cases except the copper compound nucleus, the gamma peaks are more intense at 45 deg. In fact, for the full-energy alpha bombardments of barium, holmium, and tantalum, the peaks were indistinguishable at 90 deg from the statistical fluctuations and disappeared in the smoothing of the raw spectra before unfolding. This anisotropy is evidence for the high-multipole character of the radiation. The radiation need not be the slow E_3; for instance, M2 transitions to low-lying states might be possible.

It is not certain whether the radiation comes from de-excitation of a compound nucleus through negative-parity vibrations or from inelastic excitation of the target. The latter case corresponds to gamma rays coincident with beam particles scattered through an angle large enough to miss the stopping scintillator. The two cases may be distinguished if the target and compound-state nuclei have different anomalous peak energies. In tellurium the anomalous peak is at 2.1 Mev, while in cerium it is probably about 2.7 Mev. The spectrum for the tellurium target (Fig. 16A) shows a large peak at 2.7 Mev, but there is also a suggestion of one at 2.1 Mev. Other comparisons are not possible because the peaks for target and residual nucleus are too close in energy or because data are not available.

In the barium target, the 26-Mev alpha bombardment (Fig. 19B) produced a greater peak in the spectrum than did the one at 42 Mev. In addition, the anisotropy of the peak was no longer present at the lower energy. Likewise, in holmium the peak was no longer anisotropic at the lower bombarding energy, and the average over all angles must be greater than at the higher energy. The lower yield at 42 Mev, where there are more decay channels, suggests that inelastic scattering may be responsible, though the tellurium bombardment indicates otherwise. The lower anisotropy at 26 Mev may be the result of the lower angular momentum.

V. CONCLUSIONS

From the data obtained in this experiment, one may draw several conclusions regarding the de-excitation of the compound nuclei studied in the presence of both high and moderate amounts of angular momentum:

1. The yield of gamma rays in the heavy-ion bombardments was in every case greater than the neutron binding energy. This finding is in contradiction to the frequently held assumption of evaporation theory that gamma emission does not compete with particle emission above the neutron threshold.

2. The total energy of the gamma rays in the heavy-ion bombardments was in agreement with the magnitude of the observed shifts in the excitation functions.

3. At the same excitation energy, the number of photons from the copper compound nucleus was greater in the presence of a larger angular momentum. This observation demonstrates that the increased yields is an angular-momentum effect.

4. The greater part of the angular-momentum release occurs through quadrupole transitions, except perhaps at the highest angular momenta. This conclusion may be formed from the angular distribution of the photons, and also from a comparison of the number of photons to the estimated angular momentum at the beginning of photon emission.

5. Single-particle transitions cannot account for the quadrupole emission. Therefore, it must be attributed to collective effects. The energies of the gamma rays and the insufficient amount of the rotational energy suggest that the collective effects involve vibrational modes. There is a possibility that octupole as well as quadrupole vibrations may be involved.

The effects of this experiment depend partly on knowledge of the compound-nucleus cross section. Better data on the cross sections than is presently available would make interpretation of the gamma yields more reliable.

Further work in experiments similar to this would appear to be useful in the study of collective modes of de-excitation. Longer runs with better statistics and observation of the gamma yield at a number of angles would make interpretation more accurate. With heavy ions, the collective

effects appear less strong at 100 Mev than at half that energy. The breakdown of the collective modes at high spin can perhaps be more readily studied in this way than by Coulomb excitation. It is hoped that additional experiments of the sort described here will be performed in the future.

APPENDICES

A. Calculation of the Rotating Liquid-Drop Energies

Because of the inadequacy of published tables of the elliptic functions appearing in Eqs. (24) and (28), it was necessary to calculate them on the IBM 704. For convenience, the whole calculation was programmed with the elliptic functions evaluated in a subroutine. This subroutine should be useful in any Fortran program requiring the use of elliptic functions. The calculation is carried out according to Eq. (34).

The program requires the following quantities to be furnished by the user:

XSTART, the first value of x for which energies are computed

XSTOP, the final value of x

RSTART, the initial value of $R = \lambda^2$

RSTOP, the final value in the series of R values

ISTEPS, the number of values of β between 0 and 1.0

JSTEPS, the number of values of γ between 120 deg and 180 deg

KSTEPS, the number of values of x between XSTART and XSTOP

LSTEPS, the number of values of R between RSTART and RSTOP

XFIXED and

RFIXED, exact values of x and R for use with the option described below

$W_1 \ldots W_6$ and

$Z_1 \ldots Z_6$, two series of constants given below.

The number of intervals (JSTEPS, etc.) includes the first and last value of the parameter, except for ISTEPS, which does not count $\beta = 0$.

An option is available to compute the energies for only one value of x and R, given by XFIXED and RFIXED. Sense switch No. 3 is placed down to exercise this option.

The elliptic function subroutine ELLIP was written in Fortran from the equations given in the Share program for elliptic functions, GMIEF-1-C3. The number of terms in the summation was increased for high values of k to extend the range of k. The authors of the Share program give the accuracy of the method as better than four in the eighth digit.

The equation used are:

$$F(\phi,k) = \sum_{i=1}^{n} (\phi_i - \phi_{i-1}) \sum_{j=1}^{6} \frac{W_j}{\sqrt{1-k^2\sin^2\left[(\phi_i-\phi_{i-1})\, Z_j+\phi_{i-1}\right]}}$$

and

$$E(\phi,k) = \sum_{i=1}^{n} (\phi_i - \phi_{i-1}) \sum_{j=1}^{6} W_j \sqrt{1-k^2\sin^2\left[(\phi_i - \phi_{i-1})\, Z_j + \phi_{i-1}\right]}$$

The number of terms n, in the summation is given by:

$n = 1$ for $k \leq 0.55$

$n = 2$ for $0.55 < k \leq 0.85$

$n = 3$ for $0.85 < k \leq 0.95$

$n = 5$ for $0.95 < k \leq 0.99$

$\phi_o = 0.$

$\phi_i = \frac{i}{n}\,\phi$, for i = 1, 2, ...n.

The constants used in the Gaussian integration are:

$Z_1 = 0.0337652429$

$Z_2 = 0.1693953068$

$Z_3 = 0.3806904070$

$Z_4 = 0.6193095930$

$Z_5 = 0.8306046932$

$Z_6 = 0.9662347571$

$W_1 = W_6 = 0.856622462$

$W_2 = W_5 = 0.1803807865.$

$W_3 = W_4 = 0.2339569673.$

The constants W_i and Z_i, as well as the parameters of the calculation, are read from punched cards by the main program. The format appears in the listing at the end of this appendix.

The running time depends on the number of values of the parameters for which calculations are done. For 40 values of β and 13 of γ, the time is about five seconds per pair of x,R values.

```
C     PROGRAM BLOB FOR ENERGIES OF DEFORMED ROTATING  LIQUID DROP

    1 DIMENSION BSTEP(40),INTGAM(40), SURFE(40,40), ECOUL(40,40),
     XEROT(40,40),ETOTAL(40,40),W(6), Z(6), PSI(6)
    5 READ 10, XSTART, XSTOP, RSTART, RSTOP, ISTEPS, JSTEPS, KSTEPS,
     XLSTEPS, XFIXED, RFIXED
   10 FORMAT (4F8.4 ,4I4,2F8.4)
   12 READ 13, (W(I),I=1,6),(Z(J),J=1,6)
   13 FORMAT (6F12.9 )
   30 DO 200 I=1,ISTEPS
      B = I
      BSTEPS = ISTEPS
      BETA = (B*1.0)/BSTEPS
      BSTEP(I) = BETA
   35 DO 200 J=1,JSTEPS
      G=J
      GSTEPS=JSTEPS
      GAMMA      = 120.0+((G-1.0)*60.0)/(GSTEPS-1.0)
      INTGAM(J) = GAMMA
      PI= 3.14159265
      GAMMA = GAMMA/57.2957795
   50 CANG=COSF(GAMMA)
      BANG=COSF(GAMMA+(2.0*PI)/3.0)
      AANG=COSF(GAMMA -(2.0*PI)/3.0)
   60 ASQ= EXPF ((2.0*BETA)*AANG)
      BSQ= EXPF ((2.0*BETA)*BANG)
      CSQ= EXPF ((2.0*BETA)*CANG)
   70 ALPASQ= (ASQ-CSQ)/ASQ
      DLTASQ= (BSQ-CSQ)/BSQ
      TSQ= DLTASQ/ALPASQ
      T= SQRTF(TSQ)
      ALPHA= SQRTF(ALPASQ)
      CHI= SQRTF(1.0-ALPASQ)
      PHI = ATANF(ALPHA/CHI)
   80 RHO=SQRTF(1.0-DLTASQ)
      CINVER= EXPF(-BETA*CANG)

   83 CALL ELLIP (PHI, T, W, Z, E, F)
   85 BSURF= 0.5*CINVER*(RHO*CHI+(1.0/ALPHA-ALPHA)*F+ (ALPHA*E))

C     NOW CALCULATE BCOUL AND BROT

  100  EPSLON = SQRTF(1.0/(ASQ-CSQ))
      TAU = EPSLON * SQRTF(ASQ-BSQ)
      CALL ELLIP(PHI, TAU, W, Z, E, F)
  120 BCOUL = EPSLON*F
      BROT = 2.0/(ASQ+BSQ)
      SURFE(I,J) = BSURF-1.0
      ECOUL(I,J) = BCOUL-1.0
  200 EROT(I,J) = BROT

C     WRITE TABLES OF SURFACE AND COULOMB ENERGY AND BROT

      WRITE OUTPUT TAPE 1,210
  210  FORMAT(22H1SURFACE ENERGY CHANGE)
  211 WRITE OUTPUT TAPE 1,212, (INTGAM(J),J=1,JSTEPS)
  212 FORMAT (7H0GAMMA= 14I8)
  213 WRITE OUTPUT TAPE 1,214
  214 FORMAT(5H BETA)
      DO 215 I=1, ISTEPS
  215 WRITE OUTPUT TAPE 1,216, BSTEP(I), (SURFE(I,J), J=1, JSTEPS)
  216  FORMAT (1H F5.3, F10.5, 13F8.5)
      WRITE OUTPUT TAPE 1,230
```

```
  230 FORMAT(22H1COULOMB ENERGY CHANGE)
  231 WRITE OUTPUT TAPE 1,212, (INTGAM(J),J=1,JSTEPS)
  232 WRITE OUTPUT TAPE 1,214
  234 DO 236 I=1,ISTEPS
  236 WRITE OUTPUT TAPE 1,216, BSTEP(I), (ECOUL(I,J), J=1, JSWEPS)
      WRITE OUTPUT TAPE 1,240
  240 FORMAT(27H1ROTATIONAL PARAMETER BROT    )
  241 WRITE OUTPUT TAPE 1,212, (INTGAM(J),J=1,JSTEPS)
  242 WRITE OUTPUT TAPE 1,214
  244 DO 246 I=1,ISTEPS
  246 WRITE OUTPUT TAPE 1,216, BSTEP(I), (EROT (I,J), J=1, JSTEPS)

C     OPTION FOR SINGLE X AND R VALUE

  247 IF (SENSE SWITCH 3) 248,255
  248 DO 250 I=1, ISTEPS
      DO 250 J=1, JSTEPS
  250 ETOTAL(I,J)=SURFE(I,J)+2.0*XFIXED*ECOUL(I,J)+RFIXED*EROT(I,J)
  252 GO TO 287

C     COMPUTE ENERGY TABLES FOR MESH OF X AND R VALUES

  255 DO 285 K=1,KSTEPS
      XSTEP = K-1
      XSTEPS = KSTEPS-1
      X = XSTART + XSTEP*(XSTOP-XSTART)/XSTEPS
  260 DO 285 L=1,LSTEPS
      RSTEP = L-1
      RSTEPS = LSTEPS-1
      R = RSTART + RSTEP*(RSTOP-RSTART)/RSTEPS
  270 DO 275 I=1,ISTEPS
      DO 275 J=1,JSTEPS
  275 ETOTAL(I,J)=SURFE(I,J)+2.0*X    *ECOUL(I,J)+R      *EROT(I,J)
  278 WRITE OUTPUT TAPE 1, 280
  279 WRITE OUTPUT TAPE 1, 277, X, R
  277 FORMAT (28HOFISSIONABILITY PARAMETER X=  F5.3,
     X16HLAMBDA SQUARED = F5.3)
  280 FORMAT (51H1TOTAL ENERGY CHANGE AS FRACTION OF SURFACE ENERGY )
  281 WRITE OUTPUT TAPE 1,212, (INTGAM(J),J=1,JSTEPS)
  282 WRITE OUTPUT TAPE 1,214
  284 DO 285 I=1,ISTEPS
  285 WRITE OUTPUT TAPE 1,216, BSTEP(I),(ETOTAL(I,J), J=1, JSTEPS)
  286 GO TO 299
  287 CONTINUE
  288 WRITE OUTPUT TAPE 1, 280
  290 FORMAT (51H1TOTAL ENERGY CHANGE AS FRACTION OF SURFACE ENERGY )
  291 WRITE OUTPUT TAPE 1,212, (INTGAM(J),J=1,JSTEPS)
  292 WRITE OUTPUT TAPE 1,214
  294 DO 295 I=1,ISTEPS
  295 WRITE OUTPUT TAPE 1,216, BSTEP(I),(ETOTAL(I,J), J=1, JSTEPS)
  299 CONTINUE
  300 END (0,1,0,0,1)
```

```
      SUBROUTINE ELLIP (PHI, T, W, Z, E, F)
      DIMENSION W(6), Z(6), PSI(6)

C     DETERMINE THE NUMBER OF ITERATIONS

    5 IF(T-0.55) 10,10,15
   10 N=1
   11 GO TO 30
   15 IF(T-0.85) 17,17,20
   17 N=2
   18 GO TO 30
   20 IF(T-0.95) 22,22,25
   22 N=3
   23 GO TO 30
   25 IF (T-0.99) 27 ,27,29
   27 N = 5
   28 GO TO 30
   29 E = SINF (PHI)
      DIFFE = (1.0+E)/(1.0-E)
      F = 0.5*LOGF (DIFFE)
      GO TO 91
   30 PSI(1) = 0.0

C     DO SUMMATIONS TO FIND E AND F

      DO 35 I=1,N
      FLI = I
      FLN = N
   35 PSI(I+1) = FLI*PHI/FLN
      F = 0.0
      E = 0.0
   40 DO 90 I=1,N
      FSUMJ = 0.0
      ESUMJ = 0.0
   50 DO 75 J = 1,6
      OMEGA = (PSI(I+1) - PSI(I))*W(J) + PSI(I)
      SINOM = SINF(OMEGA)
   60 CN = SQRTF(1.0-T*T*SINOM*SINOM)
      FTERMJ = Z(J)/CN
   70 ETERMJ = Z(J)*CN
      FSUMJ = FSUMJ + FTERMJ
      ESUMJ = ESUMJ + ETERMJ
   75 CONTINUE
      FTERMI =FSUMJ*(PSI(I+1) - PSI(I))
      ETERMI =ESUMJ*(PSI(I+1) - PSI(I))
      F = FTERMI + F
      E = ETERMI + E
   90 CONTINUE
   98 RETURN
  100 END(0,1,0,0,1)
```

B. The Unfolding of the Gamma Spectra

The method of Scofield was used for correcting the observed pulse-height spectrum for the response of the sodium iodide crystal.[72] It is based on the use of a response matrix, but rather than direct inversion of the matrix to obtain the incident-photon spectrum, successive approximation by correction factors is used.

The response of the counter in counts per photon is a function R(V, E) of both the gamma energy E and the pulse-height voltage V. If the incident spectrum of the photons is N(E), the observed pulse-height distribution is

$$C(V) = \int_0^\infty R(V,E)\, N(E)dE.$$

Use of a matrix is well adapted to the discrete channels of the pulse-height analyzer. In the matrix formulation, we have

$$\bar{C} = \bar{R} \times \bar{N},$$

where

$$R_{ij} = \int_{V_{i-1}}^{V_i} R(V,\bar{E}_j)dV,$$

$$R(V,\bar{E}_j) \simeq \int_{E_{j-1}}^{E_j} R(V,E)dE/(E_j - E_{j-1}),$$

$$C_i = \int_{V_{i-1}}^{V_i} C(V)dV,$$

and

$$N_j = \int_{E_{j-1}}^{E_j} N(E)dE.$$

Theoretically, inversion of the matrix gives the initial spectrum

$$\bar{N} = \bar{R}^{-1} \times \bar{C}.$$

While mathematically exact, this method is unsuitable in the presence of statistical fluctuations in the data and inaccuracy in the response function. However, the effect of matrix inversion may be obtained by successive approximations. The observed spectrum is multiplied by the response matrix to obtain a doubly-folded spectrum. Each channel or element of the observed spectrum is individually corrected by a factor of the ratio of the original to the doubly-folded value of that element. The corrected spectrum is multiplied by the response matrix and the ratios again found element by element. These ratios are applied as

corrections to the original observed spectrum, not to the first corrected spectrum. The process is repeated until the desired degree of convergence is obtained.

If we denote the original observed spectrum by $\bar{C}_o$ and the approximations to the incident gamma spectrum by $\bar{N}_i$, we have

$$\bar{N}_1 = \bar{C}_o.$$

The corrected observed spectra may be denoted $\bar{C}_i$; therefore we can write

$$\bar{C}_1 = \bar{R}x\bar{N}_1,$$

$$(\bar{N}_2)_i = \frac{(\bar{N}_1)_i}{(\bar{C}_1)_i} (\bar{C}_o)_i$$

$$\bar{C}_2 = \bar{R}x\bar{N}_2,$$

$$(\bar{N}_3)_i = \frac{(\bar{N}_2)_i}{(\bar{C}_2)_i} (\bar{C}_o)_i, \quad \text{etc.}$$

In practice, 50 iterations were found to give convergence within one part in 10^4.

In the routine GAMSPEC a group of several spectra is unfolded at one run. The spectra of this group must have the same energy intervals and angle of observation, while a gain adjustment factor is specified for each spectrum individually. The data cards for the spectrum are preceded by a card specifying the following constants:

MESH, the number of channels in the spectrum and the dimension of the response matrix;

NRUNS, the number of spectra in the group;

THRES, the lower gamma-energy limit;

EMAX, the upper gamma-energy limit.

The data cards then follow, with each spectrum preceded by the factor GAIN by which the energy scale is to be multiplied. The formats for these cards are given in the Fortran listing at the end of this appendix.

If the value of GAIN is not unity, subroutine GAINAJ is called in to apply the correction. It interpolates linearly between the points of the input spectrum and corrects for changed channel width. In extrapolating at either end of the spectrum, it assumes an exponential

dependence on pulse height. The corrected input spectrum is written on tape 3.

The response matrix may be generated in subroutine RESPON or read from tape 5, according to the position of sense switch 5. If it is available on tape, the program proceeds to smooth the spectrum if sense switch 1 is down; then it unfolds the spectrum according to the iterative scheme mentioned. The successive approximations are listed on tape 3 if sense switch 3 is depressed.

The geometry factor for 45-deg runs is used if sense switch 4 is placed down. This switch is left up for the 90-deg spectra. Sense switch 2 is used to call for smoothing of the spectrum after unfolding.

After unfolding, the resultant incident spectrum is multiplied by the response matrix as a check and the product written on tape 3. The product should be equal to the input spectrum corrected for gain and geometry. The unfolded spectra are written smoothed and unsmoothed on tape 3.

In writing the response matrix, subroutine RESPON selects the energy and pulse-height intervals according to the specified values of MESH, THRES, and EMAX. The pulse-height intervals are divided into 10 subintervals, the response of the crystal calculated in function subroutine CURVE, and an average taken. The response is calculated according to the functional dependences on energy and pulse height given in Table II Section III.

The running time for the evaluation of the response matrix is about 3 minutes for 20 channels and 18 minutes for 50 channels. If the matrix is on tape, the running time per spectrum is less than 30 seconds for 20 channels and slightly over 1 minute for 50 channels.

Fortran listings of program GAMSPEC and associated subroutines are given on the following pages.

```
C      GAMMA SPECTRUM ANALYSIS - PROGRAM GAMSPEC

       DIMENSION R(50,50), F(50),H(50), B(50,50), X(50,50),D(50,50),
      XW(50,50), SUM(50), ESUM(50), E(50), RESID(50), DIF(50,50),
      X Y(50,50)
       READ 5, MESH, NRUNS, THRES, EMAX
     5 FORMAT (2I5, 2F10.3 )
       WRITE OUTPUT TAPE 3,13
    13 FORMAT     (14H1INPUT SPECTRA     )
    10 DO 35 JS=1, NRUNS
       READ 12, GAIN, (F(I), I=1,MESH     )
    12 FORMAT (7F10.3)
       WRITE OUTPUT TAPE 3, 93, JS, (F(J), J=1,MESH)
       CALL EFM (0,0)

C      ADJUST GAIN IF REQUIRED

       IF (GAIN-1.0) 20,30,20
    20 CALL GAINAJ (F, H, MESH, GAIN, THRES, EMAX)
       DO 25 I=1, MESH
    25 B(I,JS) = H(I)
       GO TO 35
    30 DO 34 K=1, MESH
    34 B(K,JS) = F(K)
    35 CONTINUE
       FLMESH = MESH
       DO 36 J=1, MESH
       EINDEX = J
    36 E(J) = (( EMAX-THRES)/FLMESH) * (EINDEX-0.5) + THRES

C      GENERATE RESPONSE MATRIX OR READ IT FROM TAPE

       IF (SENSE SWITCH 5) 40,47
    40 CALL RESPON ( MESH, EMAX, THRES, R )
       WRITE OUTPUT TAPE 5, 45, ((R(I,J), I=1,MESH), J=1, MESH)
    45 FORMAT (1P5E18.9)
       END FILE 5
       REWIND 5
       GO TO 48
    47 READ INPUT TAPE   5, 45, ((R(I,J), I=1,MESH), J=1, MESH)
       REWIND 5
    48 CONTINUE

C      OPTIONAL SMOOTHING BEFORE UNFOLDING

       IF (SENSE SWITCH 1) 50,58
    50 DO 55 N=1,NRUNS
       MINUS = MESH - 1
       DO 53  L=2, MINUS
    53 X(L,N) = 0.25*B(L-1,N) + 0.5*B(L,N) + 0.25*B(L+1,N)
       X(MESH,N) = 0.25* B(MINUS,N) + 0.75* B(MESH,N)
       X(1,N) = 0.75*B(1,N) + 0.25* B(2,N)
       DO 55 L=1, MESH
    55 B(L,N) = X(L,N)

C      UNFOLD BY SUCCESSIVE APPROXIMATIONS

    58 DO 140 N=1,NRUNS
       DO 110 I=1, MESH
       DO 110 J=1,50
       DIF (I,J) = 0.0
       D(I,J) = 0.0
   110 W(I,J) = 0.0
```

```
      DO 115 I=1,MESH
  115 W(I,1) = B(I,N)
      DO 120 I = 1, MESH
      DO 120 J = 1, MESH
  120 D(I,1) = R(I,J) * W(J,1) + D(I,1)
      DO 130 L= 1,49
      LL= L+1
      DO 122 I=1, MESH
  122 W(I,L+1) =(W(I,L) / D(I,L)) * W(I,1)
      RESID(1) = 0.0
      RESID (LL) = 0.0
      DO 125 J=1, MESH
      DIF(J,L) = W(J,L+1) - W(J,L)
  125 RESID (LL) = RESID (LL) + DIF(J,L) * DIF(J,L)
      RESID (LL) = SQRTF (RESID(LL))
      IF (L-2) 127,127,126

C     CHECK FOR DIVERGENCE OF APPROXIMATIONS

  126  IF (RESID(LL) -RESID(LL-1) ) 127,230,230
  127 DO 130 I=1, MESH
      DO 130 J=1, MESH
  130 D(I,L+1) = R(I,J)*W(J,L+1) + D(I,L+1)
      GO TO 131
  230 LL=LL-1
  131 DO 132 I=1, MESH
  132 X(I,N) = W(I,LL)

C     OPTIONAL WRITING OF APPROXIMATIONS

      IF (SENSE SWITCH 3) 133,140
  133 WRITE OUTPUT TAPE 3, 134
  134 FORMAT (28H1 SUCCESSIVE APPROXIMATIONS  )
      DO 135 J=1,25
  135 WRITE OUTPUT TAPE 3 , 136, N,J,(W(I,J), I=1,MESH), RESID(J)
  136 FORMAT (4HORUN I2, 3H J=I2,1P10E10.3/(1PE21.3,1P9E10.3 ))
  140 CONTINUE

C     GEOMETRY FACTOR FOR 45 DEGREE RUNS

      IF (SENSE SWITCH 4) 142,150
  142 DO 146 N=1, NRUNS
      DO 146 I=1, MESH
  146 X(I,N) = X(I,N) * 2.25
  150 DO 69 J=1,NRUNS

C     COMPUTE SUM OF COUNTS AND AVERAGE ENERGY

      SUM (J) = 0.0
      ESUM (J) = 0.0
      DO 68 L = 1, MESH
      ESUM (J) = ESUM (J) + E (L)*X(L,J)
   68 SUM (J) = SUM (J) + X (L,J)
   69 ESUM (J) = ESUM (J) / SUM (J)

C     WRITE SMOOTHED INPUT SPECTRUM AND UNFOLDED SPECTRUM

   90 WRITE OUTPUT TAPE 3, 92
      DO 91 J =1,NRUNS
```

```
   91 WRITE OUTPUT TAPE 3, 93, J, ( B (I,J), I = 1, MESH )
   92 FORMAT ( 41 H0 SPECTRA ADJUSTED FOR GAIN AND SMOOTHED    )
   93 FORMAT (  11HORUN NUMBER I2,1P10E10.3/(13H              1P10E10.3)
   94 FORMAT (26H              TOTAL COUNTS  F10.1 ,  15H AVERAGE ENERGY
     X F8.3  )
      WRITE OUTPUT TAPE 3, 96
   96 FORMAT (25H0UNFOLDED GAMMA SPECTRA     )
      DO 95 J = 1, NRUNS
      WRITE OUTPUT TAPE 3, 93, J, (X (I,J), I=1, MESH )
   95 WRITE OUTPUT TAPE 3, 94, SUM (J)    , ESUM (J)

C     MULTIPLY UNFOLDED SPECTRUM BY RESPONSE MATRIX TO CHECK

      WRITE OUTPUT TAPE 3,320
  320 FORMAT (14H0CHECK SPECTRA )
      DO 325 N=1,NRUNS
      DO 324 I=1, MESH
      DO 324 J=1, MESH
  324 Y(I,N) = Y(I,N) + R(I,J) *X(J,N)
  325 WRITE OUTPUT TAPE 3, 93, N, (Y(I,N), I=1, MESH)

C     OPTIONAL SMOOTHING AFTER UNFOLDING

      IF (SENSE SWITCH 2)  240, 97
  240 WRITE OUTPUT TAPE 3, 250
  250 FORMAT (26H SMOOTHED UNFOLDED SPECTRA  )
      DO 350 N=1,NRUNS
      MINUS = MESH - 1
      DO 340 L=2, MINUS
  340 Y(L,N) = 0.25*X(L-1,N) + 0.5*X(L,N) + 0.25*X(L+1,N)
      Y(MESH,N) = 0.25* X(MINUS,N) + 0.75* X(MESH,N)
      Y(1,N) = 0.75*X(1,N) + 0.25* X(2,N)
      DO 345 L=1,MESH
  345 X(L,N) = Y(L,N)
  350 WRITE OUTPUT TAPE 3, 93, N, (X(I,N), I=1,MESH)
   97 CONTINUE
      END FILE 3
      REWIND 3
  100 END ( 0,1,0,0,0 )


      SUBROUTINE GAINAJ (F,H,NBOXES,GAIN, THRES, EMAX)

      DIMENSION E(50), EA(50), H(50), G(50), F(50)
      BOTE = THRES * GAIN
      TOPE = EMAX * GAIN
      DO 10 N=1, NBOXES
      BOXES = NBOXES
      P=N
      E(N) =(((TOPE-BOTE )/BOXES) * (P-0.5))+ BOTE
      G(N) = F(N)/GAIN
   10 EA(N)=(((EMAX-THRES)/BOXES) * (P-0.5))/     + THRES
      IF ( GAIN - 1.0 ) 60,60,14

C     GAIN TO BE INCREASED

   14 H(1) = G(1) - (G(2)-G(1))*(E(1)-EA(1))/(E(2)-E(1))
   15 DO 50 N=2,NBOXES
      DO 30 L=2,N
```

```
      M=N-L+1
      IF (EA(N)-E(M)) 30,30,45
   30 CONTINUE
   45 H(N) =G(M) + (G(M+1)-G(M))*(EA(N)-E(M))/(E(M+1)-E(M))
   50 CONTINUE
   55 GO TO 90

C     GAIN TO BE DECREASED

   60 DO 80 N=1,NBOXES
      NLESS = NBOXES - N
      DO 70 L=1,NLESS
      M=N+L
      IF (EA(N) -E(M)) 75,75,70
   70 CONTINUE
   72 H(N) = G(NBOXES) *(G(NBOXES)/G(NBOXES-1))**((EA(N)-E(NBOXES))/
     X (E(NBOXES)-E(NBOXES-1))  )
      GO TO 80
   75 H(N) = G(M) -(G(M)-G(M-1)) * (E(M)-EA(N))/(E(M)-E(M-1))
   80 CONTINUE
   90 RETURN
   95 END (0,1,0,0,1)


      SUBROUTINE RESPON (MESH, EMAX, THRES,R)

      DIMENSION R(50,50) , E(50)
      FLMESH = MESH

C     LOCATE ENERGY INTERVALS

      DO 12 J=1, MESH
      EINDEX = J
   10 E(J) = (( EMAX-THRES ) /FLMESH ) * ( EINDEX- 0.5 ) + THRES
      DO 12 K = 1, MESH
   12 R (J,K ) = 0.0

C     LOCATE PULSE HEIGHT INTERVALS

   15 DO 60 J = 1, MESH
      DO 50 I = 1, MESH
      ELEM = 0.0

C     AVERAGE RESPONSE OVER 10 PULSE HEIGHT INTERVALS

      DO 25 L = 1,10
      XINDEX = 10* ( I-1 ) + L
      X = (( EMAX-THRES) / (FLMESH*10.0)) * (XINDEX-0.5) + THRES
      ELL = L
      IF (X- 1.25*E(J)) 25,25,55
   25 ELEM = ELEM    + CURVE(E(J),X)
   50 R (I,J) = R (I,J) + ELEM   /10.0
   55 R (I,J) = R (I,J) + ELEM / ELL
   60 CONTINUE
      DO 70 I=1,MESH
      DO 70 J=1,MESH
   70 R(I,J) = R(I,J) * 100.0/ FLMESH
      RETURN
      END (0,1,0,0,1)
```

```
      FUNCTION CURVE (E,X)
C     PHOTO AND ESCAPE PEAKS
      PHOT1 = 0.0
      PHOT2 = 0.0
      PHOT3 = 0.0
      C = 0.361
      U = 0.0815* ((E)**0.5)
C     CONSTANTS FOR 10 PERCENT RESOLUTION AT 0.66 MEV
      IF (E-0.65) 5,7,7
    5 HITE1 = 0.00459 * E**(-0.033)
      GO TO 8
    7 HITE1 = 0.00253 * E**(    -1.46)
    8 PHOT1 = HITE1 * EXPF(-(X-E       )**2.0/ (C*U**2.0))
      IF (E-1.75)  11,9,9
    9 HITE2 = 1.437*HITE1*LOGF(E/1.75) /2.303
      HITE3 = 0.569*HITE1*LOGF(E/1.75) /2.303
      PHOT2 = HITE2 * EXPF(-(X-E+0.51  )**2.0/ (C*U**2.0))
      PHOT3 = HITE3 * EXPF(-(X-E+1.02  )**2.0/ (C*U**2.0))
      IF (X-0.4) 10,102,102
  102 IF (X-0.6) 103,103,10
C     ANNIHILATION PEAK
  103 ANNHT = 1.2*  (HITE2 + HITE3)
      ANNIH = ANNHT * EXPF(-(X-0.51) **2.0 / 0.00122 )
      GO TO 11
   10 ANNIH = 0.0
   11 IF (E-1.0) 14,12,12
C     COMPTON DISTRIBUTION
   12 COMPEJ = E-0.25
   13 GO TO 20
   14 IF (E-0.5) 17,15,15
   15 COMPEJ = 0.9*E - 0.15
   16 GO TO 20
   17 COMPEJ = 0.6 * E
   20 CONTINUE
      COMAR = 0.0077 - 0.001806 / (E+0.235)
      COMPHT = COMAR / ((E+COMPEJ    ) * 10.0 )
C     SCATTER PEAK
  121 IF (X-0.5) 22,21,21
   21 SCATR = 0.0
      GO TO 24
   22 SCATHT = 0.455*COMPHT
      SCATPS = 0.145 + 0.0675*E
      SCWID = 0.08
      SCATR = SCATHT * EXPF (-(X-SCATPS)**2./(C*SCWID**2.0))
C     COMPTON DISTRIBUTION WITH ESCAPE PEAKS
```

```
 24 IF (E-1.75) 25,25,30
 25 IF ( X-COMPEJ) 26,26,27
 26 COMPT = COMPHT
    GO TO 50
 27 IF (X-E ) 28,28,29
 28 COMPT = COMPHT * (E-X) / (E-COMPEJ)
    GO TO 50
 29 COMPT = 0.0
    GO TO 50
 30 IF (X-E+1.22) 31,31,34
 31 COMPT = COMPHT
 32 GO TO 50
 34 IF (X-E+0.87) 35,38,38
 35 IF (HITE2 - COMPHT) 31,31,135
135 COMPT = COMPHT+ (HITE2-COMPHT)*((X-E+1.22)/0.35)
 36 GO TO 50
 38 IF (X-E+0.51) 39,42,42
 39 COMPT = HITE2
 40 GO TO 50
 42 IF (X-COMPEJ) 43,45,45
 43 COMPT = HITE2  + (0.1*COMPHT) *((X-E+0.51)/(COMPEJ-E+0.51))
 44 GO TO 50
 45 IF (X-E)46,48,48
 46 COMPT = (HITE2 + 0.1 * COMPHT) * (E-X) / (E-COMPEJ)
 47 GO TO 50
 48 COMPT = 0.0
 50 CONTINUE
 55 CURVE = PHOT1 + PHOT2 + PHOT3 + SCATR + COMPT  + ANNIH
    RETURN
    END (0,1,0,0,1)
```

ACKNOWLEDGMENTS

This research would not have been possible without the cooperation and assistance of many people.

I particularly wish to thank Professor John O. Rasmussen for his advice and encouragement, especially in the study of the level densities and the interpretation of the data.

For proposing this experiment and for his guidance and assistance in its execution, I would like to express my gratitude to Dr. Bernard G. Harvey.

In setting up the electronic circuitry, the help of Mr. Michiyuki Nakamura was invaluable. I am indebted to him for providing me with a practical knowledge of counting electronics.

I would like to acknowledge the use of unpublished data supplied by Drs. John Alexander and Gregory Choppin. Discussions with them, and with Drs. John Morton and John Huizenga were most fruitful.

I am indebted to Professor John A. Wheeler for the proposal of the liquid-drop calculations and for his guidance in carrying them out.

For their cooperation in the sharing of electronic equipment and for their valuable discussions of experimental techniques, I wish to thank Mr. Bruce Wilkins and Dr. George Igo. The californium fission source was provided by Dr. Stanley G. Thompson.

Thanks are due to the members of the cyclotron and the Hilac crews for the difficult feat of providing very low but constant beam levels.

I am grateful for professional advice in writing the computer programs, particularly to Messrs. Douglas Brainard and Donald Zurlinden of the computing group.

I would like to thank my wife Tanya for her patient assistance both as editor and typist of this thesis.

The fellowship support of the National Science Foundation is gratefully acknowledged. This work was performed under the auspices of the U. S. Atomic Energy Commission.

REFERENCES

1. G. Choppin, Research in Nuclear Chemistry Progress Report, June 1, 1959 to May 31, 1960, Florida State University, Tallahassee (unpublished).
2. A. S. Karamyan, Y. B. Gerlit, and B. F. Myasoedov, Soviet Phys. JETP 9, 431 (1959).
3. John Alexander (Lawrence Radiation Laboratory), unpublished data.
4. J. R. Morton, Investigation of Nuclear Reactions by Recoil Studies of Radioactive Products (Thesis), Lawrence Radiation Laboratory Report UCRL 9595, 1961 (unpublished).
5. J. Gilmore, The Effect of Angular Momentum on Fission Probability (Thesis), Lawrence Radiation Laboratory Report UCRL 9304, July 1960 (unpublished).
6. G. Gordon, Fission and Spallation in Nuclear Reactions Induced by Heavy Ions (Thesis), Lawrence Radiation Laboratory Report UCRL 9083, May 1960 (unpublished).
7. T. Ericson and V. M. Strutinsky, Nuclear Phys. 8, 284 (1958).
8. T. D. Thomas, Phys. Rev. 116, 703 (1959).
9. J. M. Blatt and V. F. Weisskopf, Theoretical Nuclear Physics (John Wiley and Sons, Inc., New York, 1952).
10. D. L. Hill and J. A. Wheeler, Phys. Rev. 89, 1102 (1953).
11. W. J. Knox, (University of California, Davis), private communication.
12. G. S. Pik-Pichak, Soviet Phys. JETP 11, 557 (1959).
13. B. R. Mottelson and J. G. Valatin, Phys. Rev. Letters 5, 511 (1960).
14. V. F. Weisskopf, Phys. Rev. 52, 295 (1937).
15. H. A. Bethe, Revs. Modern Phys. 9, 69 (1937).
16. K. J. LeCouteur, in Nuclear Reactions, ed. by P. M. Endt and M. Demeur (North-Holland Publishing Company, Amsterdam, 1960).
17. J. M. B. Lang and K. J. LeCouteur, Proc. Phys. Soc. (London) A67, 586 (1954).
18. A. G. W. Cameron, Can. J. Phys. 36, 1040 (1958).
19. T. D. Newton, Can. J. Phys. 34, 804 (1956).
20. C. Bloch, Phys. Rev. 93, 1094 (1954).
21. N. Rosenzweig, Phys. Rev. 108, 817 (1957).
22. A. A. Ross, Phys. Rev. 108, 720 (1957).
23. T. Ericson, Nuclear Phys. 11, 481 (1959).

24. T. Ericson, Nuclear Phys. 8, 265 (1958).
25. K. J. LeCouteur and D. W. Lang, Nuclear Phys. 13, 32 (1959).
26. T. Ericson, Proceedings of the International Conference on Nuclear Structure, ed. by D. A. Bromley and E. W. Vogt (University of Toronto Press, Toronto, 1960).
27. S. G. Nilsson, Kgl. Danske Videnskab. Selskab, Mat.-fys. Medd. 29, No. 16 (1955).
28. C. Critchfield and S. Oleksa, Phys. Rev. 82, 243 (1951).
29. G. A. Pik-Pichak, Soviet Phys. JETP 7, 238 (1958).
30. J. Hiskes, The Liquid-Drop Model of Fission: Equilibrium Configurations and Energetics of Uniform Rotating Charged Drops (Thesis), Lawrence Radiation Laboratory Report UCRL-9275, June 1960 (unpublished).
31. R. Beringer and W. J. Knox, Phys. Rev. 121, 1195 (1961).
32. W. J. Swiatecki, Proceedings of the Second United Nations International Conference on the Peaceful Uses of Atomic Energy (United Nations, Geneva, 1958), Vol. 15.
33. C. Jordan, Cours d'Analyse de l' École polytechnique, Vol. 2 (Gauthier-Villars, Paris, 1894).
34. I. Halpern, Ann. Rev. Nuclear Sci. 9, 245 (1959).
35. L. C. Biedenharn and M. E. Rose, Revs. Modern Phys. 25, 729 (1953).
36. T. Ericson, Nuclear Phys. 17, 250 (1960).
37. H. W. Broeck, Neutron Emission from Compound Systems of High Angular Momentum (Thesis), Yale University, 1960 (unpublished).
38. V. M. Strutinsky, Soviet Phys. JETP 10, 613 (1960).
39. V. M. Strutinsky, L. V. Groshev, and M. K. Akimova, Nuclear Phys. 16, 657 (1960).
40. E. S. Troubetzkoy, Phys. Rev. 122, 212 (1961).
41. T. J. Gooding, Proton Total Cross Sections at 34 ± 2.5 Mev (Thesis), University of Minnesota, 1958 (unpublished).
42. Terphenyl in polystyrene, manufactured by Semi-Element Company, Saxonburg, Pa.
43. G. E. Gordon, A. E. Larsh, and T. Sikkeland, Phys. Rev. 118, 1610 (1960).
44. F. S. Stephens, Jr., R. M. Diamond, and I. Perlman, Phys. Rev. Letters 3, 435 (1959).
45. A. Sayres and C. S. Wu, Rev. Sci. Instr. 27, 280 (1956).

46. J. A. Northrop and J. C. Gursky, Nuclear Instr. 3, 207 (1958).
47. B. B. Kinsey, in Beta- and Gamma-Ray Spectroscopy, ed. by K. Siegbahn (Interscience Publishers, Inc., New York, 1955).
48. C. O. Muehlhause, Phys. Rev. 79, 277 (1950).
49. D. E. Alburger in Beta- and Gamma-Ray Spectroscopy, ed. by K. Siegbahn (Interscience Publishers Inc., New York, 1955).
50. E. Pollard and D. E. Alburger, Phys. Rev. 72, 1196 (1947).
51. W. F. Hornyak and T. Coor, Phys. Rev. 99, 675 (1953).
52. J. Seed and A. P. French, Phys. Rev. 88, 1007 (1952).
53. J. F. Streib, W. A. Fowler, and C. C. Lauritsen, Phys. Rev. 59, 253 (1941).
54. R. B. Day and R. L. Walker, Phys. Rev. 85, 582 (1952).
55. R. S. Foote and H. W. Koch, Rev. Sci. Instr. 25, 746 (1954).
56. H. E. Kubitschek and S. M. Dancoff, Phys. Rev. 76, 531 (1949).
57. V. A. Karnaukhov and Y. T. Organesyan, Soviet Phys. JETP 11, 964 (1960).
58. A. B. Smith, P. R. Fields, and A. M. Friedman, Phys. Rev. 104, 699 (1956).
59. V. J. Ashby, Distribution of a Finite Particle Beam after Being Multiply Scattered by a Thin Foil, University of California Radiation Laboratory Report UCRL-1414, August 1951 (unpublished).
60. Bruce Wilkins (Lawrence Radiation Laboratory), private communication.
61. R. J. Howerton, Tabulated Neutron Cross Sections, University of California Radiation Laboratory Report UCRL-5226, May 1958 (unpublished).
62. J. M. Freeman and J. H. Montague, Nuclear Phys. 9, 181 (1958).
63. J. J. Van Loef and D. A. Lind, Phys. Rev. 101, 103 (1956).
64. V. I. Strizhak, J. Exptl. Theoret. Phys. (USSR) 31, 907 (1956).
65. R. Kiehn and C. Goodman, Phys. Rev. 93, 177 (1954).
66. M. Rothmann and C. E. Mandeville, Phys. Rev. 93, 796 (1954).
67. M. A. Grace, H. R. Lemmer, and H. Halban, Proc. Phys. Soc. (London) A65, 456 (1952).
68. V. E. Scherrer, B. A. Allison, and W. R. Faust, Phys. Rev. 96, 387 (1954).
69. I. L. Morgan, Phys. Rev. 103, 1031 (1956).
70. N. Starfelt and H. W. Koch, Phys. Rev. 102, 1598 (1956).

71. J. H. Hubbell and N. E. Scofield, IRE Trans. Nuclear Sci. NS-5, 1957 (1958).

72. N. E. Scofield, A Technique for Unfolding Gamma-Ray Scintillation Spectrometer Pulse-Height Distributions, U. S. Naval Radiological Defense Laboratory Report USNRDL-TR 447, 1960 (unpublished).

73. J. Huizenga (Argonne National Laboratory), private communication.

74. W. J. Knox, Proceedings of the Second Conference on Reactions between Complex Nuclei (John Wiley and Sons, Inc., New York, 1960).

75. H. C. Britt and A. R. Quinton, Phys. Rev. Letters (to be published).

76. R. Kaufman and R. Wolfgang, Phys. Rev. 121, 192 (1961).

77. G. Choppin (Florida State University), private communication.

78. A. Ghiorso and T. Sikkeland, Proceedings of the Second United Nations International Conference on the Peaceful Uses of Atomic Energy (United Nations, Geneva, 1958), Vol. 14.

79. V. J. Ashby and H. C. Catron, Table of Nuclear Reaction Q Values, Lawrence Radiation Laboratory Report UCRL-5419, February 1959 (unpublished).

80. A. G. W. Cameron, A Revised Semiempirical Atomic Mass Formula, Chalk River Report CRP 560, 1957 (unpublished).

81. S. N. Goshal, Phys. Rev. 80, 939 (1950).

82. S. A. Moszkowski, in Beta- and Gamma- Ray Spectroscopy, ed. by K. Siegbahn (Interscience Publishers, Inc., New York, 1955).

83. L. V. Groshev, V. N. Lutsenko, A. M. Demidov, and V. I. Pelekhov, Atlas of Gamma-Ray Spectra from Radiative Capture of Thermal Neutrons, trans. from Russian by J. B. Sykes (Pergamon Press, Ltd., New York, 1959).

84. R. J. Blin-Stoyle and M. A. Grace in Handbuch der Physik, Vol. 42 (Springer-Verlag, Berlin 1957), p. 555.

85. K. Alder, A. Bohr, T. Huus, B. Mottelson, and A. Winter, Revs. Modern Phys. 28, 432 (1956).

86. B. L. Cohen and R. E. Prine, Phys. Rev. (to be published).

87. M. Crut, D. R. Sweetman, and N. S. Wall, Nuclear Phys. 17, 655 (1960).

88. B. L. Cohen, Phys. Rev. 105, 1549 (1957).

89. B. L. Cohen and A. G. Rubin, Phys. Rev. 111, 1568 (1959).

90. J. L. Yntema and B. Zeidman, Phys. Rev. 114 815 (1959).